AFCRL-63-341

Measurement of Gamma-Ray Spectra From Thermal-Neutron Capture

John M. Neill
Norman C. Rasmussen
Theos J. Thompson

Massachusetts Institute of Technology
77 Massachusetts Avenue
Cambridge, Massachusetts

Scientific Report No. 1

MITNE-37

Contract No. AF19(604)-7492

Project 4608
Task 460801

August, 1963

Prepared for

Air Force Cambridge Research Laboratories
Office of Aerospace Research
United States Air Force
Bedford, Massachusetts

Requests for additional copies by Agencies of the Department of Defense, their contractors, and other Government agencies should be directed to the:

DEFENSE DOCUMENTATION CENTER (DDC)
CAMERON STATION
ALEXANDREA, VIRGINIA

Department of Defense contractors must be established for DDC services or have their 'need-to-know' certified by the cognizant military agency of their project or contract.

All other persons and organizations should apply to:

U.S. DEPARTMENT OF COMMERCE
OFFICE OF TECHNICAL SERVICES
WASHINGTON 25, D.C.

AFCRL-63-341

Measurement of Gamma-Ray Spectra From Thermal-Neutron Capture

John M. Neill
Norman C. Rasmussen
Theos J. Thompson

Massachusetts Institute of Technology
77 Massachusetts Avenue
Cambridge, Massachusetts

Scientific Report No. 1

MITNE-37

Contract No. AF19(604)-7492

Project 4608
Task 460801

August, 1963

Prepared for

Air Force Cambridge Research Laboratories
Office of Aerospace Research
United States Air Force
Bedford, Massachusetts

MEASUREMENT OF GAMMA-RAY SPECTRA FROM THERMAL-NEUTRON CAPTURE

by

JOHN M. NEILL

Submitted to the Department of Nuclear Engineering on 3rd August, 1963 in partial fulfillment of the requirements for the degree of Doctor of Philosophy.

ABSTRACT

An investigation of the gamma-ray spectra of several isotopes from thermal-neutron capture has been carried out. The isotopes irradiated are Sc^{45}, Ir^{191}, Ir^{193}, Rh^{103}, Dy^{161}, Dy^{164} and Ho^{165}. The instruments that have been employed are a six-meter bent crystal spectrometer at M.I.T. and a scintillation pair spectrometer at Brookhaven National Laboratory.

The technique of using the bent crystal spectrometer has been refined by means of improved development of the photographic emulsion used as a detector, by means of a formalized data-taking procedure and by the use of a digital computer to analyze the results in a consistent fashion. The instrument has been used to survey the low-energy photons from neutron capture by natural scandium, iridium and rhodium.

The scintillation pair spectrometer is coupled to a two-parameter analyzer and has been used in coincidence studies of neutron-capture gamma rays from Dy^{161}, Dy^{164} and Ho^{165}. Its operation has been aided by the use of a digital computer to perform data reduction. An attempt has been made to perform stripping on the complex gamma-ray spectra obtained.

The results have been compiled and nuclear energy level schemes have been proposed for Sc^{46}, and somewhat tentatively for Dy^{165} and Ho^{166}. Possible additions to the present nuclear energy level schemes of Rh^{104} and Dy^{162} are also presented.

Thesis Supervisor: Dr. Norman C. Rasmussen
Title: Associate Professor of Nuclear Engineering

INDEX

LIST OF FIGURES

LIST OF FIGURES (Concluded)

LIST OF TABLES

LIST OF TABLES (Concluded)

ACKNOWLEDGMENT

I wish to thank Professor Norman C. Rasmussen for his guidance and unstinting help given in the course of this work. The research could not have been performed without the willing assistance of all the M. I. T. reactor operations staff, and the personnel from the machine shop and the electronics shop. Part of this work was done at the M. I. T. computation center, whose staff I also wish to thank. In addition, the help given to me by Inam U Rahman on our mutual project was invaluable.

I am most grateful for the help given to me at Brookhaven National Laboratory by Drs. Walter Kane, John Olness and Guy Emery. I must thank too, the staff of the B. N. L. computation center for their efficient processing of my results.

I am grateful to the Air Force Research, Cambridge, whose support of this project made completion of this thesis possible. I would also like to express my gratitude to the General Dynamics Corporation for their financial assistance during the 1960-61 academic year.

My thanks go finally to Miss D. Dutton and Mrs. M. Bosco for typing services, and to Miss M. Friend for help in proof-reading.

CHAPTER 2
INTRODUCTION

2.1

In the original proposal to do this work, it was intended to measure the capture gamma-ray spectrum of germanium. At that time, the spectrum was not well known; and, in addition, the information would be useful as a basis for determination of low-level impurities in that material by means of analysis of prompt gamma rays. In the course of the investigation, it was intended hopefully to develop techniques for resolving complex gamma-ray spectra and so determine the nuclear energy levels of nuclei formed in neutron capture by the five individual germanium isotopes that comprise the natural element.

The problem was essentially a determination of the line spectrum of gamma rays from the absorption of neutrons by a multi-isotope mixture. It was planned in the research work to use two instruments to measure these gamma rays. One was a six-meter, bent crystal spectrometer which had good precision and resolution at low energies. The other was a scintillation pair spectrometer which had reasonable resolution and efficiency at high energies. It was hoped to extend upwards the energy range of the bent crystal spectrometer by using a shielded scintillation detector instead of an emulsion plate. In this way, it was expected that a good quantitative measurement of gamma-ray intensity could be obtained. The details of the original research proposal were given in Reference N1, and this review of its main features has been made so as to show how a somewhat different problem was finally undertaken. Prior to working on germanium, it was decided to test some of the originally proposed ideas on the element, scandium.

The reasons for selecting scandium were many. It was monoisotopic and its absorption cross section of 23 barns was much higher than the 2.4 barns of germanium. Some knowledge of the level structure of the capture nucleus, Sc^{46}, was known from (d,p) excitation by Mazari (M2), and from capture gamma-ray studies by Bartholomew (B4), by

Groshev (G1), and by Hammermesh (H6). There was also a request by Fiebiger at Brookhaven National Laboratory for precise measurement of the low-energy neutron-capture gamma-ray spectrum of scandium, needed to couple to his coincidence data. Furthermore, the original bent crystal spectrometer, built at M.I.T., was in use and a new one needed to be constructed. It did seem more reasonable to test the operation of the new instrument, when it was built, on a mono-isotopic element about which some information was already known.

2.2

The new six-meter, bent crystal spectrometer was designed by the author and built by him and I. U. Rahman, with the latter making the initial measurement of the capture gamma rays from scandium. The construction, calibration and operation of this instrument were described by Rahman (R1). The spectrometer was placed by a port leading into the thermal column of the M.I.T. reactor, this being the only port available where there was room for this large instrument.

Unfortunately, the neutron flux available in this port was only 5×10^{11} n/cm^2-sec which was very low compared to the value of 10^{13} n/cm^2-sec available with the original spectrometer (K1). In addition, the preliminary tests of the shielded scintillation detector for the bent crystal spectrometer proved to be unsuccessful. There was too great a noise-to-signal ratio in the energy range of interest to warrant further testing. Consequently, it was felt that since germanium had a low absorption cross section, that since the flux available was limited and that since the scintillation detection scheme had not worked, there was little chance of successfully measuring all of the low-energy capture gamma rays from germanium by the methods proposed. The early conclusions were as follows. A much higher flux would be required to measure the capture gamma rays of germanium with a bent crystal spectrometer. Secondly, the efficiency of that instrument was too low to allow its use directly in the detection of impurities in a sample of low absorption cross section, such as germanium.

2.3

The second experimental part of the original program envisaged the use of a scintillation pair spectrometer to measure the high-energy gamma rays from the irradiated sample. This instrument was supplied to M.I.T. and set up in operation by Paik (P1). This instrument, as supplied, had a rather poor resolution (about 4.5% at 7.6 Mev) and a low over-all efficiency due to a very small geometrical factor. For measurement of the energy of gamma rays, the instrument did not have, for instance, the resolving power of a Compton magnetic spectrometer. The latter instrument has an extremely low efficiency and can be used only on natural elements because such large sources are required. A useful area of research for the scintillation pair spectrometer then seemed to be the measurement of gamma rays from neutron capture by separated isotopes, or the measurement of coincidences between high-energy and low-energy gamma rays. In both of these applications, the M.I.T. instrument had much too small a geometrical efficiency to be used directly. A program for the development of this instrument was therefore initiated.

2.4

Section 2.1 reviewed the original research proposal, and Sections 2.2 and 2.3 discussed briefly the problems encountered in the application of the two main instruments to that research. This section discusses the decisions made as a consequence of these problems and outlines the area of research that was finally undertaken.

The irradiation of scandium and measurement of its capture gamma rays was well under way when the decision was made not to investigate germanium due to the experimental difficulties. There was already revealed in the experiment then in progress a need for a formal, but quick, method of analysis of the emulsion plates used as detectors. Hand calculations were not too feasible when there were more than 30 lines on one plate, and use of a digital computer seemed appropriate. There was indicated an urgent need for developing the emulsions at M.I.T. to obtain a quicker inspection of results, and this required the construction of a refrigerated developing facility. Finally, it was shown that even the precise measurement of these low-energy gamma rays did

not allow construction of an unambiguous level scheme of the capture nucleus. The latter fact showed also that determination of the level schemes of the nuclei formed from neutron capture by the germanium isotopes would never have been obtained by irradiation of the natural element.

It was decided to measure the low-energy capture gamma-ray spectra of other isotopes, viz., iridium and rhodium, about which some information was already known, as was the case in scandium. Iridium was chosen because its separated isotopes were being investigated by Fiebiger at Brookhaven National Laboratory. The high-energy gamma rays from neutron capture by natural iridium had been studied by Groshev (G2). The gamma rays from the decay of Ir^{192}, which was formed by irradiation of natural iridium, were precisely measured by Muller (M3), and it was believed that the irradiated sample would provide a means of calibrating unknown sources. Rhodium was chosen because its low-energy level scheme had been investigated by the reaction, $Rh^{103}(d,p)Rh^{104}$, on the M.I.T. Van de Graaff accelerator and reported by da Silva (S1). In addition, rhodium was mono-isotopic and had an appreciable thermal-neutron absorption cross section. The capture gamma rays of rhodium were investigated also by Greenwood (G4), Buschhorn (B1), Kalinkin (K5), and Gruber (G5).

Considerable effort was put into the development of the scintillation pair spectrometer, principally in increasing the geometric efficiency and improving the resolution. This effort did not produce results that were considered good enough, and so was given up. A real, though insufficient, improvement was achieved in that the efficiency was raised by a factor of 10, and the resolution was improved to 3.4% at 7.6 Mev by the methods described in Chapter 4. The decision was made instead to use a similar instrument designed for coincidence work and coupled to a two-parameter analyzer at Brookhaven National Laboratory (B.N.L.). For comparison, this instrument could achieve a resolution of 2.5% at 7.6 Mev. The intention was to couple the coincidence studies done there with the work done on the bent crystal spectrometer at M.I.T. However, coincidence studies of scandium and iridium had already been made at B.N.L. For technical reasons described in Chapter 5, rhodium did not prove to be suitable to allow the high-energy, low-energy coincidence

measurements to be made on the apparatus at B.N.L. Instead, two further isotopes were investigated there, Dy^{164} and Ho^{165}. These two were selected because natural dysprosium and holmium had been irradiated and their capture gamma rays measured by Hickson (H1) on the original bent crystal spectrometer at M.I.T. There was information on the level structure of the capture nuclei of these isotopes from various sources, which are detailed in Chapter 7. Dysprosium and holmium were also of interest since the principal nuclei from their irradiation, Dy^{165} and Ho^{166}, were highly deformed and could be expected to exhibit many rotational excitation levels. Determination of some of the parameters relating to these rotational bands and other excitational modes would be useful in understanding nuclear structure. These parameters might be obtained if the level schemes of Dy^{165} and Ho^{166} could be inferred by combining the data from the two institutions.

At Brookhaven, the two-parameter analyzer gave prodigious quantities of information that needed to be reduced and plotted. This had been done by hand and, in order to save time, a computer code was developed to handle the data. Considerable effort was made to devise techniques of unfolding the measured pair spectra of neutron-capture gamma rays. A study of unfolding methods was made; one method was selected and programmed on a digital computer. Using this method, preliminary isotopic assignments were made of the high-energy capture gamma rays of natural dysprosium, that had been measured by Motz (M1).

The introduction may be summarized by saying that the problem undertaken required the construction and successful operation of several instruments and supporting facilities. Data handling methods were developed for these instruments and applied to measurement of neutron capture gamma rays. The results were used to formulate nuclear energy level schemes of the appropriate capture nuclei.

CHAPTER 3
BENT CRYSTAL SPECTROMETER

3.1 DISCUSSION

Bent crystal spectrometers are well described in the literature (D1, K2). A brief description of the instrument used here is given for the sake of completeness, but more detail is to be found in Reference R1.

3.2 PRINCIPLE AND DESCRIPTION OF THE INSTRUMENT

The principle of the bent crystal spectrometer of the Cauchois type is as follows. A broad beam of gamma rays is incident upon a curved quartz crystal. This crystal is a rectangle and is cut such that planes of high reflectivity are normal to the main crystal face and parallel to the sides. The planes with Miller indices 310 are used in this case. The crystal is bent so that these planes all point to a common focus about six meters away that is called the beta point. The optical properties of this system are such that if monoenergetic gamma rays are incident on these internal planes at the appropriate Bragg angle, they will be reflected to a common point at a small but definite distance away from the beta point. The locus of these common energy points is a circle, called the focal circle, whose diameter lies from the beta point to the center of the bent crystal. A detector then can be placed along this focal circle at the same horizontal level as the incident beam, and it can be used to detect the discrete gamma-ray energies in that beam.

The detector used here is an emulsion plate, 12" long by 2" wide, on which is mounted an Ilford G5 photographic emulsion. Thicknesses used typically are 600 microns for gamma rays above 70 kev; and below that energy, a thickness of 100 microns is usually used. The focussing action of the bent crystal produces a line on the emulsion plate for each discrete gamma-ray energy. The distance between these lines is measured on a Gaertner comparator, Type M1205C. If lines from a well-measured source are put on the plate with the lines from the unknown source, then the plate can be calibrated and the energies of

the unknown gamma rays may be determined in a precise manner.

Analysis of the plate is described in detail in Appendix I. The basic approach is to express the spacing of the calibration lines on the plate in a linear form. A least-squares fit of the calibration line wavelengths is made to this linear form of the functional dependence of the spacing. The coefficients so obtained are used to determine the wavelength and energy of the unknown lines. The calculations are done on the M.I.T. 7090 digital computer and provision is made for three cases:

(a) When the plate does not straddle the beta point and has two or more calibration lines,

(b) When the plate does not straddle the beta point and has only one calibration line,

(c) When the plate straddles the beta point and has one or more calibration lines.

The highest precision in wavelength is usually obtained from plates that straddle the beta point; the reasons are discussed in Appendix I. This is why considerable effort is made to obtain straddle plates, although the background level on them is invariably high. This occurs because each plate takes twice the time of a normal plate, since two images of each gamma-ray line are taken.

Figure 1 illustrates the general arrangement of the spectrometer as placed at the 9CH2 port of the M.I.T. reactor, and which leads into the thermal column. The unknown source is placed at the center of this port where the flux is 5×10^{11} n/cm^2-sec at 2 MW operation. The source is irradiated and emits prompt gamma rays which are appropriately collimated. Scattered slow neutrons from the source are stopped by a 3/16"-thick piece of borated plastic attached to a lead collimation brick in the port box. Fast-neutron shielding comprises a 1"-thick slab of polyethylene in the beam path. The direct beam is stopped by the line of lead bricks and the diffracted beam is focussed onto the focal plate. The emulsion plate views a diffracted beam whose breadth from geometrical considerations is equal to that of the unperturbed beam at the focal plate. This follows because the distance from the image of a ray to the beta point is exactly equal to the distance of the unperturbed ray from the beta point, though on the other side.

Figure 2 illustrates the arrangement with some distortion of scale to show all of the essential features. This figure shows clearly that the

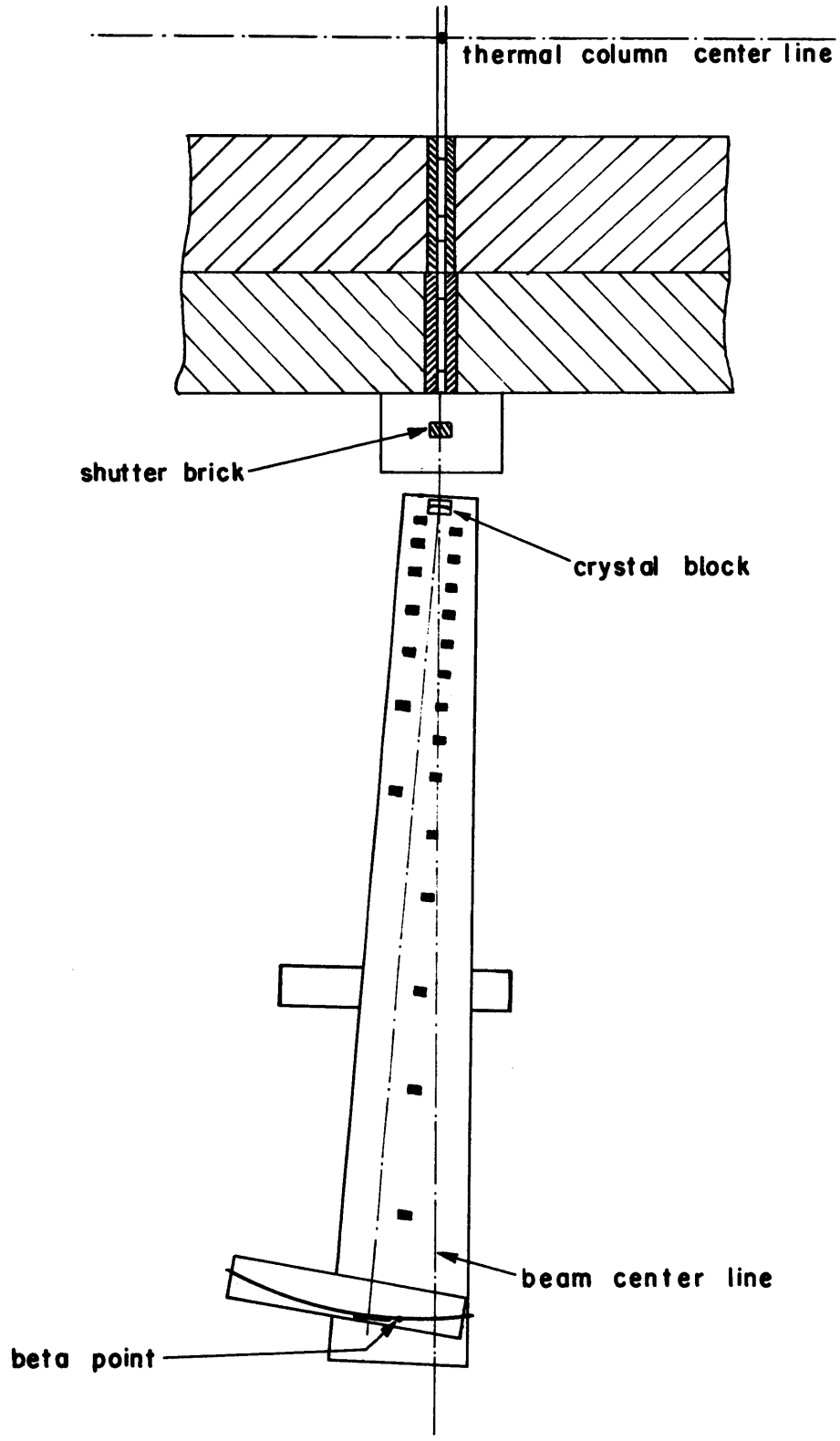

FIG I. BENT CRYSTAL SPECTROMETER ARRANGEMENT TO SCALE

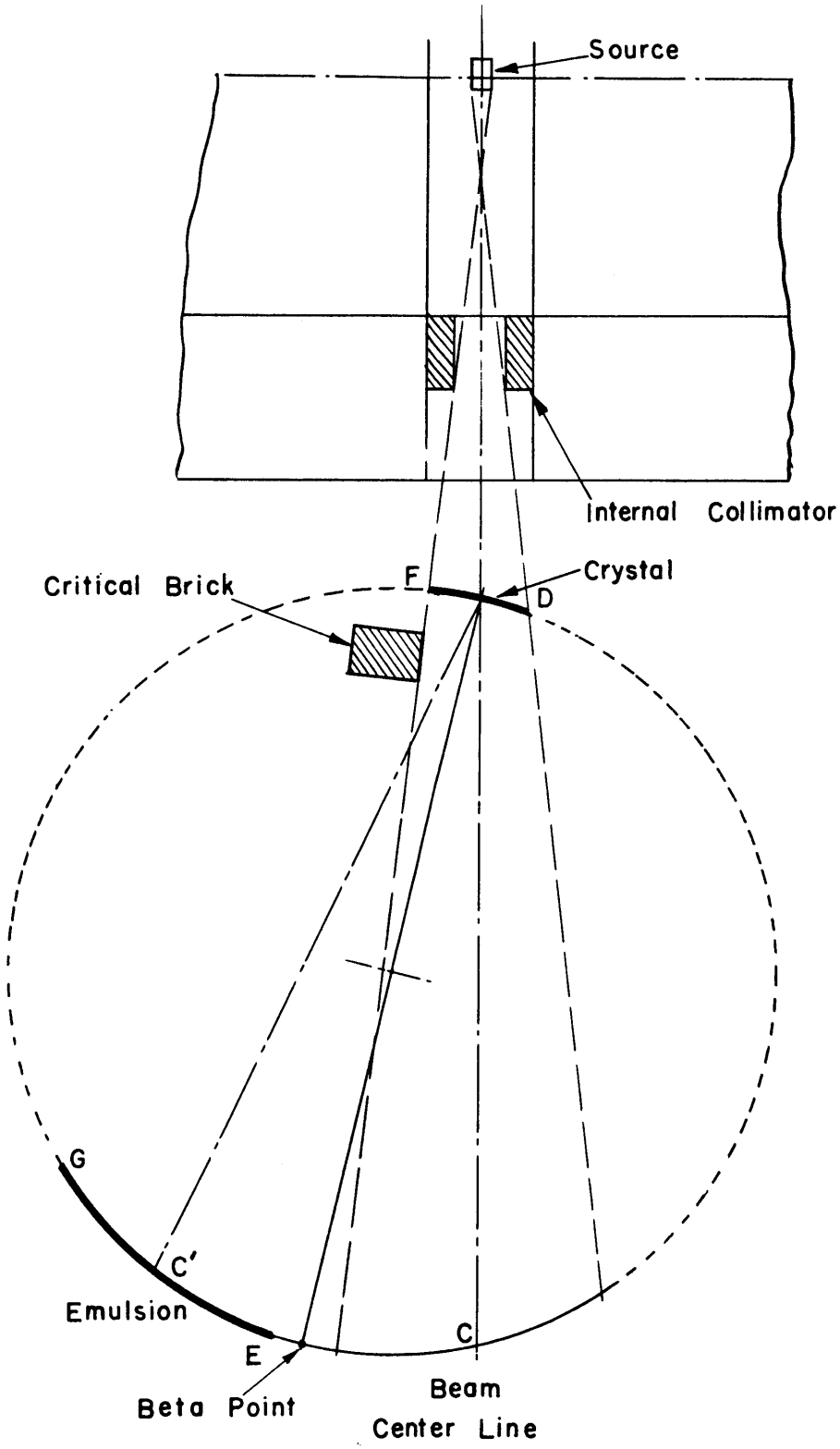

FIG 2. BENT CRYSTAL SPECTROMETER COLLIMATING SYSTEM

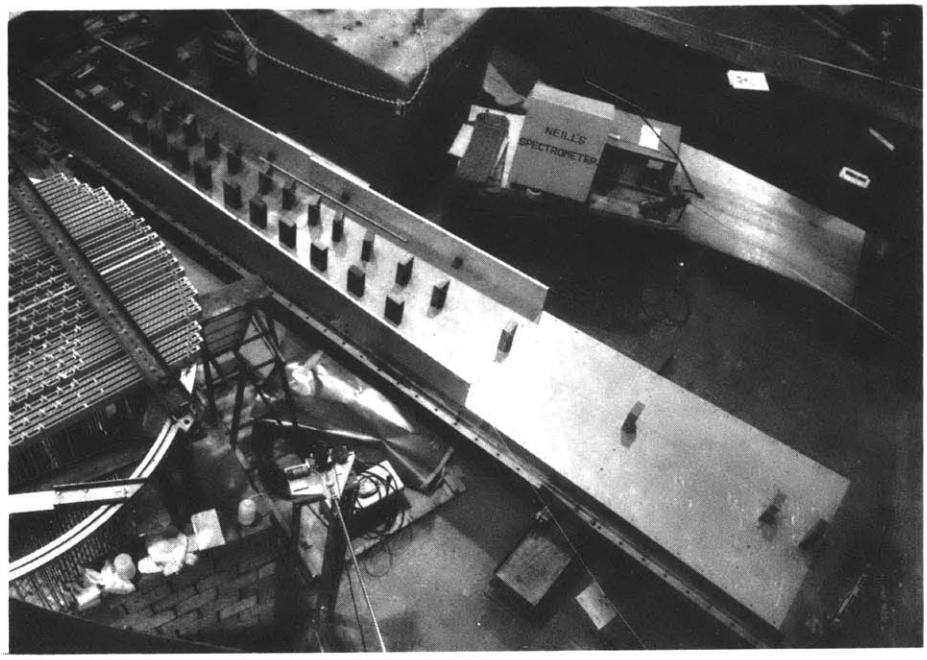

FIG 2a. PHOTOGRAPH OF THE BENT CRYSTAL SPECTROMETER

purpose of the critical brick is to provide final collimation so that the detector sees none of the direct beam. The purpose of the inner collimator is to prevent the detector from viewing directly the walls of the port. An over-all picture of the apparatus is given in Fig. 2a.

The efficiency of the instrument is extremely low, and the magnitude of its variation with energy should be appreciated when the results are interpreted. The crystal efficiency is given by Chupp (C1) in the following way.

The integrated acceptance angle θ for a 4 mm-thick crystal and the 310 planes is

$$\theta = 7.0 \times 10^{-2}/E_\gamma^2 \text{ radians}, \tag{3.2.1}$$

where E_γ is the energy of the incident gamma ray in kev. The effective solid angle Ω presented by the crystal to the source is

$$\Omega = d\theta h/d^2 = \theta h/d, \tag{3.2.2}$$

where d = distance of the source to the crystal, and h = usable vertical height of the crystal.

If H is the height of the detector and R is the diameter of the focal circle, then

$$h = \frac{Hd}{R + d}. \tag{3.2.3}$$

Hence, the ratio η_{CG} of the number of photons seen by the detector to the number emitted by the source is

$$\eta_{CG} = \frac{\Omega}{4\pi} = \frac{7.0 \times 10^{-2} Hd}{E_\gamma^2 4\pi d(R+d)} = \frac{5.56 \times 10^{-3} H}{(R+d) E_\gamma^2}. \tag{3.2.4}$$

The efficiency η_e of the Ilford G5 emulsion is taken from the same reference C1, and is given by the empirical relationship below:

$$\eta_e = 0.06\left[\frac{2.56 \times 10^6}{E_\gamma^3} + \frac{1}{E_\gamma^{1/3}}\right]. \tag{3.2.5}$$

This expression applies over the range 100 to 800 kev and is adjusted appropriately outside of it. η_e here represents the ratio of the energy absorbed by the emulsion to the amount of photon energy incident upon

it. The other factor η_a entering into the efficiency of the system is the gamma-ray attenuation in the source itself, in the neutron shielding, in the crystal and in the air path. This factor can be calculated reasonably well, using the measured gamma-ray attenuation coefficients. For this calculation, the source is assumed to have an atomic number of 45.

Hence, the over-all efficiency of the system is given by

$$\eta_T = \eta_{CG} \cdot \eta_e \cdot \eta_a \qquad (3.2.6)$$

and this is shown in Fig. 3, with Fig. 4 showing the component efficiencies. The curve shows two features of note:

(a) The efficiency changes by over 2 orders of magnitude over the useful operating range.

(b) The maximum efficiency occurs around 75 kev.

Intensity measurements on the bent crystal spectrometer are difficult to make for reasons detailed in Chapter 5. In general, only qualitative estimates by eye are made. If a gamma ray is to be detected on the emulsion, the probability will depend on the intensity of the gamma ray as well as the efficiency of the system. The lower useful limit of the instrument seems to be about 30 kev for a typical source, although X rays down to 22 kev have been detected. The upper energy limit of the instrument arises not only from the reduced efficiency but also from the difficulty of separating the reflected beam from the direct one. The background on the emulsion always increases at high energies. The upper useful limit of the instrument seems to be about 1.5 Mev, although Kazi (K2) has measured a 2.2 Mev gamma ray from neutron capture by hydrogen in the high flux port. Kazi gives a value of 1200 curie hours needed to detect a 0.511 Mev gamma ray. That value may be combined with Figure 3 to estimate the number of curie hours required at other energies.

The resolution of this instrument is energy-dependent and can be expressed approximately by

$$\text{Resolution} = 10^{-3}\, E_\gamma(\text{kev})\% \,, \qquad (3.2.7)$$

so that it has excellent resolving power over the useful energy range. The precision should be related to the resolution directly, since the

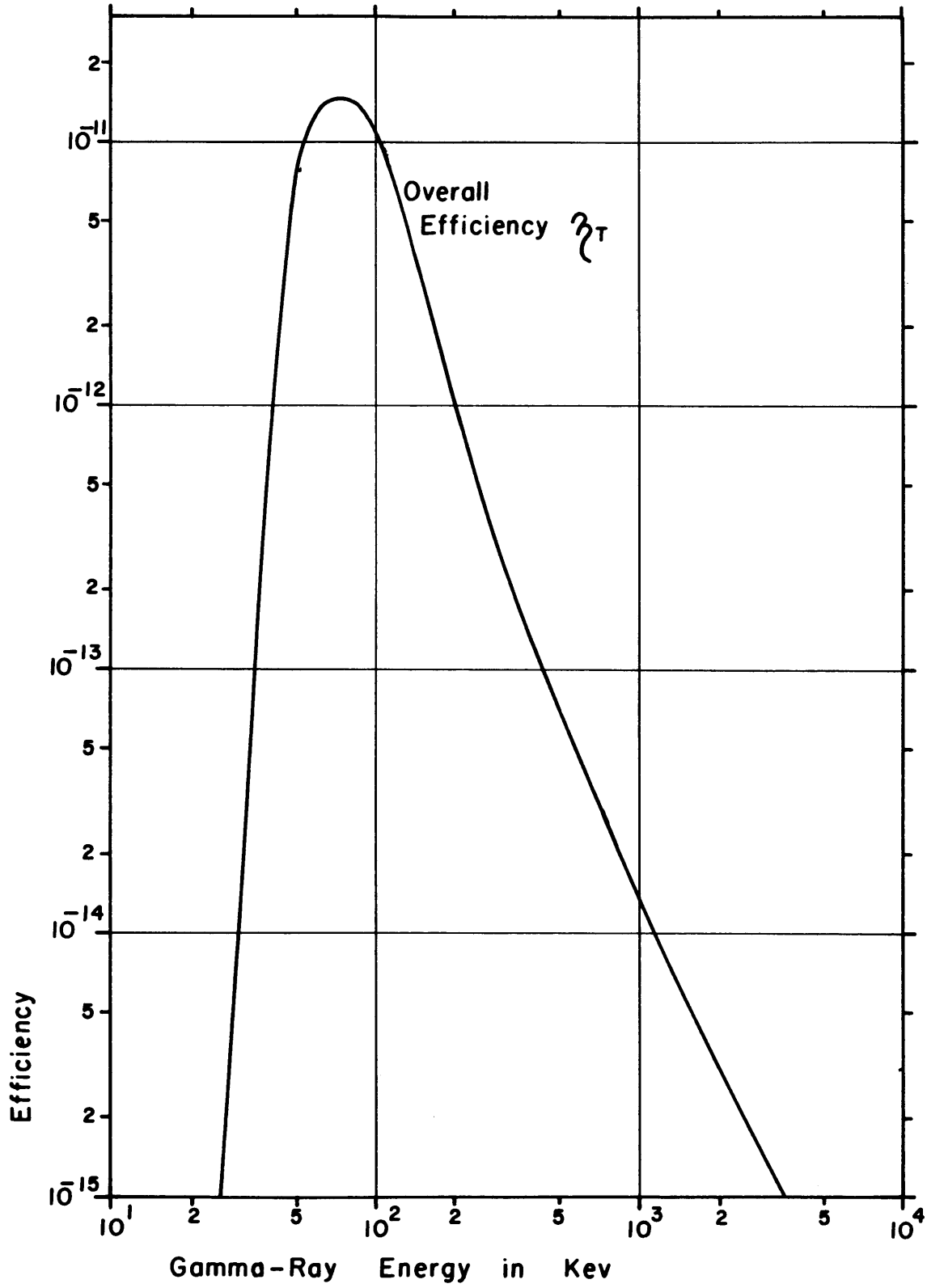

FIG 3. OVERALL EFFICIENCY OF THE BENT CRYSTAL SPECTROMETER SYSTEM

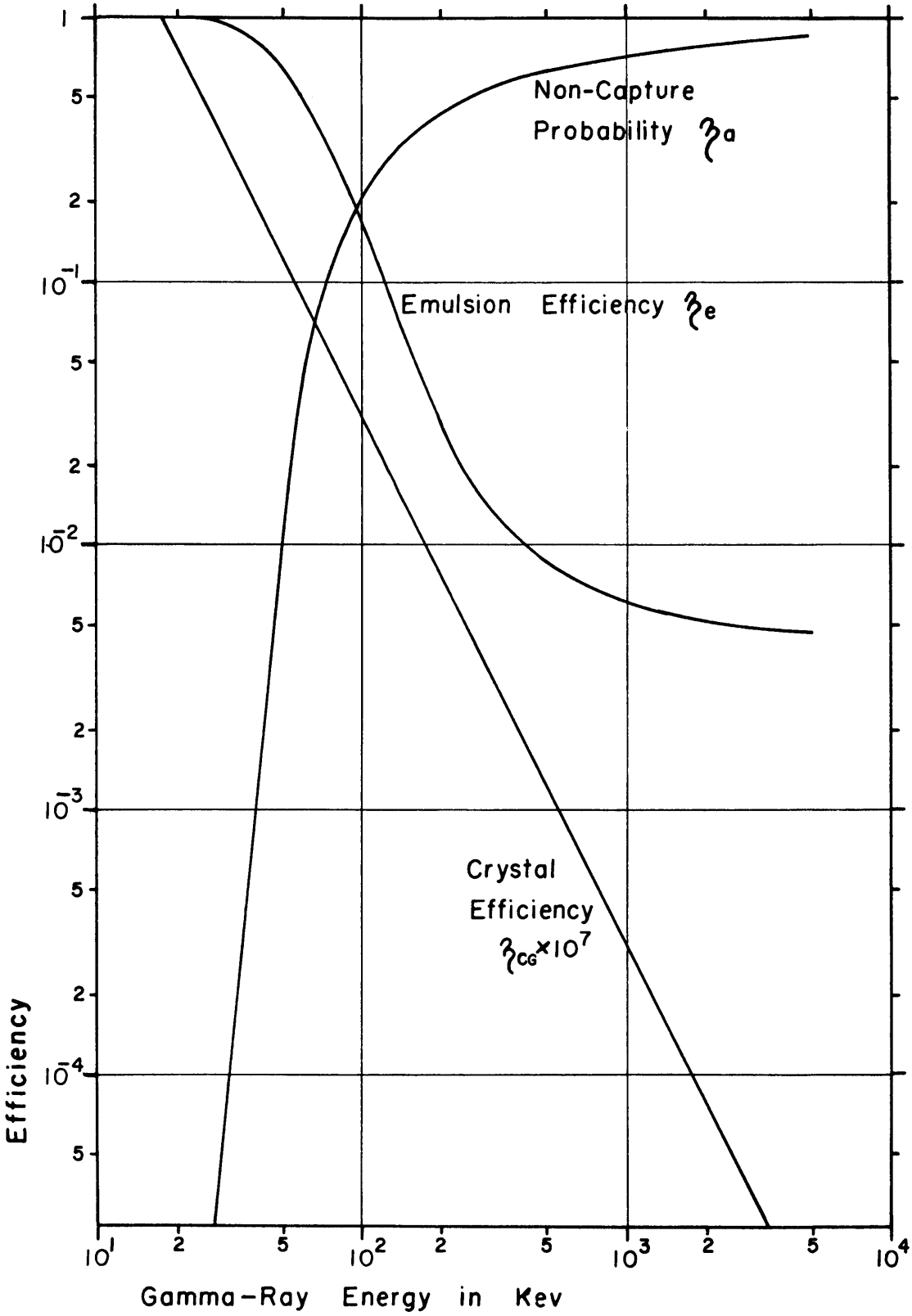

FIG 4. COMPONENT EFFICIENCIES OF THE BENT CRYSTAL SPECTROMETER SYSTEM

standard deviation of the measurement of a line center is usually about 1/20 of the line width. However, uncertainties in the calibration lines decrease the accuracy of the measurement so that it is expressed approximately as

$$\text{Precision} = 10^{-4}\, E_{\gamma}(\text{kev})\% \ . \qquad (3.2.8)$$

3.3 OPERATION OF THE INSTRUMENT

The operation of the spectrometer is not well described in Reference R1 and so is covered more fully here. The dimensions of the source and final collimator are such that a view of about 4" is possible at the focal plate. Exposure ranges are therefore selected at a spacing of 4" except near the beta point, where the range must be less if the detector is not to see the direct beam.

Operations are commenced initially with the lead shutter brick down so that the direct beam is cut off, and with no detector on the focal plate. The spectrometer is rotated about its pivot until the center line of the incident beam of gamma rays lies at the center of the range of interest at point C on the direct beam side of the focal plate. The spectrometer frame is locked in this position. If a gamma ray directed towards C is incident at the correct Bragg angle, it may be reflected towards point C′ which is at the same distance away from the beta point as C, though on the other side. A string is drawn taut from point D on the crystal to point E on the focal plate. A line of lead bricks is placed against this string as indicated in Fig. 2. The shutter brick is raised and the critical brick is pushed in until the radiation level at point E is low enough, usually about 2 mr/hr or less. The shutter brick is closed down again. A string is now drawn from point F on the crystal to point G which is to be the extremity of the emulsion plate away from the beta point. Lead bricks are placed on the spectrometer frame up to this latter string. The purpose of these bricks is to stop side-scattered gamma rays. In addition, these bricks support shielding over the beam necessary to stop gamma rays scattered vertically upwards. The emulsion plate is strapped to the focal plate and the shutter brick is raised to allow exposure.

Calibration of the emulsion plate in the high energy range is achieved by exposure to decay gamma radiation from a Ta^{182} source.

This tantalum source is located in the port box and is pulled into the beam center line by means of a wire. This operation is usually done at the weekend when the reactor is shut down. Calibration of the emulsion plate in the low energy range is achieved by use of a Picker hot-shot X-ray machine. The shutter box assembly at the head of the spectrometer is removed, and the X-ray machine is put in its place at the correct level and shielding placed around. It is found to be more convenient to use the machine with a simple transmission target instead of the more efficient reflection target. In this type of usage, a transmission target is selected of a sample whose X rays are of the desired energy. It is attached to the front of the X-ray machine beam hole, the machine is lined up and then set to run over the weekend. Since the beam source is now much closer to the crystal face, considerable care must be taken with shielding to ensure that the emulsion does not see the direct beam.

In determining which material the transmission target must be made of the following simple rules are useful.

1. The $K\alpha_1$ X ray of the target material should be placed about 20 cms away from the edge of the emulsion plate nearest the beta point, so that the $K\beta$ X rays will be seen, too.

2. The relationship between gamma or X-ray calibration energy E_γ and distance y from the beta point is

$$y(\text{cms}) = \frac{3120}{E_\gamma(\text{kev})}. \qquad (3.3.1)$$

The X-ray machine is aimed at a point on the other side of the beta point that corresponds to the center of the emulsion plate. The lead bricks that cut off the direct beam must be behind a line drawn from the crystal to the position of the $K\beta_2$ X ray on the emulsion plate.

The practice has been to use two emulsion plates at one time, to provide insurance against one being broken or improperly processed. They are covered individually in a household plastic wrapping to prevent drying out and are then bound together with two separate layers of black photographic paper. It has been found, however, that below 60 kev, the transmission through the first emulsion plate is small enough that the image on the second plate is weak. It is felt, therefore that one plate alone is adequate below 60 kev. On the high flux port used by Hickson (H1),

in which intensities are 20 times greater, this conclusion is less applicable. In addition to the emulsion, an X-ray film is usually mounted just above the focal plate. The film can be developed quickly and serves to monitor the primary detector.

It has also been found that at energies above 200 kev, a distinct improvement in contrast can be obtained by using a filter in front of the emulsion. The filter captures the large number of low-energy gamma rays from the source, that arise presumably from Compton scattering in the crystal, while the discrete energies of the reflected beam are affected little. A convenient filter is sheet cadmium, 0.020" thick.

3.4 PHOTOGRAPHIC EMULSION DEVELOPING SYSTEM

The emulsion plates require special processing because they are so thick. If the developing time is rapid, compared with the diffusion time of developer through the emulsion, then very uneven developing will occur and there will be considerable surface blackening. For this reason, a refrigerated developing system is required for the emulsion since the developing rate is much less at low temperatures, relative to the diffusion rate.

Prior to the installation of this system, the practice had been to send the plates to California for processing and this resulted in excessive plate breakage and too great a time lag between exposure and inspection.

The processing requires a facility that will provide a constant bath temperature of 5°C and yet can be raised to 23°C within 5 minutes and lowered back down in the same time. This is needed because developing is done dry at 23°C after the developer fluid has completely diffused into the emulsion at 5°C. The latter requirement is the most severe and essentially determines the refrigerator capacity. The capacity necessary is excessively large, and so the system has been designed with a large thermal reservoir and a smaller refrigerator to do the same job.

Figure 5 illustrates the system. It comprises two stainless steel trays, each with a double-walled bottom. The bottoms of these trays are connected to each other and to the refrigerator unit by copper pipes and with appropriate valving. The refrigerator is a water-cooled unit and is placed in a cupboard underneath the trays. The refrigeration fluid that cools the trays is water. The whole system is placed in a stainless

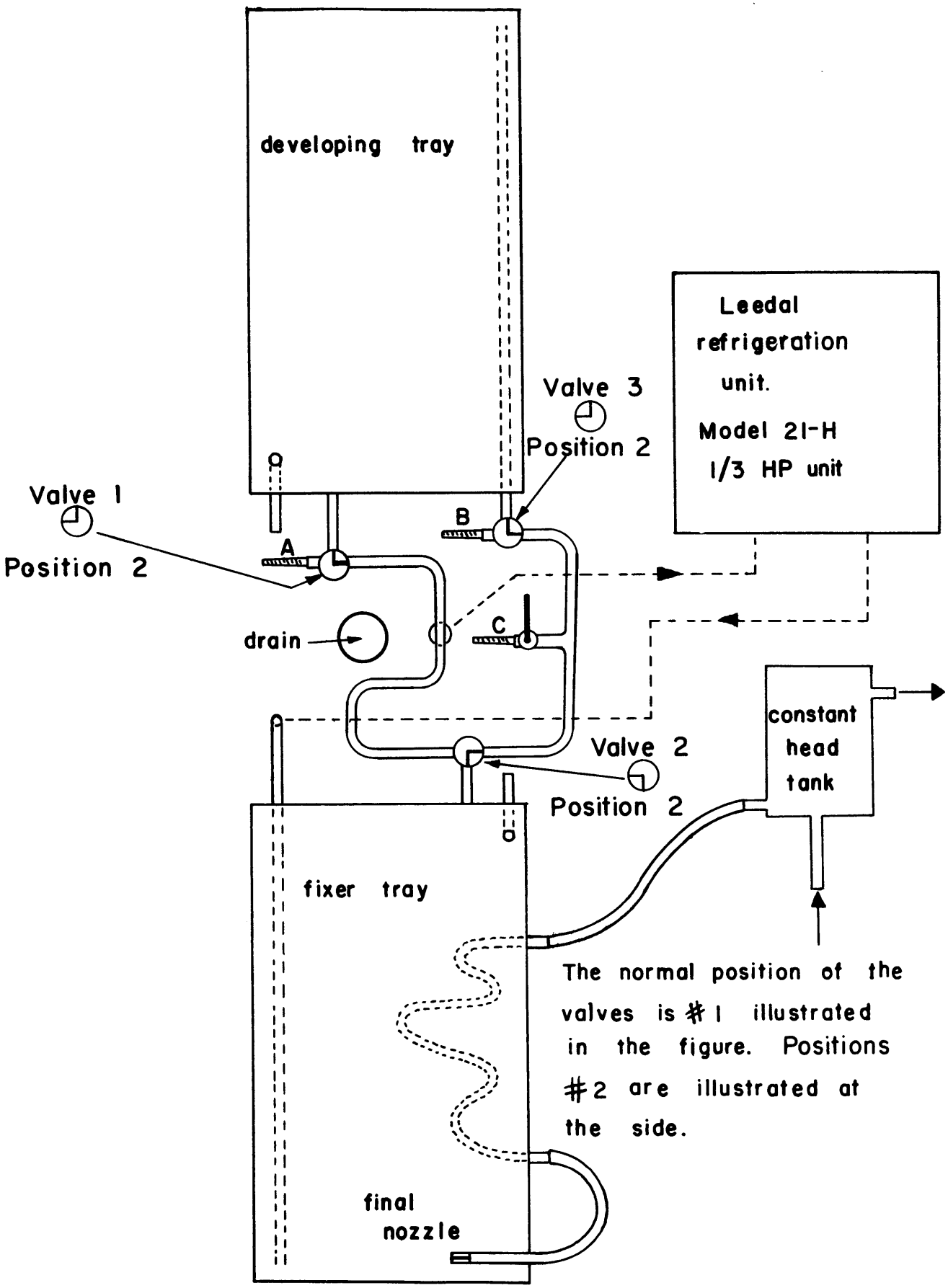

FIG 5. REFRIGERATED DEVELOPING SYSTEM

steel pan and is enclosed in a wooden locker located in the dark room of the reactor building at M.I.T. Each tray is provided with a drain which is connected by tygon tubing to the open drain indicated in Fig. 5. The drain in each tray is closed by screwing a short stainless steel pipe into the tapped drain hole and by using a screw clip on the tygon tubing. The fixer tray has a stainless steel coil in its bottom, which is to provide cooling of the water for washing the emulsions after fixing. A simple constant head tank provides a constant flow of this wash water when required, via rubber tubing to a small final nozzle at the mouth of the tubing. Each tray is provided with a stainless steel cover. The cover for the fixer tank has a slow-speed electric stirrer mounted in it to provide agitation during fixing. Neither tray is designed for pressurized operation and care must be taken to prevent mains water pressure being applied in full to the double-walled bottom of each tray.

The procedure for processing plates is described by Cohan (C2), who did an extensive literature survey and some experimentation. The procedure for a 600 micron-thick emulsion is described in detail here to show the proper use of the developing system. All of the operations in the dark room must be done in the dark or safe light until near the end of fixing.

1. The required amounts of developing and fixer fluids are made up 16 hours prior to commencing the processing. The developer is made up with distilled water, if possible. These fluids are stored in the refrigerator in which emulsion plates are stocked.

2. At the same time, the trays are cleaned thoroughly and the fixer tray is filled with cold water to a depth of 5 cms.

3. The refrigeration system is checked for air leaks. A piece of rubber tubing is connected from faucet C to the drain. Inlet water is fed via rubber tubing to inlet nozzle B with valve 3 in position 2, and trapped air and excess water are bled off through faucet C. This faucet and valve 3 are switched to their normal positions simultaneously, to prevent either pressurization or air voids in the system.

4. With the valves all in their normal position #1, as in Fig. 5, the refrigeration unit is turned on and the system allowed to cool for 16 hours to its operating temperature of 5°C.

5. The processing is commenced by putting the cold developing fluid into the developing tray. The emulsion plates are unwrapped, labelled if necessary with a scriber and placed with the emulsion upwards in the soak bath of cold water in the fixer tray.

6. After soaking for 2-1/2 hours, the emulsion plates are transferred to the developer tray and allowed to soak for 2 hours.

7. The flow mixer in the darkroom is checked during this interval to make sure its temperature scale is calibrated properly and it is then connected to inlet nozzle B.

8. At the end of this time, the developing fluid is drained out and excess on the emulsions is wiped off carefully with a tissue soaked in cold water.

9. The refrigerator is turned off temporarily to prevent pressurization of the system during the next operation.

10. All valves are turned to position 2. The bottom of the developer tank is heated up to 23°C by passing 23°C water from the flow mixer in through nozzle B and out to the drain from nozzle A. The refrigeration unit is turned on again so that the fixer tank is kept cool. This is the dry developing stage.

11. The cold water in the fixer tray is converted to stop bath mixture by the addition of 120 mls of 28% vol acetic acid.

12. Twenty-five minutes after operation 10 has started, the flow mixer is turned to the fully cold position, and the developer tray is brought down to mains cold water temperature as quickly as possible.

13. The refrigeration unit is turned off again. Valves 1 and 3 are turned simultaneously back to position 1. Valve 2 is also turned back to position 1. The refrigeration unit is turned on again.

14. The stop bath mixture is now scooped up out of the fixer tray and poured gently into the developer tray and the plates are soaked for 2-1/2 hours in the stop bath.

15. During this interval, the fixer tray is thoroughly cleaned and is filled with the first batch of fixer fluid.

16. The emulsion plates are then transferred, one by one, to the fixer tray. Before insertion into the fixer, they are wiped thoroughly but quickly with tissues soaked in cold fixer, in order to remove surface scum that arises from the developing. Wiping is best done at this stage while

the emulsions are reasonably firm, since they are softened by the subsequent fixing.

17. The emulsions are soaked in fixer for 3 days. During that time, part of the fixer is drained off and fresh fixer is added at regular intervals. This is done until all the required amount of fixer has been used and terminates after about 2-1/2 days. During the fixing, electric stirring is utilized continuously.

18. After 3 days, washing is commenced. This is done by passing tap water into the constant head tank until it overflows in a regular manner. Water from this little tank is fed through the cooling coil in the bottom of the fixer tray and then through the final nozzle in the rubber tube into the tray, itself. This provides a slow flow which gradually dilutes the fixer which overflows into the drain. The wash flow is about 6 liters/hour. Washing is carried out for 3 days.

19. The developer tray is cleaned, and the four batches of drying mixture are made up and stored in the stock refrigerator. The drying mixtures comprise various amounts of water and ethyl alcohol, and are needed to dry the emulsion plates which are grossly swollen after fixing.

20. The plates are then dried by soaking for two hours in successive batches of cold drying mixtures which are placed successively in alternate trays.

21. The plates are then placed on paper towels in front of a fan for 2 days, by which time they are firm enough for handling.

22. A final wipe with pure alcohol at this stage may prove beneficial in removing any remaining surface scum.

CHAPTER 4
SCINTILLATION PAIR SPECTROMETER

4.1 PRINCIPLE AND DESCRIPTION OF THE INSTRUMENT

A description is given here of the scintillation pair spectrometer used in the present work and located at Brookhaven National Laboratory. This apparatus has been described in an earlier form by Segel (S5) and Fiebiger (F3). It has been extensively modified by Fiebiger to its present state, but there is no detailed description available of its present form and of its operation. This chapter and Appendix IV remedy the situation.

The principle of the scintillation pair spectrometer may be seen from Fig. 6. The kinetic energy of the positron and negatron from a pair interaction of a primary gamma ray in the central sodium iodide crystal B of the instrument is measured, if the two side crystals simultaneously detect the 0.51 Mev photons arising from the annihilation of the positron. The source of gamma rays is from neutron capture by a sample placed in position, Fig. 6, where the neutron beam from the reactor is perpendicular to the plane of the figure. The fourth crystal, A, used to detect low-energy coincident gamma rays, is shown placed closely to the source point in order to provide a high geometric efficiency. The source itself is placed on the neutron beam center line inside a surrounding teflon tube. This tube is double-walled and comprises three sections. In the vicinity of the source, the wall of the tube is packed with lithium carborate enriched in Li^6 to capture scattered neutrons without producing gamma rays. The wall of the other two sections is filled with cheaper boron for the same reason. Boron does, however, produce a low-energy photon, and so it is not desirable to have it in the vicinity of the source.

The source itself consists of a chemically stable form of the isotope under investigation, packed in a suitable container. If the isotope has a low capture cross section, the container may be aluminum whose outside diameter is equal to the bore of the teflon tube. If the isotope

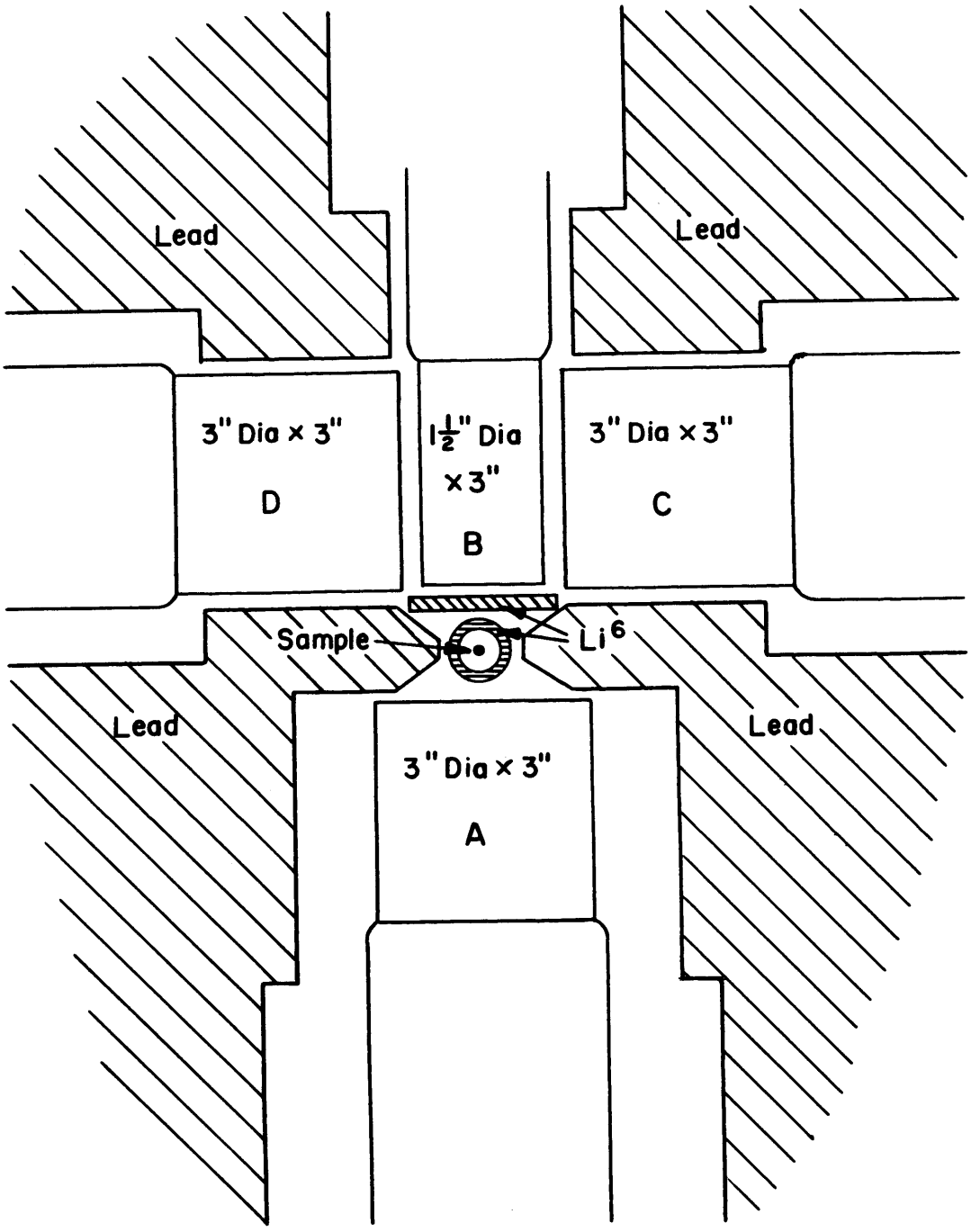

FIG 6. ARRANGEMENT OF CRYSTALS IN THE B.N.L SCINTILLATION PAIR SPECTROMETER.

has a reasonably high capture cross section, the container may be a gelatin capsule mounted on nylon cross wires inside a cardboard supporting tube.

Figure 7 indicates the over-all general arrangement, though not to scale. The detectors themselves are heavily shielded with lead and paraffin wax to reduce the external background of neutrons and photons. The lead shielding has four stepped holes bored through it to the crystal positions. Placed in these holes are plugs, at the tip of which a small source may be put in order to calibrate or stabilize the appropriate crystal. The unperturbed neutron beam is stopped by a beam catcher comprising borated paraffin wax backed by lead. Primary collimation of the neutron beam is achieved by 0.5"-diameter lead collimators placed in the reactor shield. Final collimation is achieved by a removable collimator mounted in a socket on the shielding of the detection system. This final collimator is 4" long and is made of 2" of lead and 2" of epoxy resin, loaded with boron carbide. There are several of these final collimators with different bores ranging from 3 mm diameter to 9 mm diameter, and it is practice to select the one that gives the desired counting rate in the crystals. The apparatus is located next to the Brookhaven graphite pile. The neutron beam is well thermalized and provides a flux of 10^6 n/cms^2-sec with a cadmium ratio of 50 at the source position. The beam can be cut off at the reactor shield face by insertion of an 8"-long, steel rod into the open beam port and then by covering the hole with a boral plate, 1/4" thick. There are three sodium iodide crystals in the scintillation pair spectrometer, and when only these three are used, it is termed throughout this thesis as a singles run. When a coincidence is demanded at the same time from the fourth crystal, A, it is termed a fourfold run.

An electronic block diagram of the system is shown in Fig. 8. Since a fourfold run may easily be six days long, it is necessary to eliminate drift that is normally common to scintillation detectors. Stabilizers of the deWaard type, (W1), are incorporated on each circuit. The principle of these stabilizers is to sample a peak in the unknown spectrum and adjust the high voltage of the system to maintain that peak at a predetermined pulse height. On the side crystals, which are run by a common high voltage, the stabilizers feed back instead to the voltage on the focussing electrode of the photomultiplier tube to achieve the same effect.

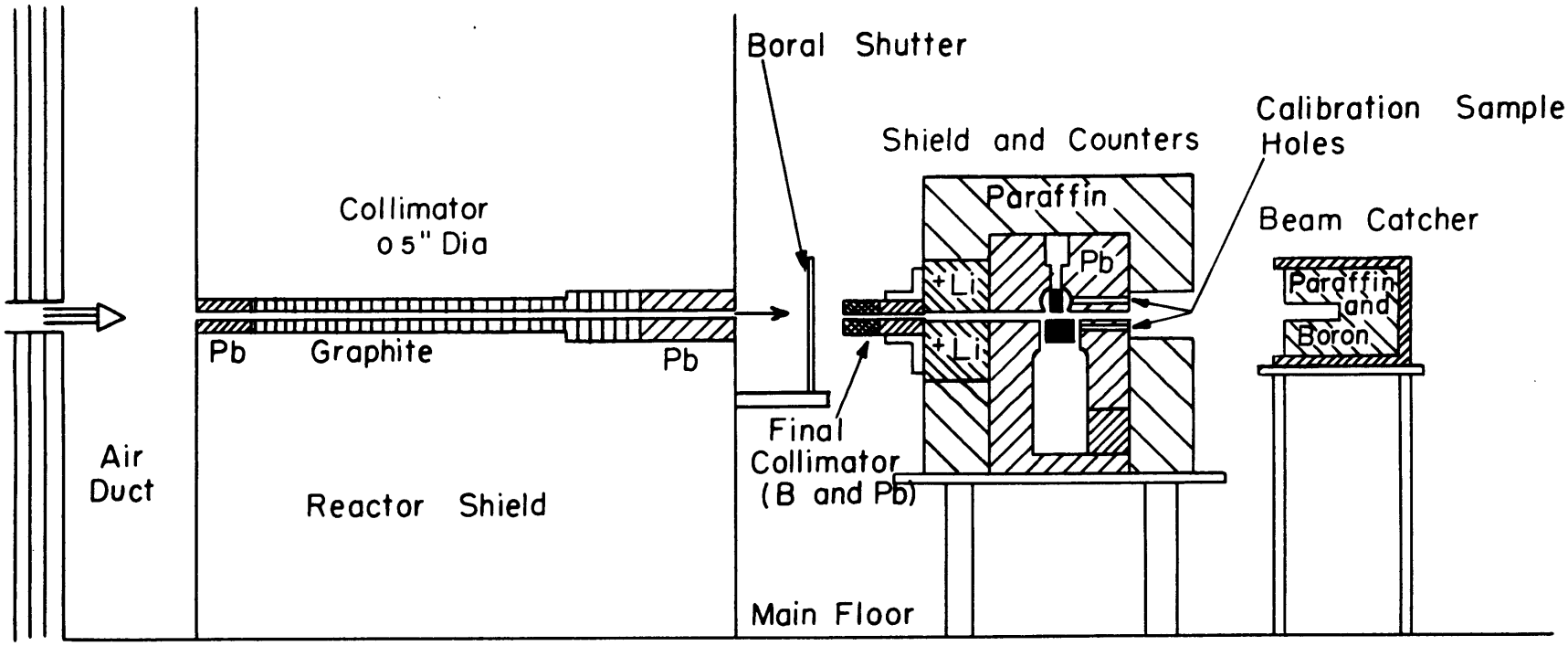

FIG 7. PHYSICAL ARRANGEMENT OF THE B.N.L SCINTILLATION PAIR SPECTROMETER. (SCALE DISTORTED)

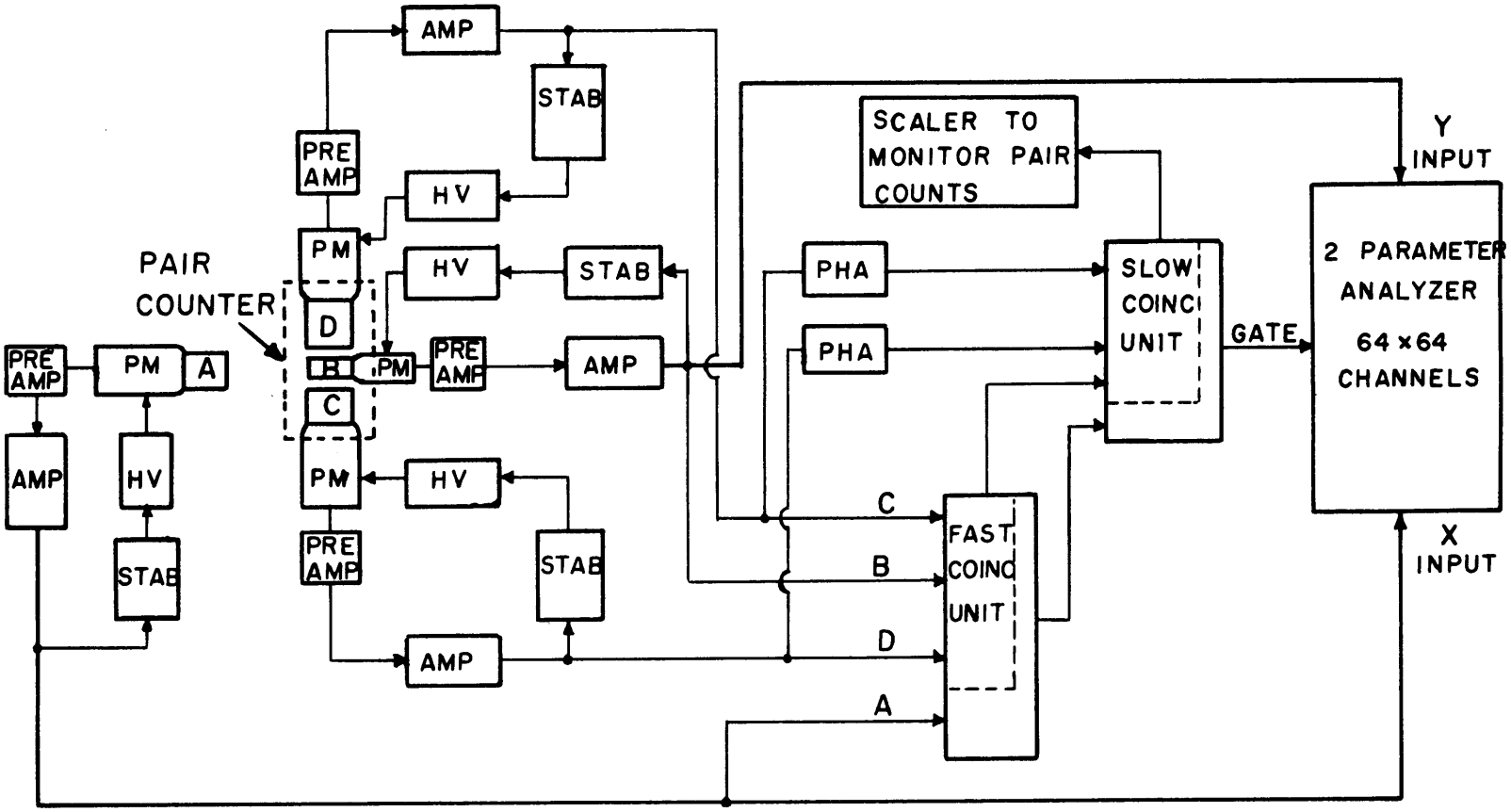

FIG 8. ELECTRONIC BLOCK DIAGRAM FOR THE B.N.L SCINTILLATION PAIR SPECTROMETER

The amplifiers used are Franklin double delay line clipped units, and their use permits minimization of spectral distortion from pile-up. Their cross-over type pulse also permits full advantage to be taken of the capabilities of the coincidence circuitry.

The coincidence requirements of the system are that fast coincidences are demanded of all four crystals, and that the energy measured in the two side crystals is 0.51 Mev, which requires two slow coincidences. The usual fast-slow coincidence circuits are transistorized units designed by Chase of Brookhaven National Laboratory. Each unit has a single-channel analyzer built into it which may be switched in, where appropriate, to meet the slow coincidence requirements. One feature of these units is that two modes of pulse timing are provided, permitting coincidence signals to be derived either from the leading edge or the zero transition of the input signals. The use of the latter, which is possible due to the type of pulse given by the Franklin amplifier, makes the coincident pulses independent of signal amplitude and almost independent of discriminator bias setting. In this way, the variation in fast-coincidence pulse timing is minimized and a resolving time of about 50 nanoseconds can be achieved.

If the coincidence requirements are met, the simultaneous pulses from the pair spectrometer Y and the fourth crystal X are delayed and then fed with a final coincident pulse to a 64 × 64 two-dimensional pulse height analyzer. The address of each count is determined then by the pulse height in the X and Y channels and the count is stored at the appropriate point in the 64 × 64 matrix. This analyzer is an early Brookhaven design with a drum-type memory, and it provides for display of each Y channel on a scope. There are two window controls on both channels of the analyzer; and in the usual case, the X channel, used for the A system, operates with the x1 window; and the Y channel, used for the B system, operates with the x5 window. Read-out from the analyzer is obtained by means of a Hewlett-Packard parallel printer at the rate of about 3 numbers/sec. No provision is made on this particular analyzer for punched paper tape output so that data handling is difficult. The scintillation pair spectrometer is highly developed and gives a resolution of about 2.5% for an incident 7.6 Mev gamma ray. This high degree of development has been obtained by the following means:

(a) Careful selection by the Harshaw Chemical Company of the central sodium iodide crystal, mounted as an integral unit without a light pipe, to provide minimum intrinsic resolution.

(b) Optimization of the crystal performance by variation of the cathode-dynode potential on the photomultiplier, by variation of the focussing electrode potential and by variation of the over-all high voltage.

(c) Careful attention to shielding to reduce the external background and to reduce background arising from scattered neutrons.

(d) Careful collimation and limitation of the maximum counting rate in the central crystal.

(e) Selection of side crystals with good resolution so that channel requirements there may be tight without sacrificing efficiency.

A description of the operation of the instrument is given in Appendix IV.

4.2 SUMMARY OF DATA REDUCTION METHODS

Reduction of the data from two-parameter coincidence runs is done by an IBM 7090 computer with a code called CAPGAM that will perform the following operations as desired:

(a) Subtract off background.

(b) Subtract off accidental counts.

(c) Calculate the standard deviation of the corrected count.

(d) Subtract off coincidences in the fourfold runs that arise from the bremsstrahlung tails of peaks.

(e) Print out and plot the corrected data.

(f) Sum channels in either X or Y directions, and plot and print out these sums.

(g) Subtract off a normalized average vector from each row to accentuate differences from a mean. This process is termed singularization. These differences are plotted and printed out.

(h) Sum singularized channels; print out and plot these sums.

(k) Plot data in subranges to provide effective changes of scale.

Details of the CAPGAM code are given in Appendix III.

Data from singles runs on the scintillation pair spectrometer can be processed by another code called PAIRSTRIP. This code smooths the counts and attempts to determine the line spectrum of incident high-

energy gamma rays. In addition, the code will calculate what the measured spectrum should be, knowing the incident line spectrum and the response function of the spectrometer. Details of the PAIRSTRIP code are given in Appendix II, together with a discussion of its applicability.

CHAPTER 5
MEASUREMENTS MADE ON THE BENT CRYSTAL SPECTROMETER

5.1 DISCUSSION OF INTENSITY MEASUREMENTS

Before discussing the energy measurements made on the bent crystal spectrometer, an explanation is given as to why no detailed study of the gamma-ray intensities has been made. Intensities are estimated qualitatively by eye and their range varies from very, very weak to very, very strong. See Table 1 for example. These qualitative values are quite useful. It is believed that quantitative estimates made from measurement of line densities are very inaccurate and the effort cannot be justified. Instead, it is felt that the qualitative values given and use of Fig. 3, showing the over-all efficiency of the system, provide sufficiently meaningful answers without unnecessary effort. Since the belief is a point of contention, the reasons for it are detailed below.

(a) The more intense transitions produce lines that are too dark to be measured by a photo densitometer. Consequently, line density measurements must be made by comparison with a set of photographic density standards. The comparative method has poor precision, even in a simple case.

(b) The exposure schedule of the emulsion plates is not simple. In general, it is not as practiced by Cohan (C2), who set his collimating system such that his whole emulsion plate was exposed at one time without moving either spectrometer frame or critical brick. The plates in this case are exposed over different length ranges, for different exposure times, for different amounts of exposure overlaps and for different critical brick settings. The consequence is that the background along the plate is extremely variable, particularly in the energy range above 200 kev where intensity measurements would be most useful. The density comparison method depends considerably on background and this factor produces a very large uncertainty in the measurements.

(c) The view factor for the source depends on the critical brick setting which is varied, depending on the energy range studied. At high

energies, the critical brick is moved in considerably; and its position relative to the beam center line is badly known and this uncertainty further contributes to the inaccuracy of measurement of the line intensities.

(d) The source intensity is not well known, due to the uncertainty in the flux level and due to a large uncertainty in neutron self-shielding factor. The latter depends on source geometry and cross section and also the directionality of the neutron current at the sample. The self-shielding factor cannot be calculated easily or with any real degree of certainty. This consideration is important only if an attempt is made to obtain an absolute intensity.

(e) A principal uncertainty is that the relationship between gamma-ray intensity and line density is not well known.

(f) Each plate may develop differently due to variations in emulsion thickness or simply by being processed in different batches. Hence, each plate must be considered separately from the others, and intensity measurements made on one plate can be related to those on another plate only by common lines which may be obtained under different exposure conditions. This introduces an uncertainty in one set of measurements relative to another.

(g) There are also other uncertainties, though of a less important nature. These arise from uneven development along a single emulsion plate, from the accuracy with which the integrated reflectivity of the bent crystal is known, and from the uncertain amount of gamma self-shielding in the source, related in turn to the pattern of neutron absorption.

5.2 SCANDIUM MEASUREMENTS

The measurements made on scandium were both a reanalysis of the work of Rahman (R1) plus an extension of the energy range that he covered. The sample consisted of 36 grams of Sc_2O_3, doubly encased in aluminum and placed at the center of the 9CH2 port of the M.I.T. reactor, where the flux was estimated as 5×10^{11} n/cm^2-sec. Neglecting self-shielding, this produced a source strength of 102 curies. The principle problem in the measurement of the scandium capture gamma rays was the calibration of the emulsion plate in the range 30 cms to the beta point. Provision was made for calibration with a tantalum source located in the port box, since

the gamma rays from Ta^{182} had been well measured by Muller (M3) by means of a bent crystal spectrometer of the Dumond type.

The first set of plates exposed in this range were badly processed and could not be relied on to give accurate results. This was not realized, due to the long delay between exposure and inspection, as discussed in Section 3.4. When the next set of plates was exposed in this range, it was discovered that the tantalum source had grown too weak to give anything but the 68 kev and 100 kev lines. This meant that only one calibration line (100 kev at 31 cms) could be used in the range nearest to the beta point. The tantalum source could have been removed and reactivated, but this would have been difficult. The difficulties were that the spectrometer would have needed to be raised out of the way in order to remove the plugs in the port box where the tantalum source was located. This would have had to be done in the presence of a 600 mr/hour beam coming from the activated scandium source. The earlier insertion of the fresh tantalum source had proved difficult and had given rise to high dose rates to the operations personnel. Furthermore, removal of the spectrometer would have required unbolting of the crystal blocks, and there was no guarantee that the line-up of crystal and focal plate could be maintained when the blocks were replaced. The decision was made then to make the calibration by means of requiring consistency between the measurements taken on two overlapping plates. One plate ranged from +5 cms to +35 cms away from the beta point, and the other plate straddled the beta point −15 cms to + 15 cms. It was hoped, in addition, that the presence of a cross-over transition would further tie down the energy calibration of the emulsion plates in this range.

The results obtained in this way were not satisfactory. They had an uncertainty four or five times larger than what was obtainable by direct calibration. In addition, no cross-over transition could be found since no lines above 300 kev were observed. It was felt that irradiation at a higher flux level would be beneficial since the ratio of background-to-signal would be smaller. There is a general level of 1 to 2 mr/hour from activated argon in the reactor room, and a shorter irradiation time would reduce its effect. However, irradiation at a higher flux level could not be done at the time. The source geometry needed to be modified, which was impossible with a scandium decay activity of 25 curies. The

scandium oxide was expensive and a new source could not be easily justified. In addition, one week of irradiation of a new source in a high flux port would have allowed the accumulation of 30 more curies of Sc^{46}. Licensing restricted the total activity of any one isotope at M.I.T. to 50 curies. Finally, there was no high flux port at the M.I.T. reactor that was available at the time with sufficient room to operate the instrument. The results obtained by that time, February 1962, were combined with those of Fiebiger (F2).

The scandium source was removed from the 9CH2 port and stored. About a year later, when its decay activity was about 2 curies, it was inserted into the high flux port at which the spectrometer used by Hickson (H1) was located. Exposure was made on a set of emulsion plates straddling the beta point. On this set, a line was identified as annihilation radiation which was an excellent calibration. Furthermore, cross-over transitions were observed and it was thus possible to improve and extend the results quoted earlier. It had not been expected that annihilation radiation would be seen, since scandium had too low an atomic number for significant pair creation by self-absorption of its high-energy gamma rays. The principle mechanism for the source of the annihilation quanta must then have been pair internal conversion, and was significant in this case due to the large proportion of gamma rays with high energy in the decay from the scandium capture state. The probability for pair emission has been illustrated on Page 226 of Reference E1, and simple calculations have been made for the intensity of the annihilation quanta. For scandium, an intensity of 7% per captured neutron could have been expected, and the conclusion was drawn that in the high flux port any normal sample would have been an adequate source of annihilation radiation in itself.

The final measurements of gamma rays from thermal neutron capture by scandium are given in Table 1. Figure 9 illustrates two of the scandium plates. The higher energy one nearest to the beta point shows the significant variation in background along the plate that leads to the difficulty in intensity measurement discussed in Section 5.1.

A strong 31 kev transition was observed on the scandium plates and also the plates exposed to the other sources. Hickson (H1) observed the same transition when using other sources and a different port at the M.I.T. reactor. This transition has been identified as being from the

Table 1. Gamma Rays from Thermal-Neutron Capture by Scandium

Energy, kev	Intensity
52.014 ± 0.008	M
61.788 ± 0.005	W
79.514 ± 0.008	W
88.938 ± 0.011	VW
89.821 ± 0.011	W
142.451 ± 0.029	VVS
146.974 ± 0.032	VVS
181.918 ± 0.067	W
216.39 ± 0.09	VS
227.71 ± 0.10	VVS
228.65 ± 0.10	VS
280.66 ± 0.15	VW
295.39 ± 0.14	VVS
383.74 ± 0.25	VVW?
485.94 ± 0.28	W
539.31 ± 0.29	W
546.55 ± 0.32	VW
554.34 ± 0.30	M
584.60 ± 0.33	M
627.12 ± 0.37	M
775.17 ± 0.74	VVW

Nomenclature for intensity used in Table 1 and elsewhere in this thesis is as follows:

S = Strong
M = Medium
W = Weak
V = Very
? = Questionable

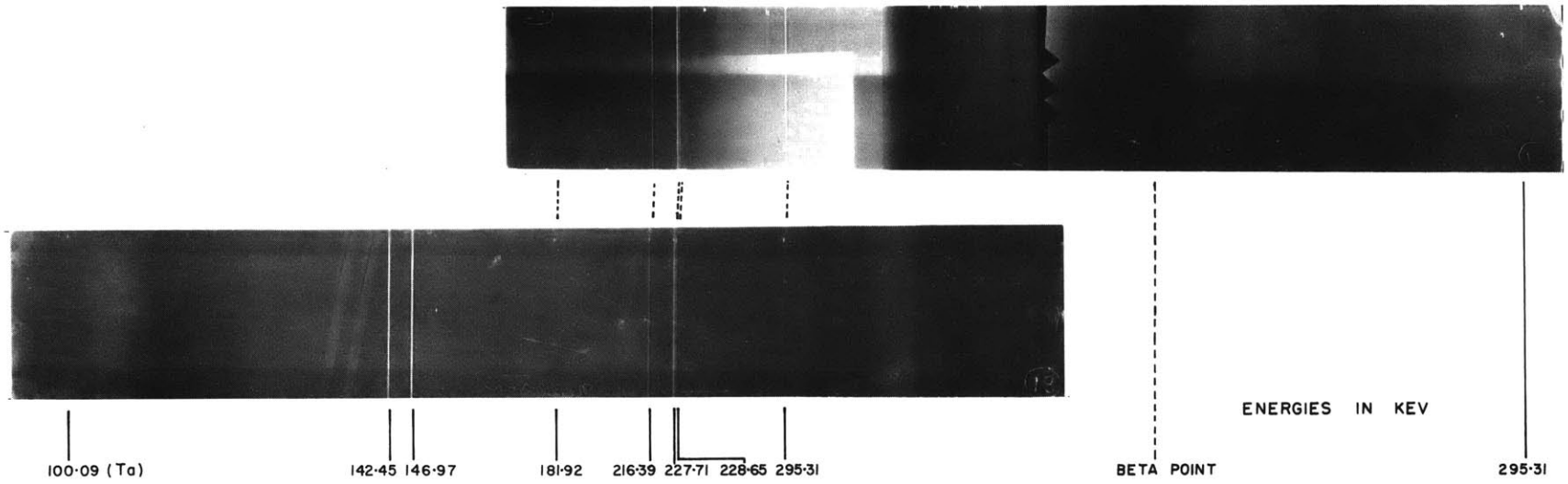

FIG 9. SAMPLE EMULSION PLATES FROM IRRADIATION OF SCANDIUM

decay of the 31 kev level in Al^{28} and a precision measurement can be quoted as 30.6415 ± 0.0020 kev.

In a separate experiment on another six-meter, bent crystal spectrometer away from the reactor, the gamma rays from the decay of Sc^{46} were measured. This spectrometer frame was not very rigid, and the results were suspect because they differed so much from those in the literature. The values measured here are 895.2 ± 2.1 kev and 1129.0 ± 3.7 kev. These can be compared with the measurements of Johansson (J3) and Lindquist (L3), who obtained 892 ± 3 kev and 1118 ± 3 kev, and 885 ± 2 kev and 1119 ± 3 kev, respectively.

5.3 IRIDIUM MEASUREMENTS

The basis for investigating iridium was that a calibration source was required which had intense, well measured gamma rays above 220 kev. The poor calibration of scandium plates had demanded this. A 220 kev gamma ray will just produce a line on both extremals of an emulsion plate straddling the beta point. Iridium comprises 2 isotopes, Ir^{191} and Ir^{193}. The gamma rays from the decay of Ir^{192} have been well measured by Muller (M3), by means of bent crystal spectroscopy. In addition, there are strong transitions in the range 300 to 600 kev. It appeared that it would be useful to look at its neutron-capture gamma rays while this calibration source was being made. In addition, Fiebiger at Brookhaven National Laboratory was investigating capture gamma rays of each iridium isotope by coincidence studies.

A 20.3-gram sample of natural iridium was packed in a doubly-sealed, standard size, aluminum can. The standard can was used because the geometry of the calibration setup, in which it was to be later employed, so required it. If neutron self-shielding factors were neglected, then an activity of 517 curies would have been obtained and this would have manifested itself as a dose rate of at least 120 R/hour at the face of the bent crystal. It was then with some surprise that a maximum dose rate of only 6 R/hour was measured. The discrepancy was put down as being due to large neutron self-shielding and some gamma-ray self-shielding. Consequently, the source was removed and another was put in its place, similar in external geometry to the scandium source. The second iridium source comprised 60.3 grams of iridium mixed with 20.2 grams of powdered

reactor-grade graphite as a dispersive medium. The mixture was packed in a doubly-sealed, aluminum can and it was much larger than the first source.

The second iridium source was placed in the middle of the 9CH2 port of the M.I.T. reactor and the neutron-capture gamma rays were surveyed by the bent crystal spectrometer. The range, 22 kev to 1 Mev, was covered in this way over a period of 3 months. Calibration was obtained internally since the decay gamma rays automatically appeared on the emulsion plates. Annihilation radiation was also observed which improved the energy calibration. The dosage rate at the crystal face was only 19 R/hour so that it was clear that neutron self-shielding was still very large. The results of this survey are given in Table 2.

No isotopic assignment has been made to those gamma rays. It was felt again that irradiation at a higher flux level would have permitted higher-energy gamma rays to be observed, but it was not possible to do this. The iridium was costly so that the manufacture of a fresh source did not seem justifiable. Transfer of the existing large iridium source to a high flux port required machining of a very radioactive component when there were no facilities for remote machining readily available. Furthermore, this same source would have exceeded the residual activity limit of 50 curies if it had been placed in the high flux port for the usual minimum operating period of one week. This minimum operating period arises since the source must be inserted and withdrawn when the reactor is shut down, and, generally, the reactor is operated continuously for about 100 hours. Consequently, no further work has been initiated on the capture gamma rays of iridium. The poor quality in the measurements is shown by comparing Table 2 with the measurements on scandium in Table 1; and it reflects the flux limitation experienced. It reflects also on the difficulty of reading extremely dark plates.

No photograph has been shown of an emulsion plate from exposure to iridium capture gamma rays because the plates were so very dark. The one plate straddling the beta point had five calibration line pairs. The analysis of the plate showed that the positional variation in the beta point from weighted reading errors was 2.5 microns, but the positional error arising from the weighted variation of each pair was 24.3 microns. The conclusion drawn was that there must have been a large random error

Table 2. Gamma Rays from Thermal-Neutron Capture by Iridium

Energy, kev	Intensity	Energy, kev	Intensity
961.16 ± 2.55	VVW?	144.84 ± 0.09	VW
477.56 ± 1.41*	VVW?	136.08 ± 0.09	W
418.30 ± 0.51	VVW?	112.13 ± 0.08	VVW
351.76 ± 0.14	M	107.95 ± 0.08	VW
334.03 ± 0.35	VVW?	94.318 ± 0.054	VVW
278.34 ± 0.35	VVW?	90.648 ± 0.072	VVW?
226.28 ± 0.18	VVW	90.376 ± 0.072	VVW?
218.77 ± 0.17	VVW?	88.724 ± 0.026	W
216.93 ± 0.15	VVW	86.826 ± 0.045	VVW?
214.91 ± 0.30	VVW?	84.257 ± 0.016	M
211.63 ± 0.17	VVW?	77.941 ± 0.008	W
178.90 ± 0.12	VVW	76.047 ± 0.021	VW
169.11 ± 0.12	VVW?	58.844 ± 0.012†	VVW
151.49 ± 0.10	VW	48.058 ± 0.018	VW

*Possible doublet.

†Isomeric decay transition in Ir^{192}.

in the position of each line in addition to the reading error, and this may have been due to emulsion distortion. New values for gamma rays from the decay of Ir^{192} have not been quoted, although they were detected easily up to 605 kev. A precision value of a gamma ray assigned to the decay of Ir^{194} has been measured as 328.72 ± 0.13 kev. This may be compared with the recent value of 328.54 ± 0.04 kev measured by Marklund (M7).

5.4 RHODIUM MEASUREMENTS

Capture gamma rays from rhodium were measured by the bent crystal spectrometer primarily because the nuclear levels in Rh^{104} had been well measured by the (d,p) reaction and it was felt that a precise measurement of the radiative transitions would lead to a good formulation of the nuclear energy level scheme up to 1 Mev. Experience had

shown that for a sample with a high absorption cross section, a better utilization would be obtained if it were mixed with a nonabsorbing spacer material such as carbon. Consequently, rhodium with an absorption cross section of 156 barns was treated as such, and the sample comprised 24.4 grams of rhodium mixed with 70 grams of powdered graphite. The sample was packed in a doubly-sealed, aluminum can of the same design used for scandium and the second iridium sample. It was placed at the center of the 9CH2 port and irradiated for 3 months. The capture gamma rays were surveyed over the range 22 kev to 1 Mev.

During the irradiation, it was discovered that a similar investigation had been recently carried out by Buschhorn (B1), up to 350 kev. It was decided to carry on the experiment to see if the range could be extended. Again, the problem of a limited flux was encountered. The source geometry was therefore changed to permit its insertion into the high flux port. Unfortunately, the Rh^{104} formed by irradiation of natural rhodium decays to Pd^{104} by the emission of high-energy beta rays which are nearly all absorbed in the source itself. These beta rays are almost 100% of a group with a maximum energy of 2.44 Mev so that self-heating was considerable. Hence, the source had to be instrumented with a thermocouple prior to placement in the high flux port. The temperature measurements, though of a dubious nature, indicated excessive temperature levels and so the source was prematurely withdrawn from the reactor. As a consequence, the extension in energy range over Buschhorn's measurements was not considerable since exposure time was so limited. It turned out that this same isotope was simultaneously under investigation by Gruber (G5), using a bent crystal spectrometer of the Dumond geometry, and his range and sensitivity were better. The results then quoted here in Table 3 provide an independent confirmation of some of Gruber's measurements.

Energy calibration of the high-energy region was obtained by means of the annihilation radiation and use of Buschhorn's data (B1). Low-energy calibration was obtained by means of X-ray standards. It had been intended to use decay gamma rays from iridium as calibration initially. This was, in fact, done in the low flux port, but double exposures of lines appeared on the plate. This was put down to a slight movement of the crystal block and interpretation of that emulsion plate was rendered

Table 3. Gamma Rays from Thermal-Neutron Capture by Rhodium.

Energy, kev	Intensity	Energy, kev	Intensity
645.42 ± 0.42	VVW	219.94 ± 0.12	VVW?
556.12 ± 0.31*	W	217.90 ± 0.04	M
538.47 ± 0.28	VW	215.54 ± 0.04	M
447.30 ± 0.19	VVW?	213.08 ± 0.04	VW
440.59 ± 0.17	W	202.96 ± 0.04	VW
427.70 ± 0.21	VW	200.92 ± 0.05	VVW
420.89 ± 0.15	W	196.17 ± 0.06	VVW?
385.25 ± 0.13	VVW	185.97 ± 0.04	VW
374.98 ± 0.13	W	180.85 ± 0.03	S
371.10 ± 0.14	VVW?	178.84 ± 0.03	W
356.87 ± 0.13	VVW?	177.77 ± 0.04	VW
353.21 ± 0.12	VVW	169.42 ± 0.03	VW
333.55 ± 0.09	M	168.36 ± 0.06	VVW
323.88 ± 0.09	W	161.39 ± 0.06	VW
317.18 ± 0.08	VW	157.04 ± 0.03	VW
305.99 ± 0.08	VW	135.22 ± 0.03	W
303.69 ± 0.08	VVW	134.602 ± 0.022	S
290.25 ± 0.10	VVW?	127.317 ± 0.020	S
288.63 ± 0.10	VVW?	118.212 ± 0.018	VVW
286.18 ± 0.08	VVW	100.804 ± 0.017	M
273.54 ± 0.07	W	97.104 ± 0.016	VS
269.22 ± 0.06	W	51.421 ± 0.008	W
266.71 ± 0.06	M	45.292 ± 0.010	VVW
261.53 ± 0.06	VW		

*From a level in Pd^{104}.

difficult. It did, however, provide interesting information about emulsion shrinkage along the plate by comparison of the separation distance between the double exposures of a single line. These results are given in Table 4.

Table 4. Separation of Double Exposures on the Rhodium Emulsion Plate No. 44.

Relative Position	cms	cms	cms	cms
Weak exposure	1.7174	11.5212	15.9328	17.1119
Strong exposure	1.3951	11.2113	15.6181	16.7971
Separation	0.3223 ±0.0021	0.3099 ±0.0014	0.3147 ±0.0008	0.3148 ±0.0010
Mean separation	0.3154 ± 0.0026 cms			

There did not appear to be any correlation between the separation distances and position on the plate. The variation of the separation was larger than the reading errors and could be due to emulsion distortion. The plate with the double exposures was neglected and its range was not repeated because Buschhorn had covered it adequately. This explains the absence in Table 3 of measurements between 52 and 97 kev.

CHAPTER 6
MEASUREMENTS MADE ON THE SCINTILLATION PAIR SPECTROMETER

6.1 TWOFOLD MEASUREMENTS

A series of runs was made, using the apparatus at Brookhaven National Laboratory, simply as two crystals in coincidence (see Fig. 6), and measuring their coincident outputs on the two-parameter analyzer. This was termed a twofold run. The purpose of these runs was to attempt to determine predominant low energy coincidences independently of using the system in the typical fourfold arrangement. Furthermore, when two strong gamma rays of the same energy are in coincidence, the twofold arrangement indicates this fact without any confusion. The isotopes studied in this way were Sc^{45}, Rh^{103}, Dy^{161}, Dy^{164} and Ho^{165}.

The different mode of operating the apparatus from that described in Appendix IV is noted here. The central crystal whose dimensions were 1-1/2" in diameter × 3" deep was felt to be too long, and it was believed that a higher photo-fraction could be achieved with a smaller crystal. A 1-1/2"-diameter × 1-1/2"-long crystal was put in its place. The discriminator bias on the B coincidence circuit was reduced nearly to zero and the coincidence units were set to demand fast coincidences only of the A and B crystals. Both crystals were stabilized with external sources, Mn^{54} on the 3" × 3" A crystal and Cs^{137} on the 1-1/2" × 1-1/2" B crystal. Calibration of each crystal was made by means of external sources, and also by self-calibration from the samples whose coincident gamma rays were to be determined. The energy range encompassed 0 to 890 kev with the B crystal and 0 to 1620 kev with the A crystal. Each run took about 5 or 6 hours, a time limit reached when the counts in any one channel exceeded the memory of the analyzer. The live time reading on the analyzer was recorded on each run. The maximum delay was then inserted into the coincidence circuit; the analyzer was switched to the subtract mode and the accidentals were directly subtracted for a duration equal to the corresponding live time.

The printed output of the analyzer was punched onto cards and was plotted by the IBM 7090 computer. The output was "singularized" (see Appendix III), and examination of this data indicated the coincidences listed in Tables 5 to 9. In general, no coincidence has been listed unless it was seen by both crystals in both directions. The capture gamma-ray spectra of the isotopes, as seen by the smaller crystal with no coincidence requirements, are shown in Figs. 10 to 14. The photopeak from the Cs^{137} stabilizing source is to be seen on each figure.

The coincidence of back-to-back annihilation quanta was observed in each run, but it has been excluded from Tables 5 to 9. Interpretation of the data in these tables has not been easy, since the coincidences need not have been all from prompt capture but could have been gamma-ray coincidences following beta decay. In addition, the coincidence of a gamma ray and either a lead X ray or an X ray from the source itself further complicated the interpretation. Finally, the output of the analyzer was not "clean" enough to permit calculation of relative intensities.

Table 5. Low Energy Gamma-Ray Coincidences from Irradiated Sc^{45}

Energies of Coincident Gamma Rays, kev		Probability
294 ± 5	143 ± 5	Definite
549 ± 17	227 ± 7	Definite
208 ± 8	224 ± 7	Definite
841 ± 18	222 ± 7	Probable
350 ± 13	448 ± 15	Possible
396 ± 16	231 ± 11	Possible
118 ± 13	100 ± 7	Possible
440 ± 20	184 ± 8	Possible

Table 6. Low Energy Gamma-Ray Coincidences from Irradiated Rh^{103}

Energies of Coincident Gamma Rays, kev		Probability
634 ± 20	179 ± 7	Definite
92 ± 7	320 ± 20	Probable
177 ± 13	176 ± 6	Probable
174 ± 9	335 ± 16	Probable
441 ± 24	92 ± 10	Possible
174 ± 7	276 ± 20	Possible

Table 7. Low Energy Gamma-Ray Coincidences from Irradiated Dy^{161}

Energies of Coincident Gamma Rays, kev		Probability
185 ± 7	283 ± 8	Probable
76 ± 4	819 ± 14	Possible
307 ± 8	336 ± 10	Possible
200 ± 6	604 ± 15	Possible
385 ± 13	438 ± 13	Possible

Table 8. Low Energy Gamma-Ray Coincidences from Irradiated Dy^{164}

Energies of Coincident Gamma Rays, kev		Probability
181 ± 5	380 ± 10	Definite
74 ± 5	101 ± 8	Probable
182 ± 8	1100 ± 30	Possible

Table 9. Low Energy Gamma-Ray Coincidences from Irradiated Ho^{165}

Energies of Coincident Gamma Rays, kev		Probability
170 ± 7	234 ± 7	Definite
181 ± 6	450 ± 15	Probable
633 ± 12	191 ± 11	Probable
178 ± 8	320 ± 11	Probable

6.2 PAIR MEASUREMENTS

Pair measurements were made, using the scintillation pair spectrometer at Brookhaven, for the following reasons:

(a) To make isotopic assignments to high energy gamma rays that had been measured elsewhere more precisely in the irradiation of the natural element.

(b) To determine high energy gamma rays where the statistics of this instrument were better than those of instruments with higher resolution.

(c) To provide data for determining the response function of the system and for checking the feasibility of calculating the line spectra by the computational methods discussed in Appendix II.

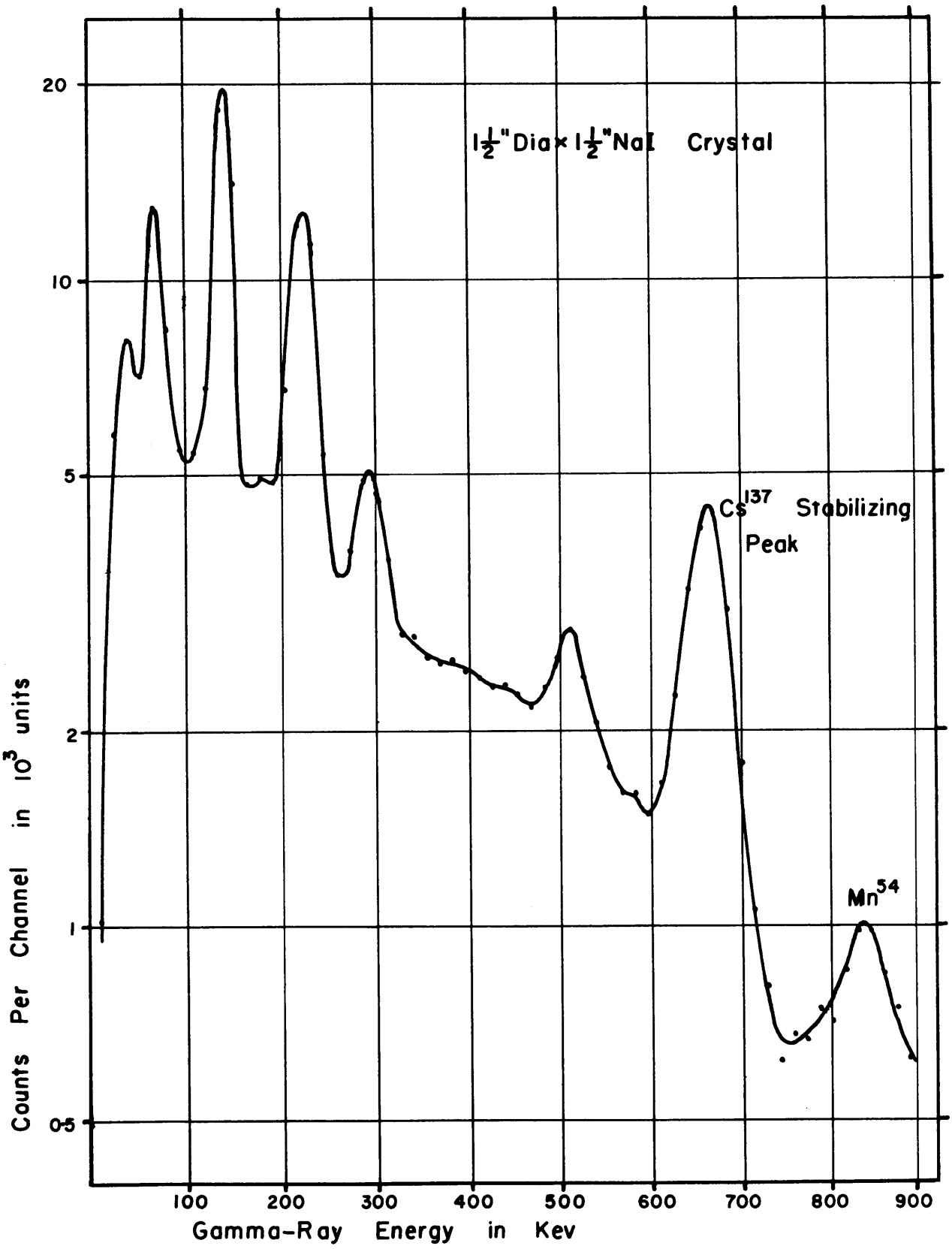

FIG 10. CAPTURE GAMMA-RAY SPECTRUM OF Sc^{45}

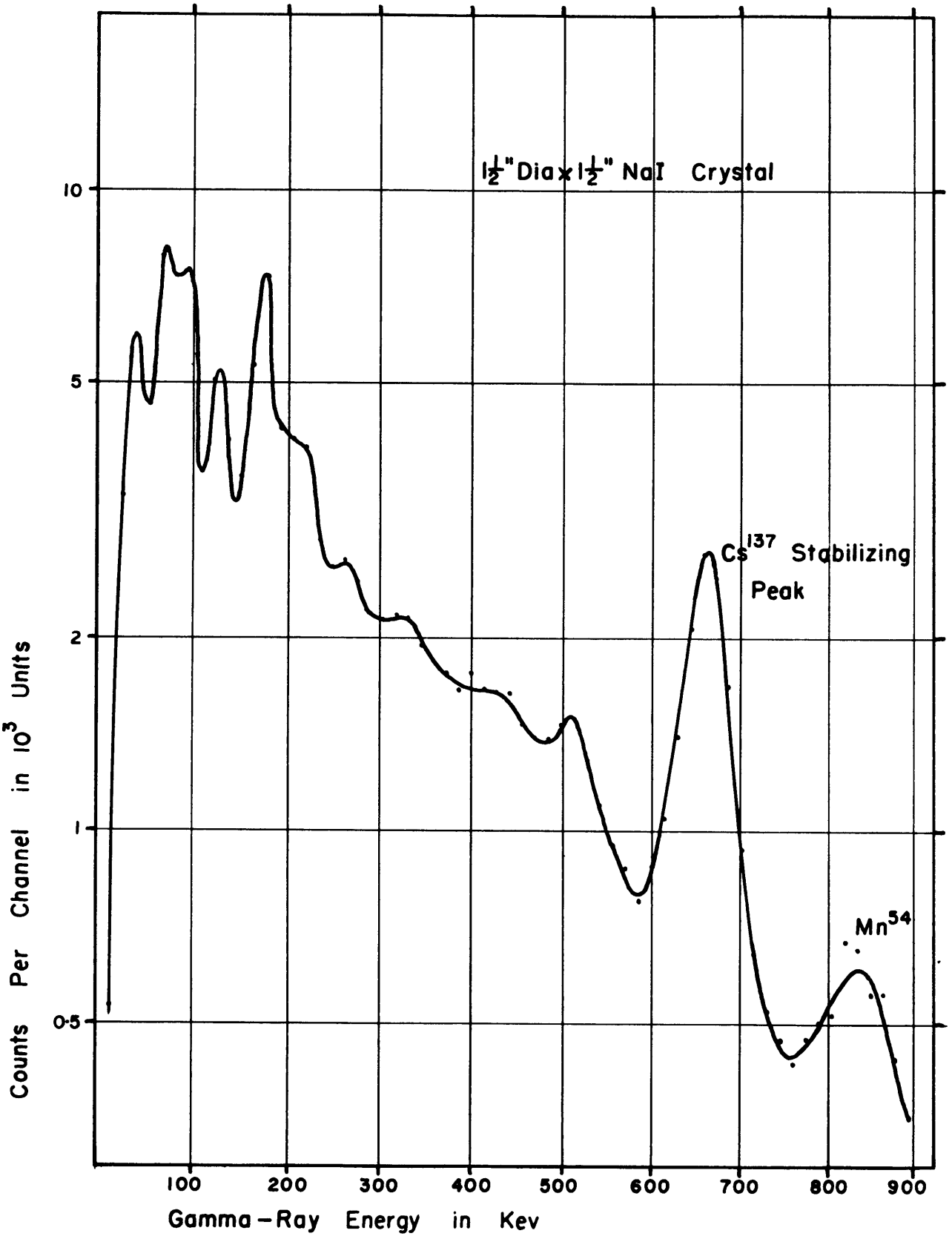

FIG 11. CAPTURE GAMMA-RAY SPECTRUM OF Rh^{103}

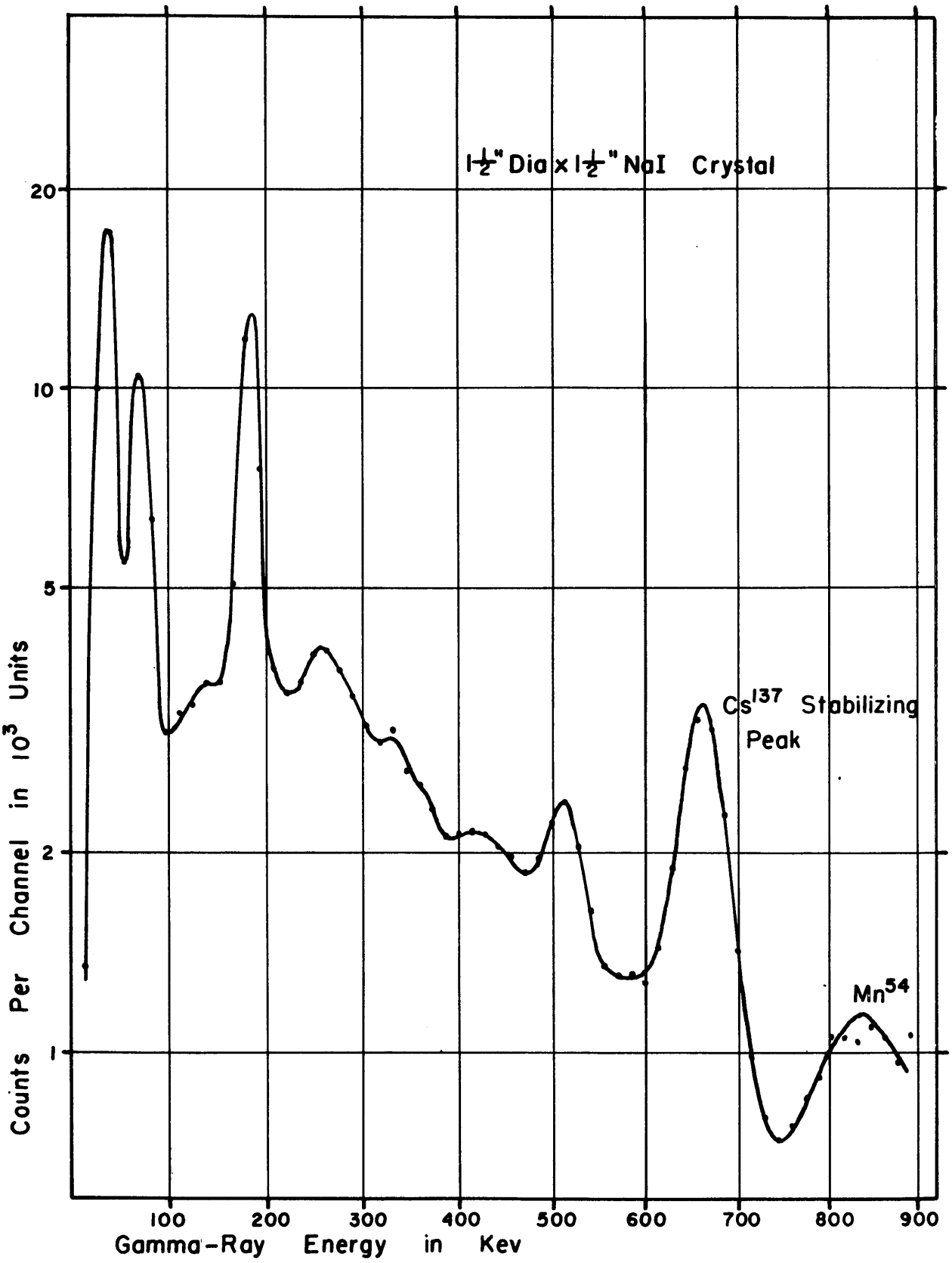

FIG 12. CAPTURE GAMMA-RAY SPECTRUM OF Dy^{161}

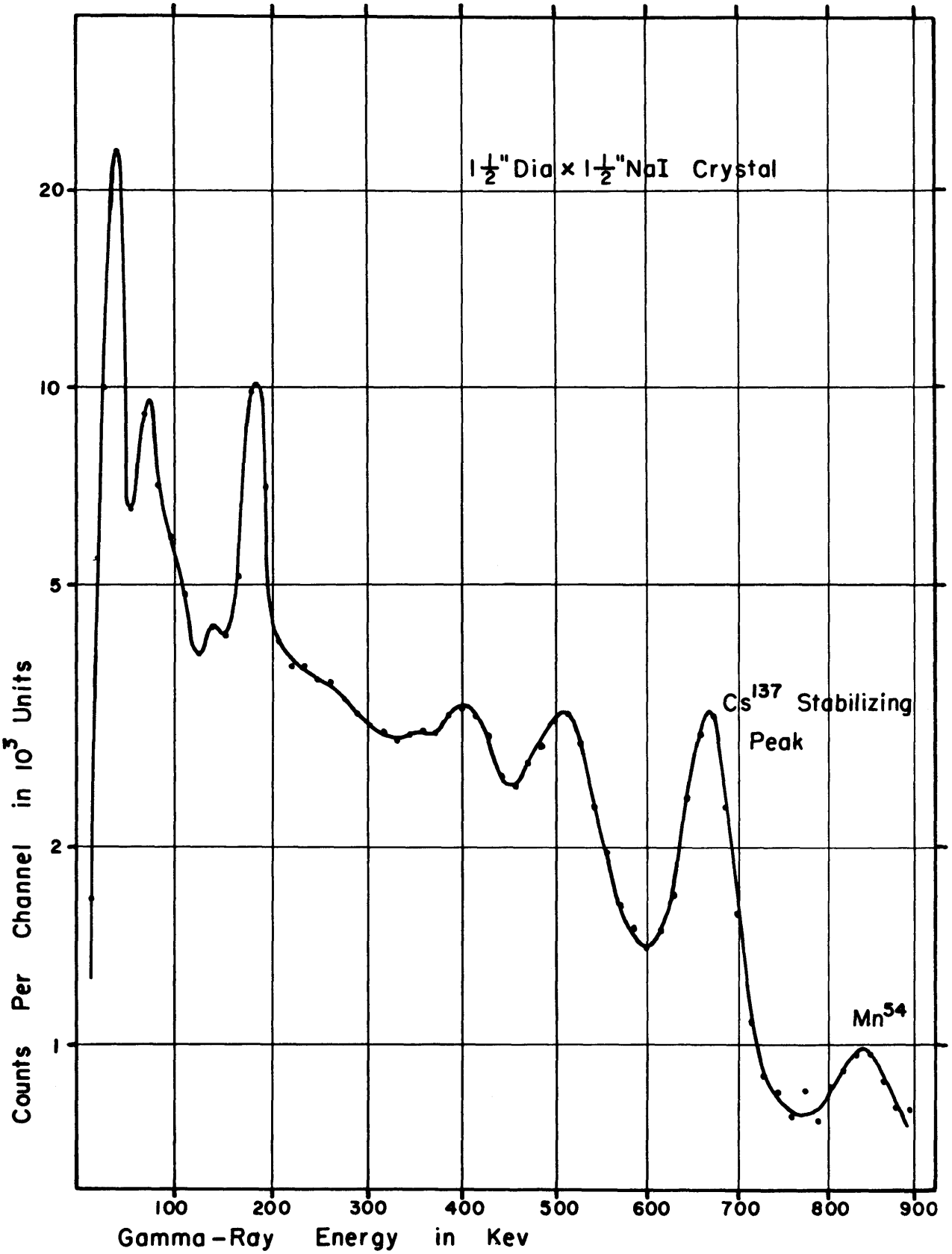

FIG 13. CAPTURE GAMMA — RAY SPECTRUM OF Dy^{164}

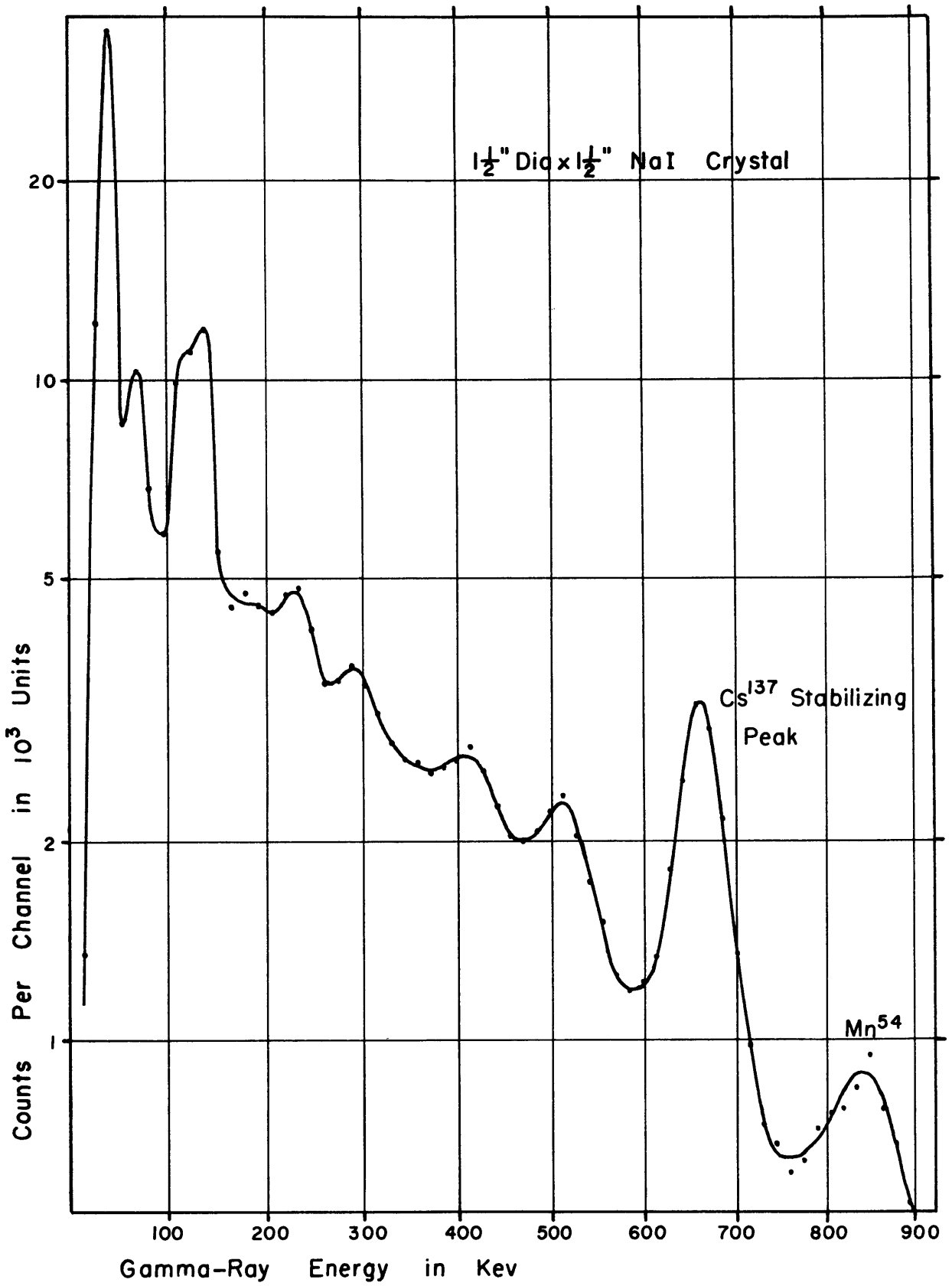

FIG 14. CAPTURE GAMMA-RAY SPECTRUM OF Ho^{165}

The spectrometer was operated without requiring any coincidences in the A crystal. In order to improve the resolution, the normal 1-1/2" × 3" B crystal of the pair spectrometer was raised up by about 1" from the close position used for the fourfold coincidence work. The final collimator was selected to keep the total count rate in the B crystal below 600,000 counts/min. In addition, the width of the single channel analyzers, that were used on the two side crystals, was reduced from the usual 30% to about 20%, to further improve the resolution of the system. Stabilization of the central crystal was achieved by means of an external Mn^{54} source. The output of the pair spectrometer was fed to an RIDL 400 channel analyzer. Calibration of the system was achieved by using capture gamma rays from iron, which have been well measured. It was hoped that the stabilization would maintain the energy calibration over the series of runs though a check was made at the end. Each run took about 40 hours to obtain good statistics on predominant peaks. Typical pair count rates under these conditions were 300 counts/min.

Figure 15 shows the measured spectrum from natural iron. Also shown on Fig. 15, displaced from the measured curve, is a calculated spectrum. This latter curve was obtained by adjustment of constants in the functional dependence of the response, and then by multiplying this response by the input line spectrum and the efficiency. The line spectrum of iron was derived from measurements made by both Kinsey (K3) and Ad'yasevich (A1). In general, Kinsey energy values were used where they were more accurate than those of Ad'yasevich, but the relative intensity values of the latter were used with three exceptions since they seemed to be more consistent. The three exceptions were the intensities of the 8.872 Mev, 7.639 Mev and 7.285 Mev gamma rays, and the set of intensities, therefore, has been renormalized. The set of gamma rays used then as the line spectrum of iron is listed in Table 10.

The comparison between the measured and calculated spectrum, as shown in Fig. 15, seemed quite good and provided reasonable confidence in the estimation of the response function over the energy range. Figure 16 shows the estimated response of the system to absorbed monoenergetic line gamma rays of 2, 4, 6 and 9 Mev. Figure 17 shows

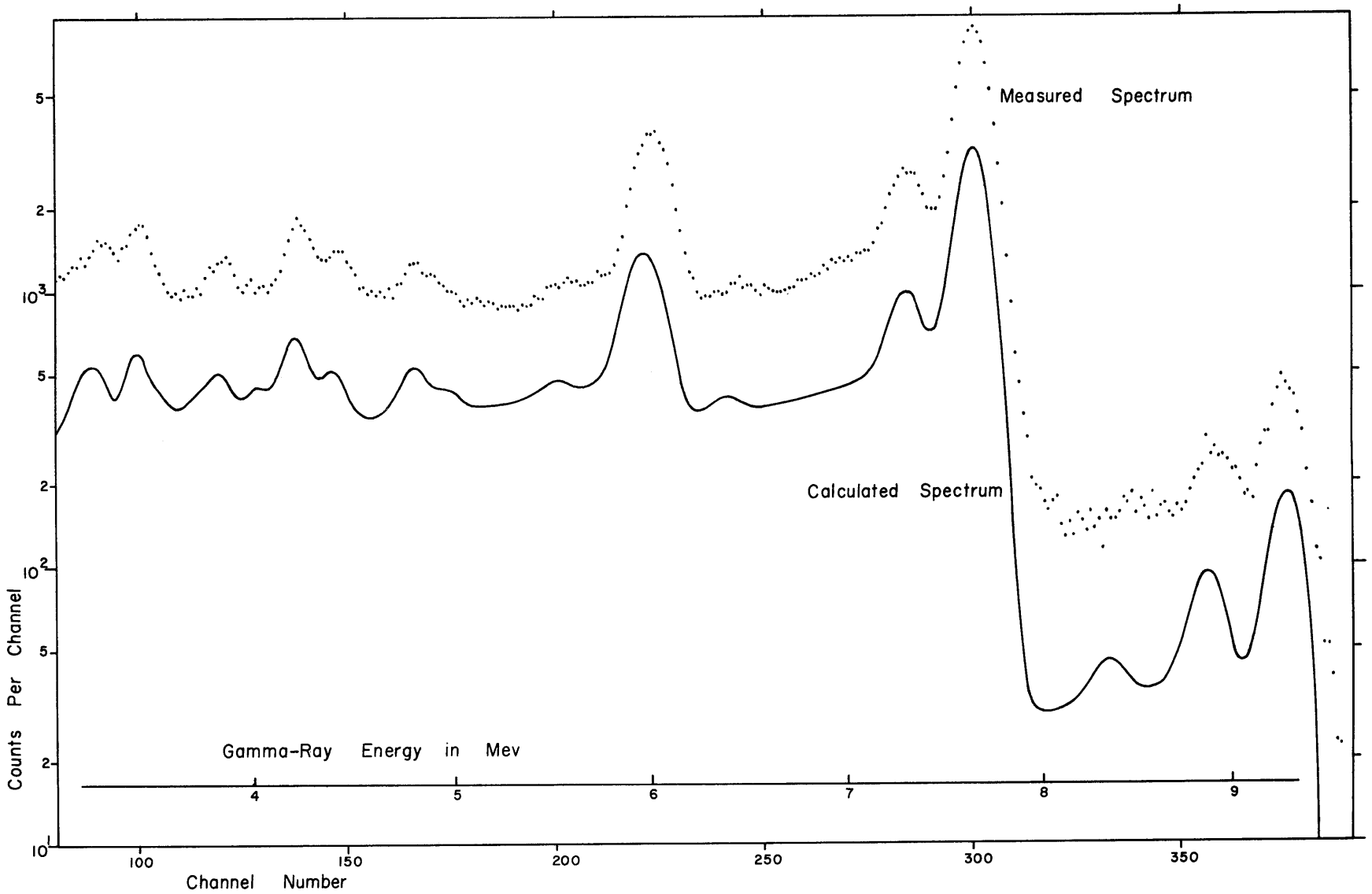

FIG 15. MEASURED AND CALCULATED PAIR SPECTRA FROM IRRADIATED IRON

Table 10. Modified Line Spectrum of High Energy Gamma Rays from Irradiated Iron.

Energy (Mev)	Intensity (Number/100 Neutrons Captured)
9.298	2.4
8.872	0.8
8.345	0.2
7.639	38.6
7.285	6.5
6.369	0.6
6.015	7.0
5.914	7.7
5.51	0.5
4.908	0.8
4.805	1.8
4.405	1.9
4.220	3.8
4.03	1.2
3.844	2.0
3.72	1.0
3.55	1.2
3.43	3.9
3.24	2.6
3.15	1.8
2.84	1.8
2.73	2.6
2.67	0.9
2.143	1.2
1.80	2.0
1.72	5.6
1.626	5.4
1.530	1.7
1.236	1.3

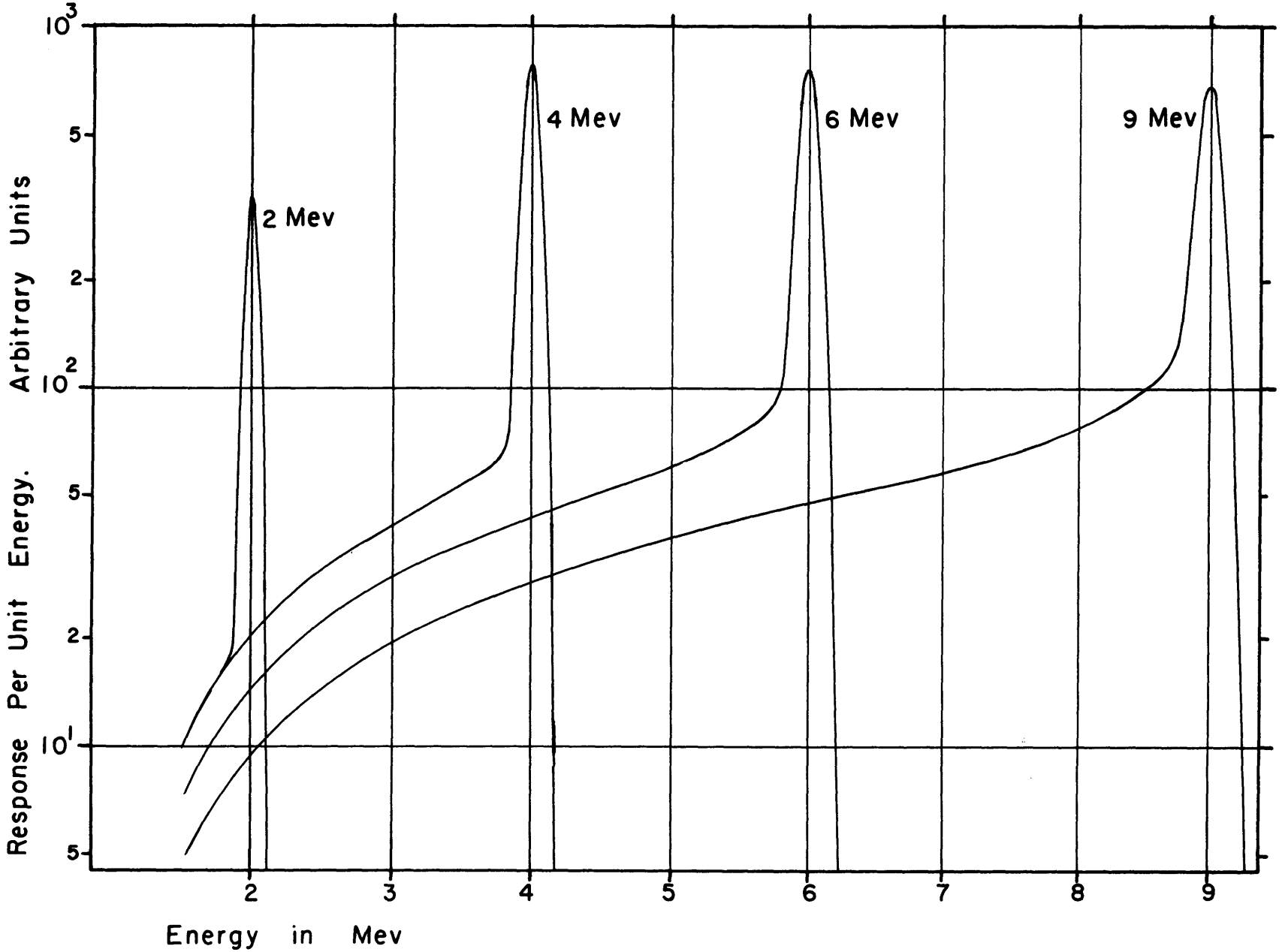

FIG 16. CALCULATED RESPONSE OF THE SCINTILLATION PAIR SPECTROMETER

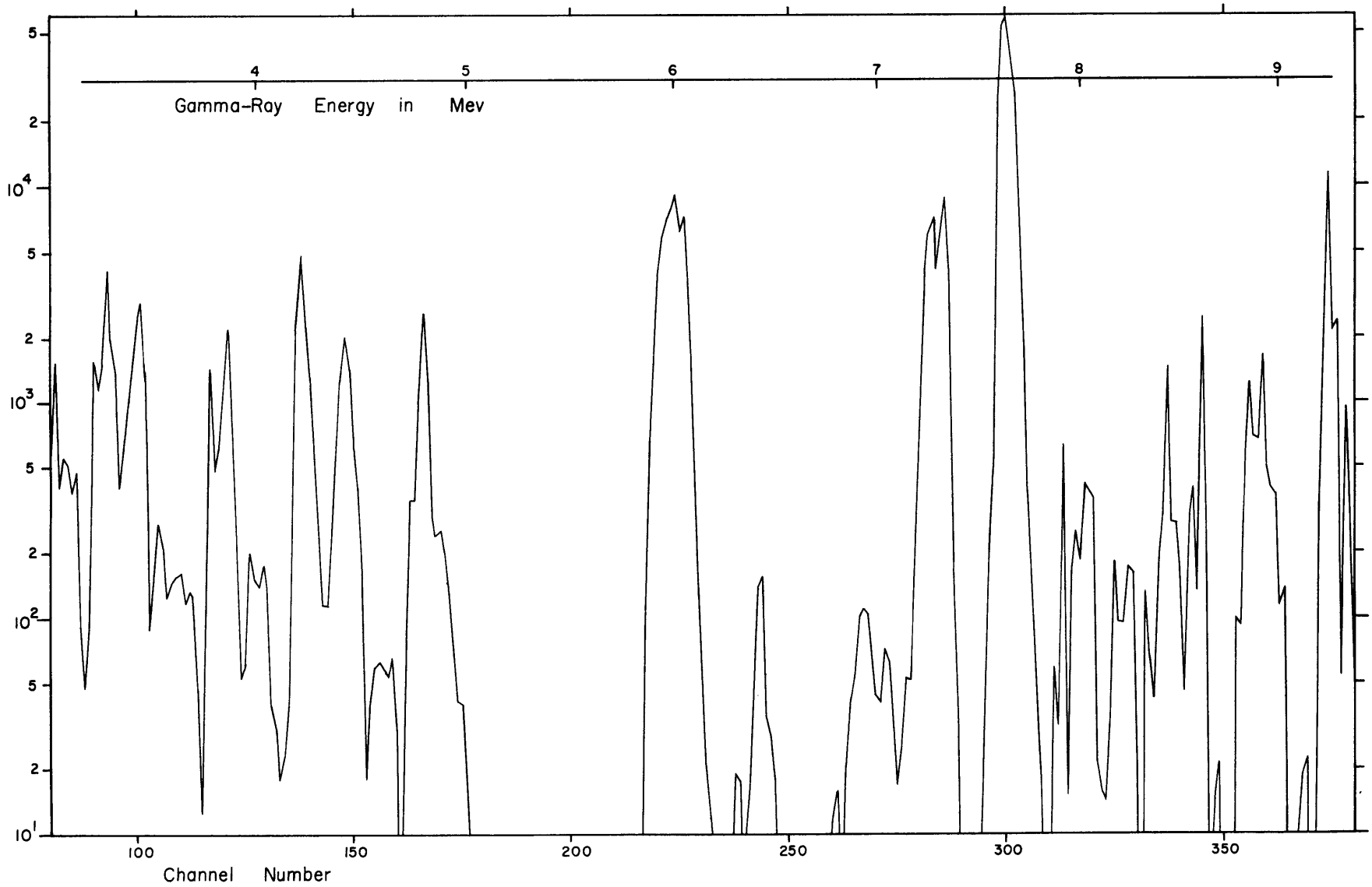

FIG 17. CALCULATED LINE SPECTRUM OF GAMMA RAYS FROM IRRADIATED IRON

an estimation of the line spectrum of iron calculated from the measured spectrum by the methods described in Appendix II and using the response function already obtained. Line gamma rays were not obtained, but the grouping was good enough to show the predominant features listed by Ad'yasevich with the exception of the separation of the doublet at 6 Mev and a gamma ray at 8.345 Mev. There were some gamma-ray groups of low intensity and high energy that were not accounted for. Their energy and magnitude were not reproducible, so they are not tabulated here.

Figure 18 shows the measured spectrum of holmium, using a sample consisting of about 1 gram of Ho_2O_3 in a large gelatin capsule. The spectrum has greatly improved statistics over that measured by Groshev (G2). Despite the poorer resolution, some added features are indicated which are interpreted as monoenergetic gamma rays or predominant groups of gamma rays. The energies of these gamma rays are given in Table 11. These gamma rays are not well resolved and therefore no intensities are given.

Table 11. High Energy Neutron Capture Gamma Rays of Ho^{165}.

Measured Here	Measured by Groshev (G2)	
Energy, Mev	Energy, Mev	Intensity**
6.073 ± 0.022	6.07 ± 0.03	0.4
5.853 ± 0.031		
5.805 ± 0.030	5.79 ± 0.02	1.2
5.554 ± 0.038	5.57 ± 0.03	0.5
5.445 ± 0.036		
5.164 ± 0.026	5.13 ± 0.03	0.8
5.073 ± 0.036		
4.866 ± 0.026		

**Intensity is quoted as gamma rays/100 neutrons captured.

An attempt was made to resolve the complex spectrum of Fig. 18 into monoenergetic gamma rays, using the procedure of Appendix II. It was not possible to resolve the spectrum below 4.5 Mev, and the resolvable components above that energy were not reproducible from a second

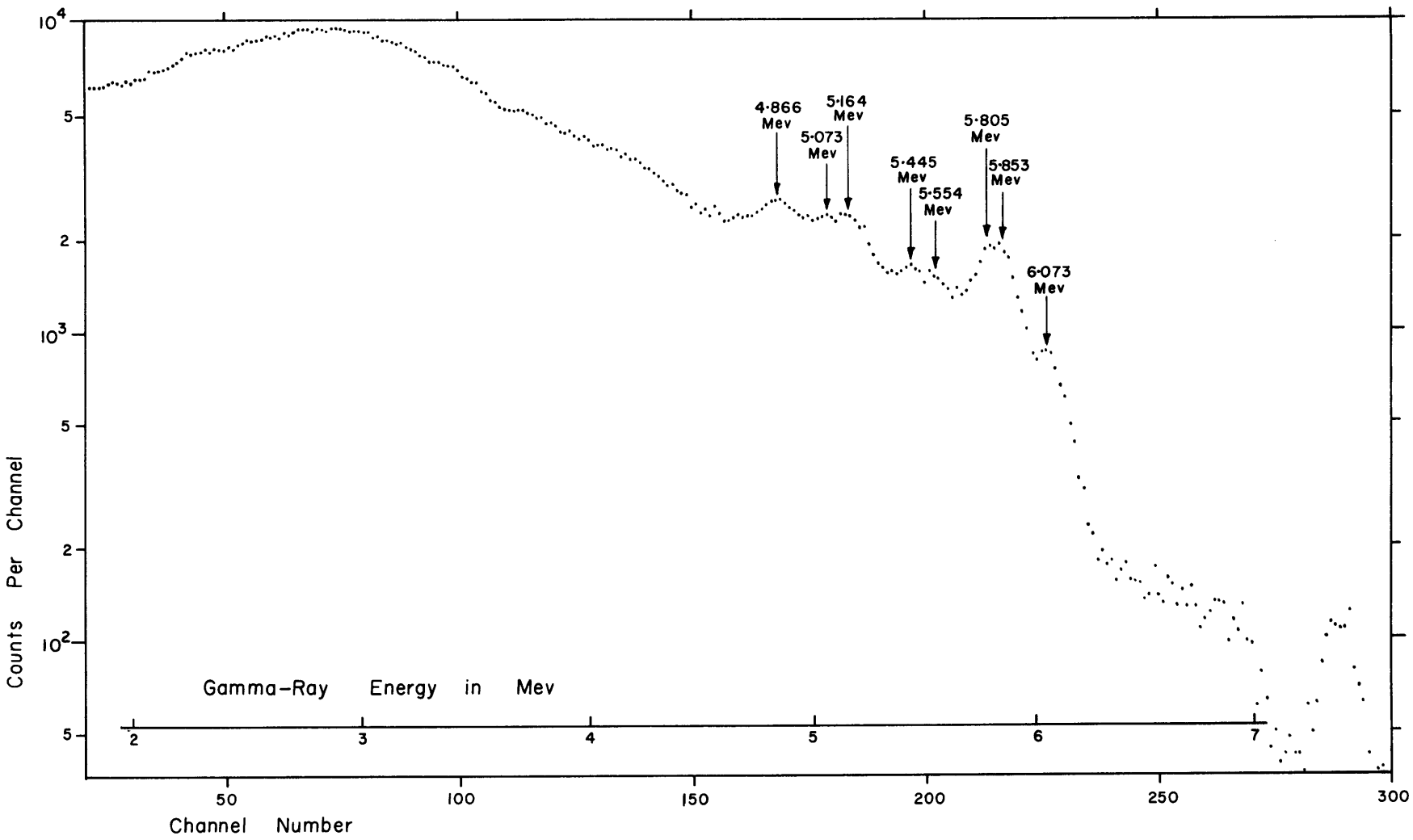

FIG 18. PAIR SPECTRUM OF IRRADIATED Ho^{165}

measured spectrum of holmium. The failure of the computational methods to resolve even the high energy part of the spectrum was believed to come from two things. One was that the response function needed to be known better than it was; the other was that the calculational method used was not quick enough and comparisons were made only with an intermediate answer. It was felt that a quicker approach should be found, which would provide a line spectrum that gave a fit which was better in the mathematical sense, such as a least squares fit. It should be added that the holmium capture gamma-ray spectrum was a difficult case with few prominent resolvable peaks.

Figure 19 shows the measured capture gamma-ray spectrum of Dy^{161} from a sample comprising about 100 mg of $Dy_2^{161}O_3$ in a small gelatin capsule. The isotopic purity of the sample is given in Table 12, together with absorption cross sections measured by House (H1).

Table 12. Isotopic Purity of Dy^{161} Sample and Dysprosium Isotopic Cross Sections.

Atomic Weight	Atom %	σ_a Barns	% Absorption in Sample
156	0.1	–	–
158	0.1	–	–
160	0.59	(130 ?)	0.1
161	90.0	580	94.9
162	7.75	140	2.0
163	1.10	120	0.2
164	0.56	2750	2.8

Gamma rays or predominant groups can be picked out from Fig. 19 and are listed in Table 13, though without specifying intensity. A tentative identification of each gamma ray is made wherever possible. It was believed that the 2.8% absorption by Dy^{164} in the sample gave rise to two of the resolvable high energy components in the spectrum.

Figure 20 shows the measured spectrum from Dy^{164}, using a sample comprising about 100 mg of $Dy_2^{164}O_3$ in a small gelatin capsule. The isotopic purity of the sample is given in Table 14. Figure 20 shows

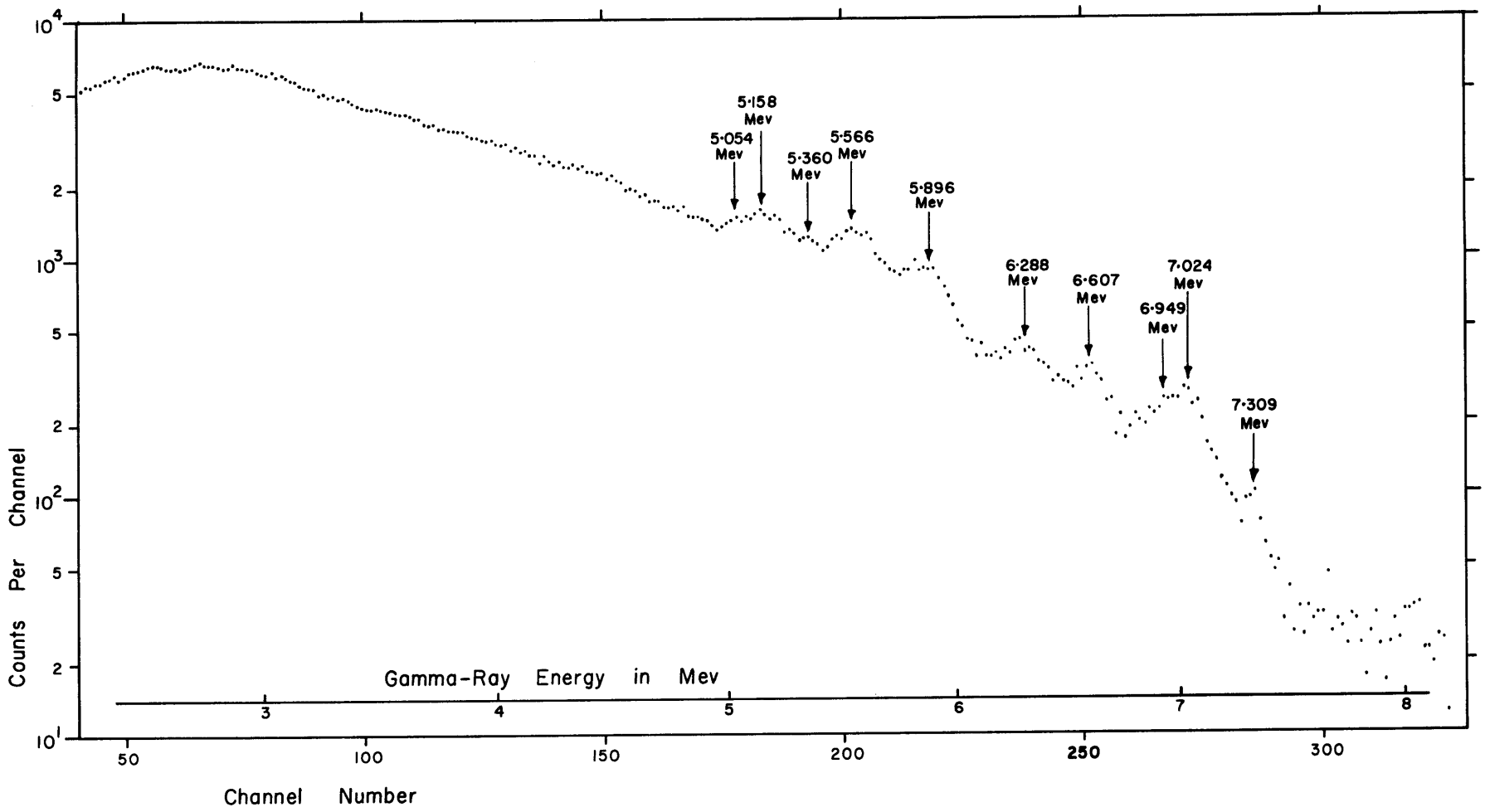

FIG 19. PAIR SPECTRUM OF IRRADIATED Dy^{161}

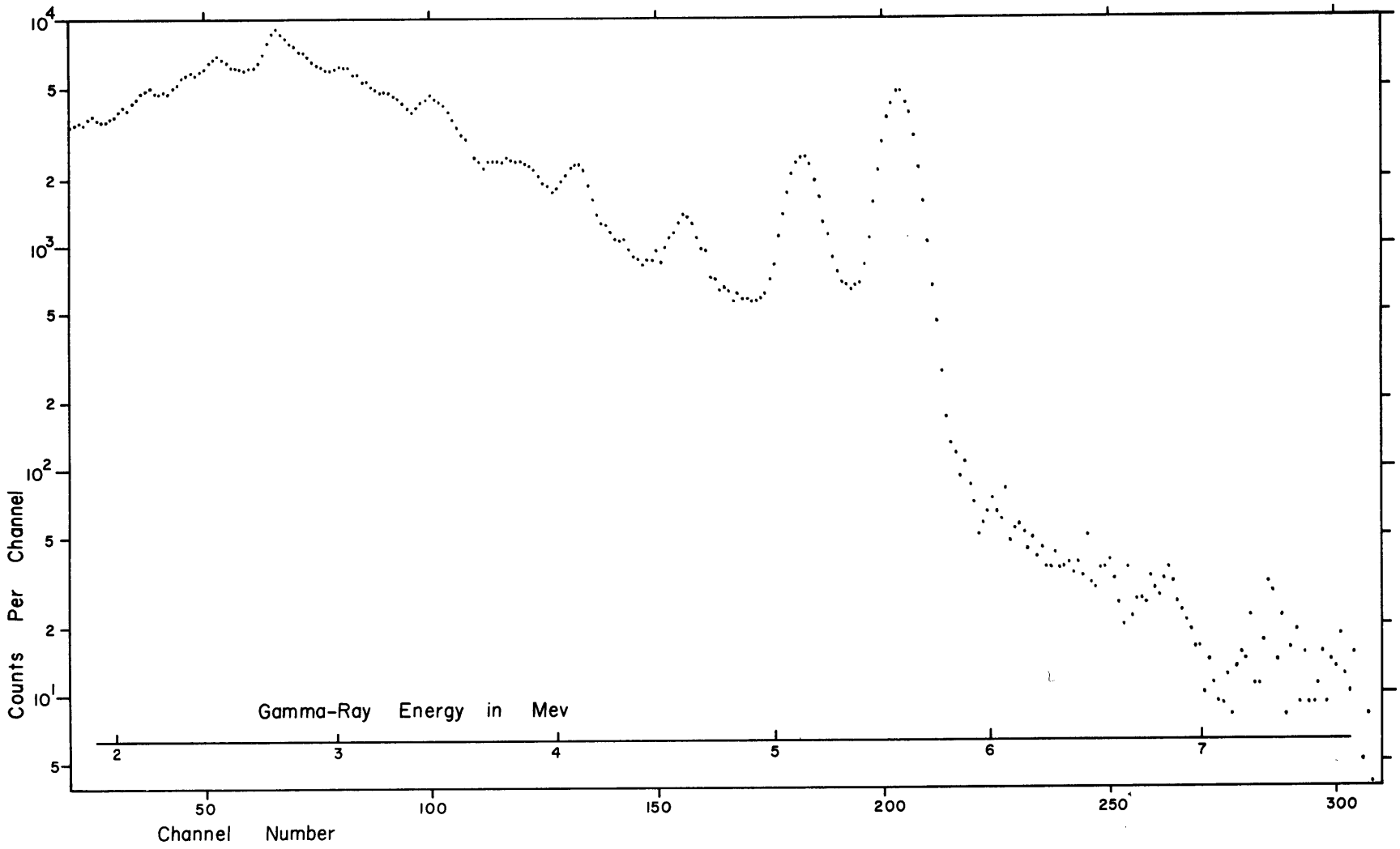

FIG 20. PAIR SPECTRUM OF IRRADIATED Dy^{164}

Table 13. High Energy Neutron Capture Gamma Rays from Dy^{161} Sample.

Energy of Gamma Ray, Mev	Isotope	Energy, Mev	Reference
7.309 ± 0.034	Pb^{208}	7.380	K4
7.024 ± 0.033	Dy^{162}		
6.949 ± 0.046	Dy^{162}		
6.607 ± 0.035	Dy^{162}		
6.288 ± 0.031	Dy^{162}		
5.896 ± 0.032	Dy^{162}	5.876 doublet	M1
5.566 ± 0.026	Dy^{165}	5.598 doublet	M1
5.360 ± 0.029	Dy^{162}		
5.158 ± 0.029	Dy^{165}	5.147 triplet	M1
5.054 ± 0.037	Dy^{162}		

Table 14. Isotopic Purity of Dy^{164} Sample

Atomic Weight	Atom %	% Absorption
156	0.02	-
158	0.02	-
160	0.02	-
161	0.40	-
162	1.34	-
163	5.55	0.2
164	92.71	99.8

the same features indicated by Groshev (G1). One important point to be noticed is that the strong 4.954 Mev gamma ray shown by Motz (M1) cannot be assigned to a transition in Dy^{164}. The high energy end of this isotope was reasonably well resolved and so seemed to be suitable for a fourfold run on the pair spectrometer.

Figure 21 shows the measured pair spectrum from natural dysprosium. On the same figure are placed part of the calculated spectra of natural dysprosium, using the data of Motz with and without the 4.954 Mev transition. The calculated spectra were obtained by knowledge of the incident line spectrum of gamma rays, the efficiency of the system,

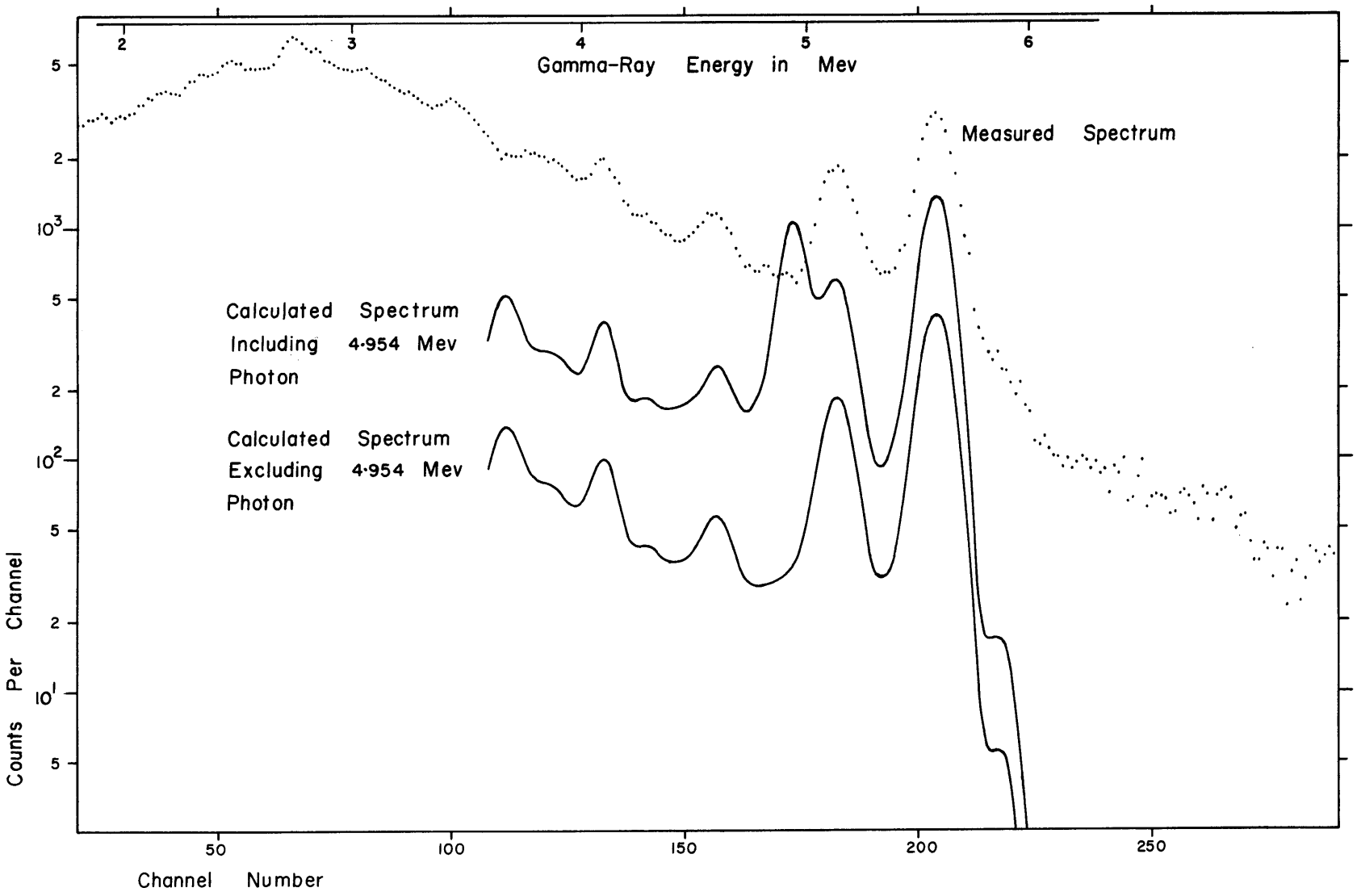

FIG 21. MEASURED AND CALCULATED PAIR SPECTRA FROM IRRADIATED NATURAL DYSPROSIUM

the energy calibration and the response function. The agreement between the measured spectrum and the spectrum calculated with no 4.954 Mev gamma ray was good. The conclusion was drawn that this gamma ray was from an impurity, probably carbon, since $C^{12}(n,\gamma)C^{13}$ had a strong 4.95 Mev transition, according to Groshev (G1).

6.3 FOURFOLD MEASUREMENTS OF Dy^{164}

Two runs were made on the same Dy^{164} sample described in the previous section. The operation and setup were the typical arrangement described in Chapter 4 and Appendix IV. In both cases, both crystals were stabilized by means of external Mn^{54} sources. The range on the scintillation pair spectrometer was about 4.0 to 6.0 Mev in both cases. The range of the fourth crystal was 0 to 2.3 Mev for run E10 and was 0 to 1.1 Mev for run E27. The second run was made because the first one, E10, indicated that the predominant low energy coincident gamma rays were below 1.1 Mev. However, E27 run was limited by the remaining time available during a reactor operating period and had poor statistics. The results are quoted in Table 15 as combined from these two runs.

It was unfortunate that the low energy calibration was poor: no external sources under 0.51 Mev were available and self-calibration was necessary with the data of Hickson (H1). None of the values quoted in Table 15 were clearly resolved and interpretation was thereby rendered difficult. Some examples of the information gathered are given in Figs. 22 and 23. Figure 22 shows the normal pair spectrum and also the pair spectrum when a coincidence was required in the fourth crystal. Easily noticeable is the disappearance of the 5.58 Mev gamma-ray group in the coincidence case, implying transitions to either the ground state or a state with a measurable lifetime, or to a state which de-excites almost completely by internal conversion. Figure 23 shows the spectra in the X channels (fourth crystal) for alternate Y channels (pair spectrometer), and the difficulty in quoting clearly resolved coincidences can be understood. Again, due to this difficulty, no intensities are given.

Table 15. High Energy - Low Energy Gamma-Ray Coincidences from Irradiated Dy^{164}.

High energy gamma ray	Coincident low energy gamma rays in kev, and remarks.
5.58 Mev	Essentially no coincidences. The small 170 and 50 kev peaks are probably from the spread of the 5.15 Mev primary gamma ray.
5.15 Mev	Broad definite peak whose half width extends from 330 to 540 kev. Definite peak of 170 kev, slightly broad, which seems to shift up slightly as primary gamma-ray energy is reduced. Small 50 kev peak.
4.62 Mev	Broad definite peak whose half width extends from 434 to 594 kev. Two possible smeared peaks of 131 and 192 kev. Possible peaks at 271 and 358 kev. Probable peak at 615 kev.
4.10 Mev	Definite broad peak at 185 kev. Broad definite peak whose half width extends from 420 to 560 kev. Definite 1450 kev peak. Broad definite peak comprising perhaps two gamma rays of energies 968 and 1068 kev. Possible peaks at 754 and 1153 kev. Small peak at 1640 kev, but this builds up as the energy of the primary gamma ray is reduced.
3.88 Mev	This primary gamma ray is almost off the Y scale, and coincidences are not well defined. Definite 180 kev peak. Broad definite peak whose center is at about 480 kev. Unresolved coincidences up to a resolved definite peak at 1630 kev.

The results are not tabulated in a normal coincidence table because it is desirable to present as many as possible of the nuances in the data.

6.4 FOURFOLD MEASUREMENTS OF Ho^{165}

Two runs were made on the same Ho^{165} sample described in Section 6.2, and using the typical arrangement described in Chapter 4. In the first run, No. A10, the fourth crystal used was the 3" × 3" unit, and it was stabilized with an external Mn^{54} source and was allowed to range from 0 to 2.1 Mev. The singles count rate of this crystal was 2.70×10^6/min, while a fourfold coincidence count rate of 28/min was

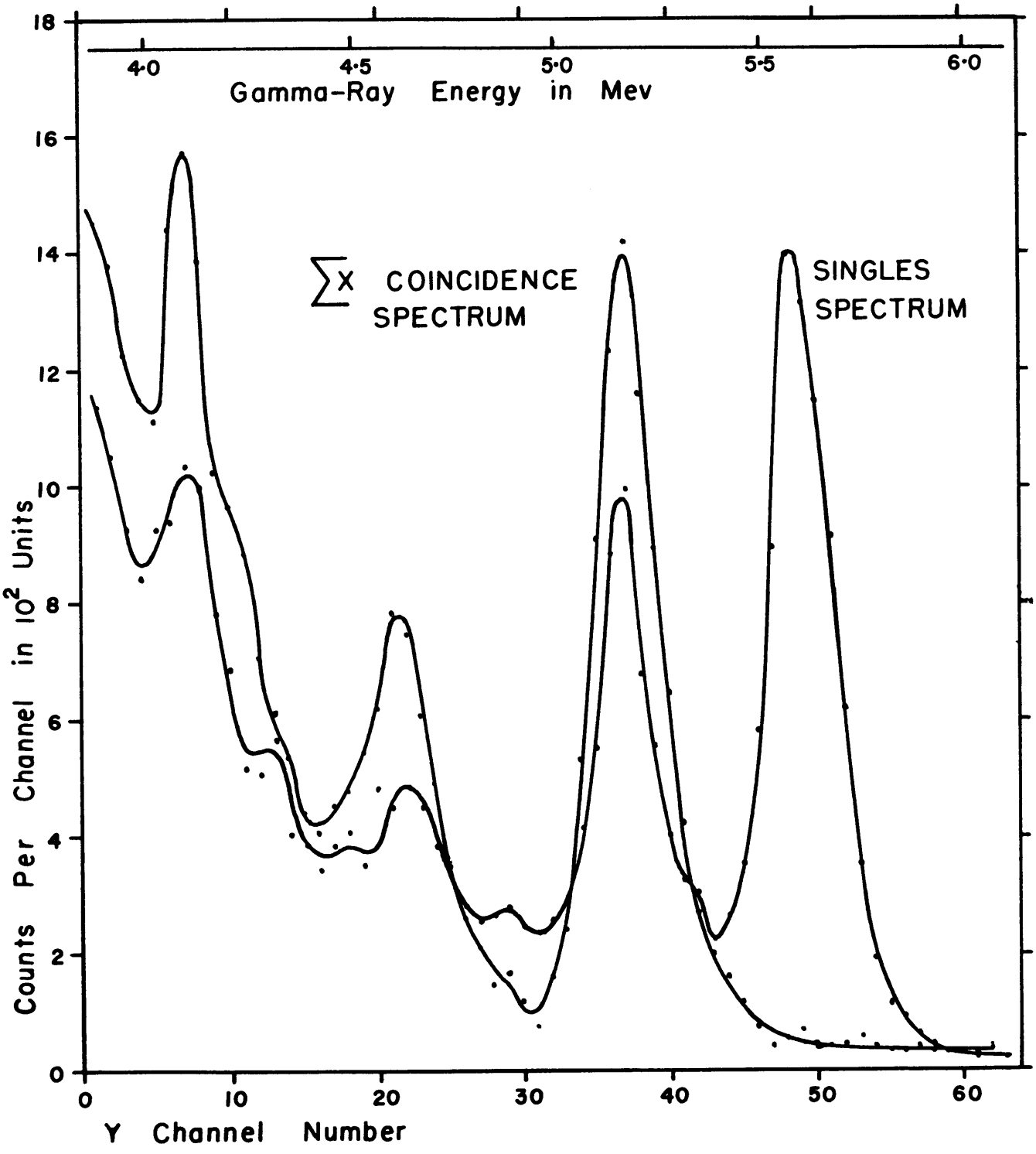

FIG 22. SINGLES AND COINCIDENCE PAIR SPECTRA FROM IRRADIATED Dy^{164}

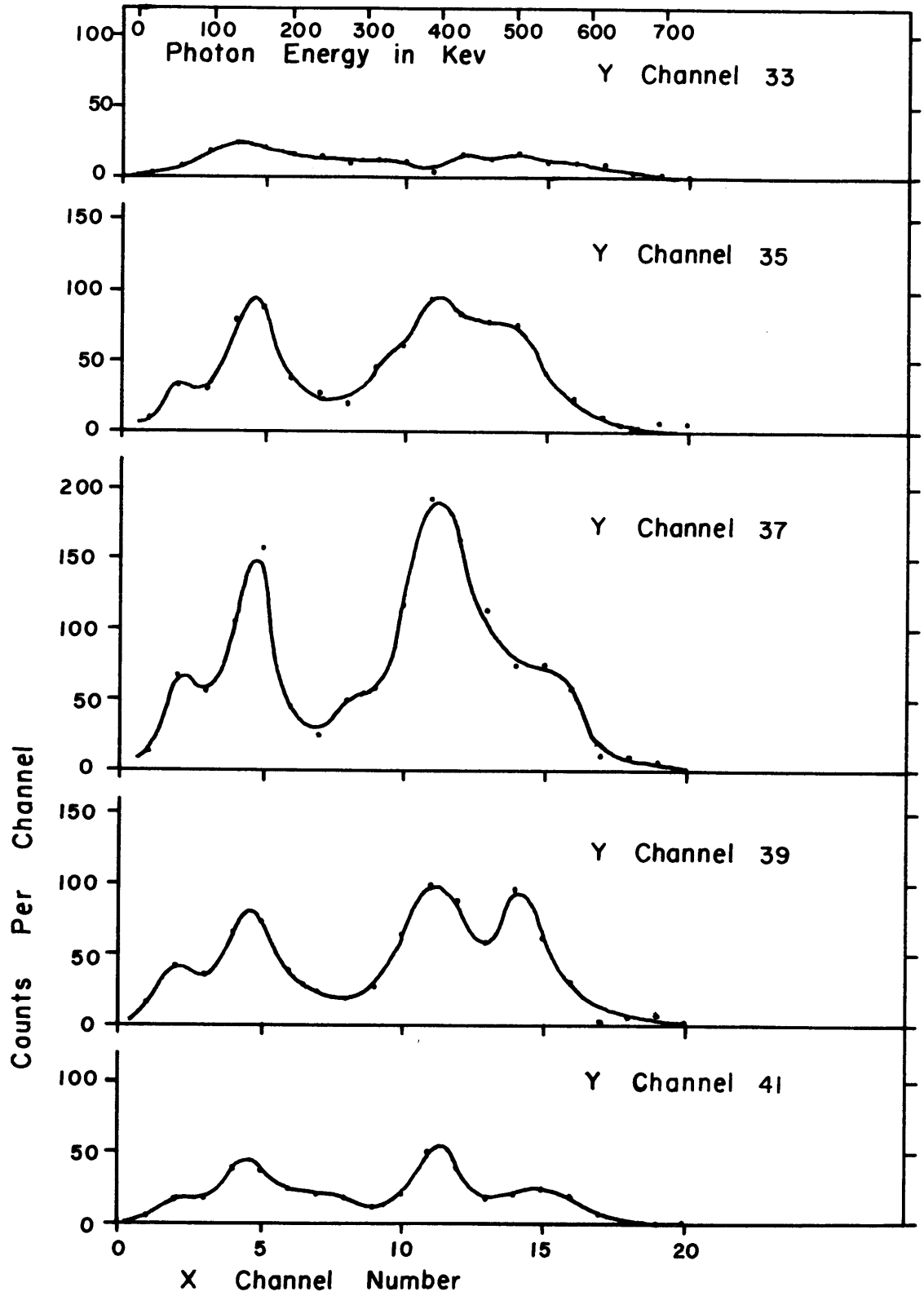

FIG 23. LOW ENERGY GAMMA RAYS IN COINCIDENCE WITH THE 5·15 MEV GAMMA-RAY GROUP FROM IRRADIATED Dy^{164}

obtained; so that the statistics of this run were poor. There were no clearly resolved low energy gamma rays in the fourfold spectrum above 700 kev, so it seemed that it would be logical to reduce the scale of the A crystal so as to allow a better calibration of the low energy peaks. In addition, it seemed plausible that one could obtain a higher fourfold coincidence count rate in a tighter geometry with a smaller crystal at the same maximum A singles count rate. Hence, on the next run, No. D9, the A crystal used was the 1-1/2" × 1-1/2" unit, and it was pushed closer to the beam center line. This crystal was allowed to range from 0 to 800 kev and it was stabilized with Cs^{137}. In this arrangement, the A crystal was run at 3.52×10^6 counts/min and the fourfold coincidence count rate was 60/min. The results from this run have better statistics and have a better low energy calibration. In both runs, the B crystal of the pair spectrometer was stabilized with an external Mn^{54} source.

It did appear later that the count rates were too high, and this resulted in a high accidental count rate of 6.62%. However, the added disadvantages of high count rates were a smearing of peaks and a poor stability. Experience later showed that stability of the system could not be guaranteed unless the height of the stabilizing photo peak was at least twice the height of the background. This condition was not achieved in run D9 on Ho^{165}, so that it was possible that the gain may have wandered somewhat during the course of the run. Figure 24 shows evidence of a small gain change between the singles and the fourfold run.

The results were poor for several reasons. Primarily, the high energy peaks could not be well resolved by the pair spectrometer. In addition, these peaks were small compared with the large number of completely unresolved high energy gamma rays, that were outside the energy range considered but which contributed substantially to the gross count rate. As a consequence, the number of counts recorded in the analyzer memory was small compared with the count rates involved, and the statistics were not good.

The results are illustrated in Fig. 24 and detailed in Table 16. The figure shows the normal pair spectrum and also the pair spectrum when a coincidence was required in the fourth crystal. The figure may also be compared with the holmium spectrum shown in Fig. 18. Comparison with Fig. 22 shows how poorly the high energy peaks from Ho^{165} have been resolved relative to those of Dy^{164}.

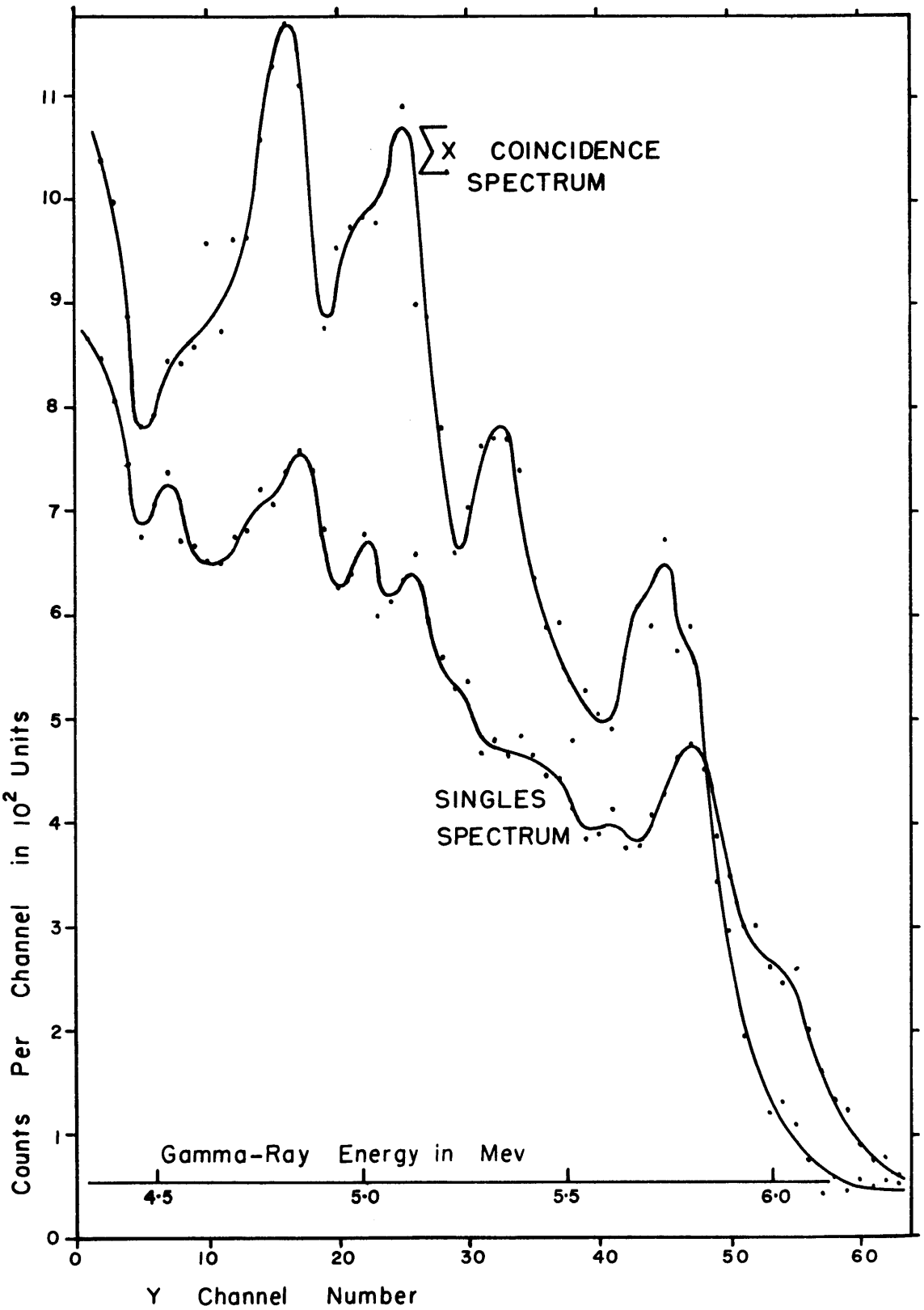

FIG 24. SINGLES AND COINCIDENT PAIR SPECTRA FROM IRRADIATED Ho^{165}

Table 16. High Energy - Low Energy Gamma-Ray Coincidences from Irradiated Ho^{165}.

High energy gamma ray	Coincident low energy gamma rays in kev, and remarks.
6.07 Mev	Essentially no coincidences. The small 47 and 230 kev peaks are probably from the spread of the 5.82 Mev primary gamma-ray group.
5.82 Mev	Definite 52 kev peak. Probable 120 kev peak. Definite 246 kev peak. Probable 220 kev peak spreading in from a primary gamma ray of lower energy. Possible 172 kev peak.
5.80 Mev	Definite 52 kev peak. Definite 226 kev peak. The peak of 246 kev is probably all from the spread of the 5.85 Mev primary gamma ray. Possible 199 and 86 kev spreading in from a primary gamma ray of lower energy.
5.54 Mev	Definite 52 kev peak. Unresolvable gamma rays from 80 to 200 kev. Probable double peak comprising gamma rays of energies 242 and 213 kev. Broad probable peak at 342 kev. Definite broad peak at 438 kev.
5.45 Mev	The coincidences from this gamma ray cannot be resolved easily from the 5.54 Mev primary gamma ray. The coincidence pattern is similar except that the 242 kev gamma ray is slightly more emphasized in the double peak. The 342 kev peak is somewhat more pronounced and a probable 504 kev peak has appeared.
5.12 Mev	Definite 49 kev peak. Probable 132 kev peak. Possible 170 kev peak. Probable double peak averaging at 230 kev. Definite 287 kev peak. Hint of a 504 kev peak. Unresolvable gamma rays over the whole energy range.
4.87 Mev	Definite 47 kev peak. Possible broad 124 kev peak. Possible 185 kev peak. Definite 239 kev peak. Hint of peaks at 276, 359 and 636 kev. Broad probable 404 kev peak. Unresolved gamma rays over the whole energy range.

CHAPTER 7
LEVEL DIAGRAMS AND SYNTHESIS OF DATA

7.1 LEVELS IN Sc^{46}

The principal information on levels in Sc^{46}, in existence prior to this work, is as follows:

(a) Nuclear energy level scheme of Groshev (G2) which is illustrated in part in Fig. 25.

(b) Nuclear energy levels obtained by Mazari (M2) using (d,p) excitation and illustrated in part in Fig. 26.

(c) Measured gamma ray of 142 kev with a half life of 20 secs, reported by Burson (B3).

(d) Coincidence measurements by Fiebiger (F1) listed in Table 17.

(e) High-energy gamma rays measured by Bartholomew (B4) and given in part in Table 18.

Table 17. Coincident Gamma Rays from Irradiated Scandium Measured by Fiebiger (F1).

Primary Gamma Ray, Mev	8.83	8.54	8.30	8.175
Coincident Gamma Rays, Mev	None	0.230	0.230, 0.310 and 0.090?	0.310, 0.150

Table 18. High Energy Gamma Rays from Irradiated Scandium Measured by Bartholomew (B4).

Energy, Mev
8.85 ± 0.08
8.539 ± 0.01
8.31 ± 0.02
8.175 ± 0.011
7.65 ± 0.03

The measurements listed in Table 17 are not very consistent with those of (a) above. Furthermore, the Q values for the reaction from

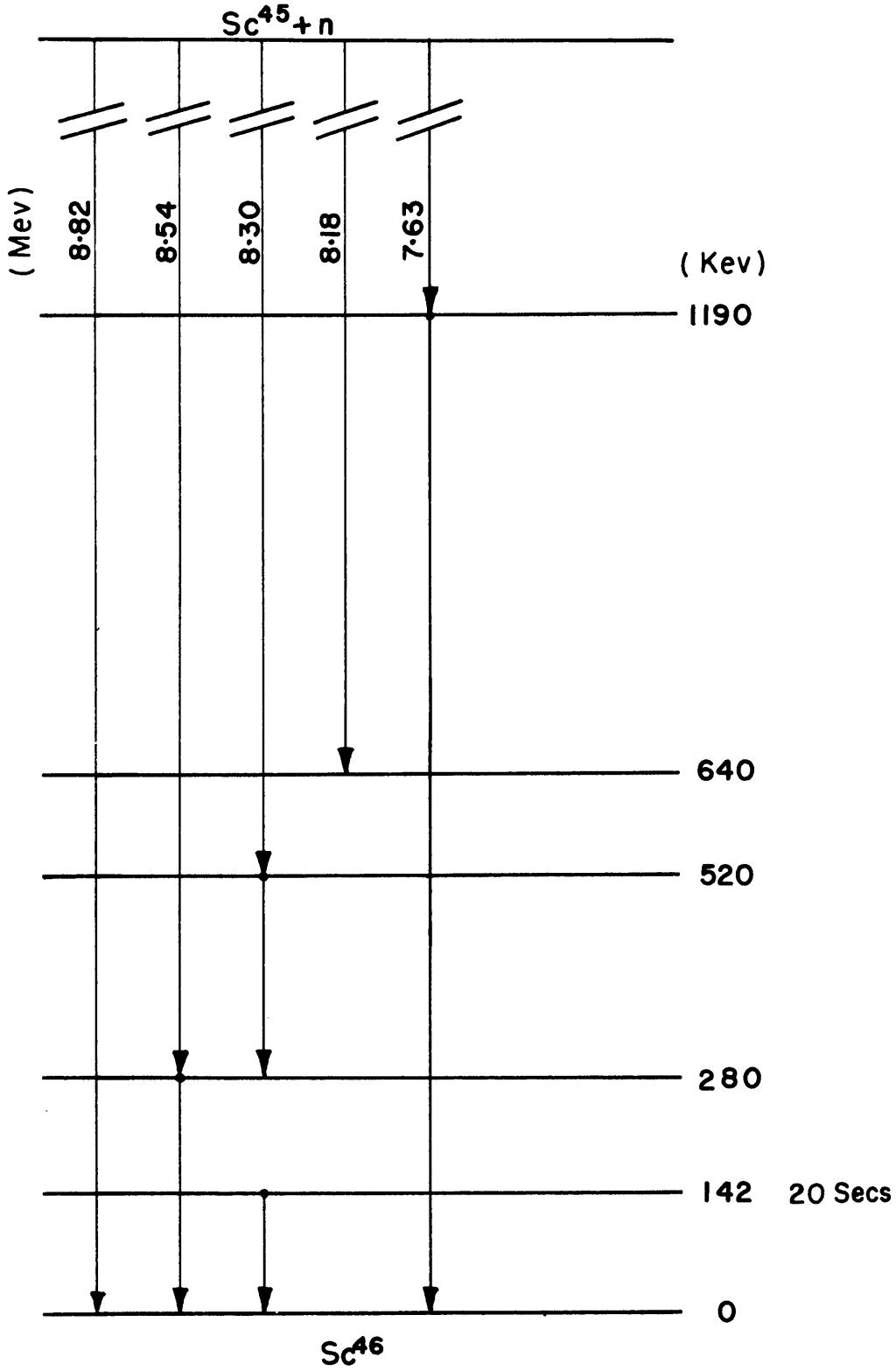

FIG 25. NUCLEAR ENERGY LEVEL SCHEME OF Sc^{46} PROPOSED BY GROSHEV G2

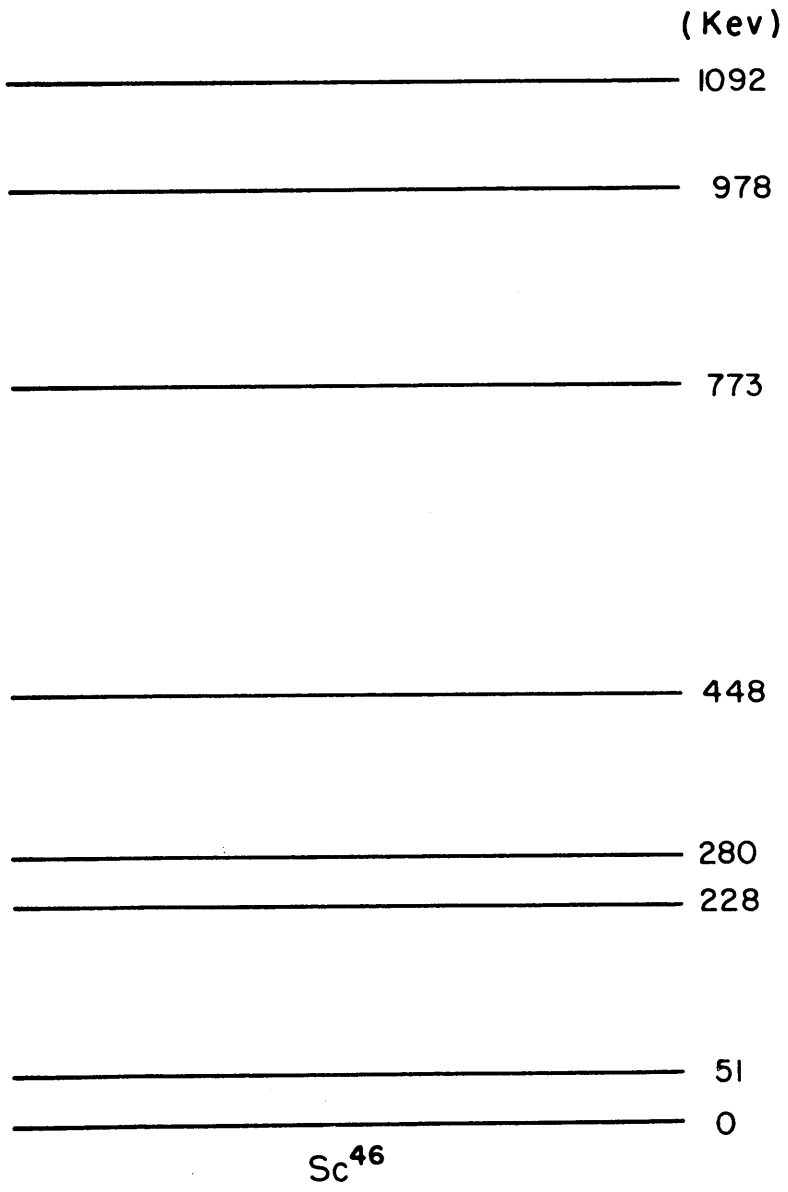

FIG 26. NUCLEAR ENERGY LEVELS OF Sc^{46} MEASURED BY MAZARI M2

different sources are at variance. The Q value for $Sc^{45}(d,p)Sc^{46}$ is given by Mazari (M2) as 6.534 ± 0.008 Mev. The Q value for the $p(n,\gamma)d$ reaction is quoted by Kazi (K2) as 2.225 ± 0.002 Mev; and hence the Q value for the $Sc^{45}(n,\gamma)Sc^{46}$ reaction would be 8.759 ± 0.008 Mev which is some 90 kilovolts less than the highest gamma-ray measurement.

After preliminary measurements on the bent crystal spectrometer had been made, it was decided that the inconsistencies in the above data could be minimized by presuming the information of Mazari to be correct. The more intense high-energy gamma rays could then be fed into appropriate levels in Sc^{46} to satisfy the coincidence measurements of Fiebiger. This preliminary level scheme was published with further information of Fiebiger in Reference F2 and is illustrated in Fig. 27. The essentials of this scheme have been confirmed by the later measurements on the bent crystal spectrometer given in Section 5.2, which indicate two definite cross-over transitions of 584 and 627 kev. Confirmation of the 142, 582 and 627 kev levels has now been made by Rapaport (R3), whose data in part are given in Table 19. Rapaport also gives a new Q value for the $Sc^{45}(d,p)Sc^{46}$ reaction as 6.541 ± 0.008 Mev.

Table 19. Nuclear Energy Levels in Sc^{46} Measured by Rapaport (R3).

Energy, Mev	ℓ_n
0	3
0.051	3
0.140	-
0.227	3
0.279	1*
0.444	3
0.577	-**
0.623	-
0.772	3
0.833	3
0.975	3
1.090	1

*A slight $\ell_n = 3$ component also
**Possible doublet

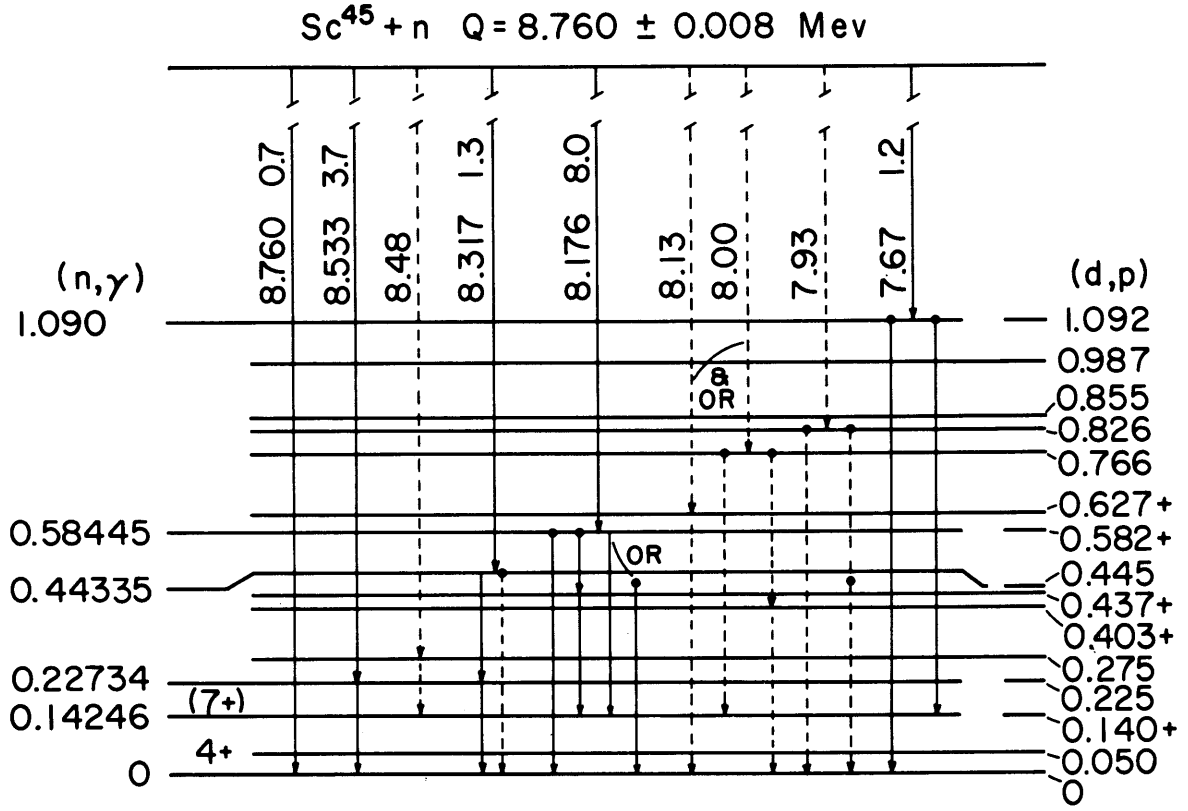

FIG 27. NUCLEAR ENERGY LEVEL SCHEME OF Sc^{46} PROPOSED BY FIEBIGER F2

Furthermore, Bartholomew, in a private communication to Fiebiger, indicates that the highest energy gamma ray might well be 8.76 Mev instead of 8.85 Mev. Bostrom (B5) reproduces many of the basic features of the scheme in an independent set of measurements. Finally, the low energy coincidence measurements given in Section 6.1 also support the correctness of the scheme.

The information from all these sources can be put into the level scheme of Fig. 28, again attempting to minimize remaining inconsistencies. A separate experiment has been performed by both Fiebiger and the author, independently, to show that the transition from the isomeric state is the lower of the two gamma rays at 145 kev. The results of this experiment are presented graphically as the spectrum from Sc^{46m} in Fig. 29 and the calibration curve in Fig. 30. A least squares fit gives the value of the gamma ray from the decay of the scandium isomer as 143.3 ± 2.4 kev.

The final scheme shows some features of note. A definite decay pattern is established for the decay of the level reached by means of the intense 8.175 Mev gamma ray. There is no sure way of deciding whether the 585 level decays initially by the 295 kev or by the 147 kev gamma ray, so that the alternative to the 289 level is a 438 kev level. The former has been chosen because it is more feasible energetically, and because it permits Ritz combinations to be made to the 775 and 829 kev levels and agrees with the coincidence data. In addition, Rapaport shows that the ℓ_n for the nearby 280 kev level is 1 with a small $\ell_n = 3$ component. The fact that a VVS 227.9 kev transition feeds the 52 kev level without the decay of that level being observed requires explanation. Presumably, it must be because the transition is highly converted, and we note that the internal conversion coefficient would be 5.5 for an E2 transition of this energy. Since the 50 kev range on the bent crystal spectrometer was surveyed only at the low flux port, it might then have been possible for this other 52 kev gamma ray not to have been observed.

7.2 LEVELS IN Rh^{104}

There is at present a considerable amount of information on the nuclear energy levels of Rh^{104} – to much, in fact, to be detailed here. The primary sources of information are as follows:

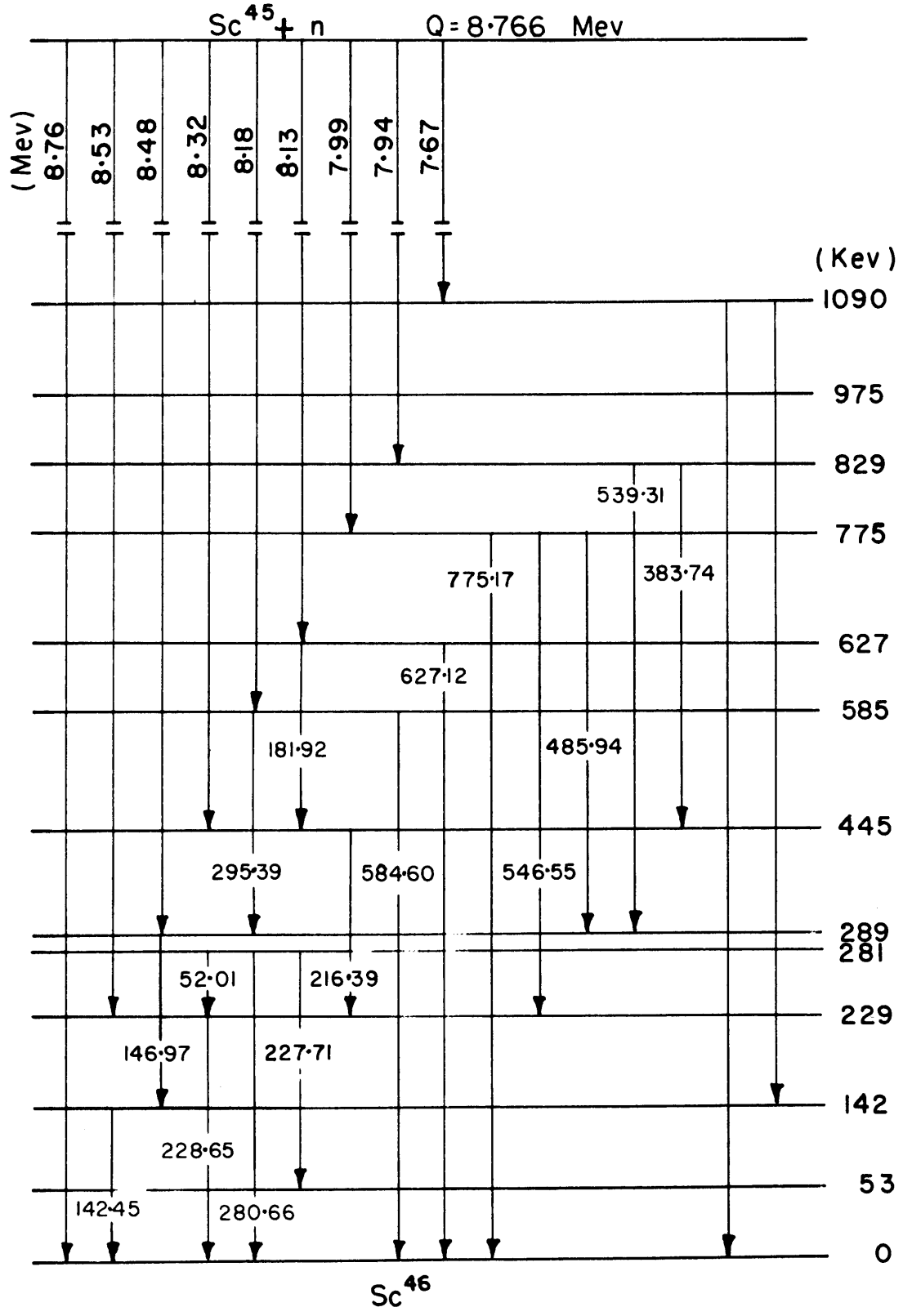

FIG 28. FINAL PROPOSED NUCLEAR ENERGY LEVEL SCHEME OF Sc^{46}

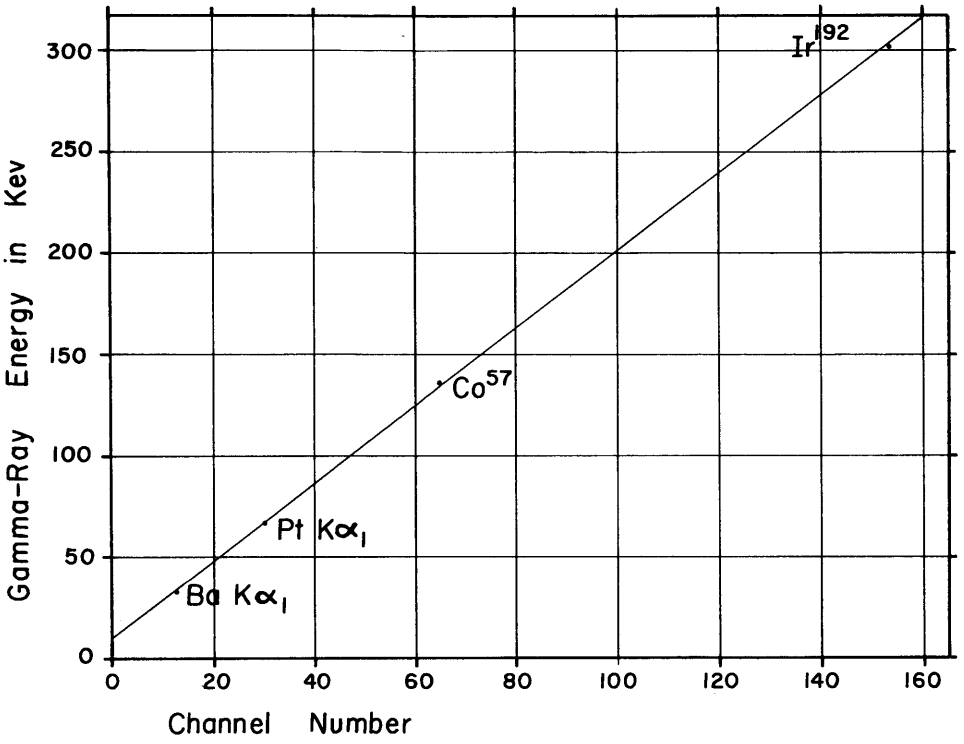

FIG 30. CALIBRATION CURVE FOR FIGURE 29

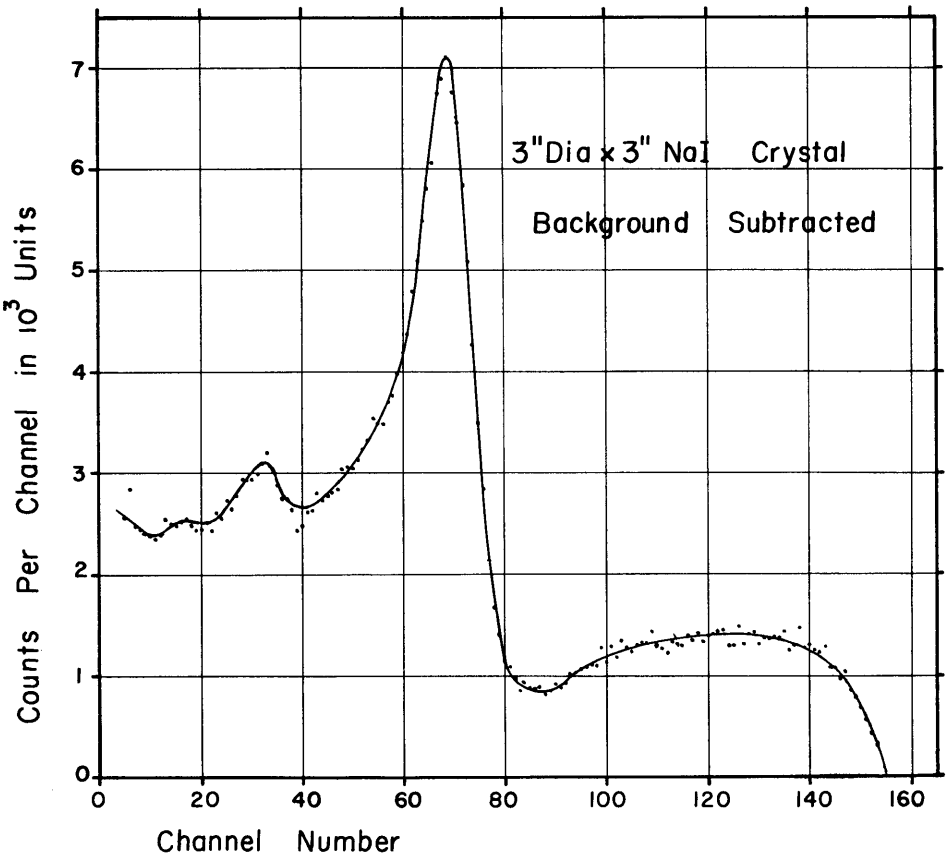

FIG 29. GAMMA-RAY SPECTRUM OF Sc^{46m}

(a) (n,γ) studies with a scintillation spectrometer by Greenwood (G4).

(b) (n,γ) studies with a scintillation spectrometer by Kalinkin (K5).

(c) Level studies from the $Rh^{103}(d,p)Rh^{104}$ reaction by da Silva (S1).

(d) Bent crystal spectroscopy data by Buschhorn (B1).

(e) Unpublished bent crystal spectroscopy data by Gruber (G5).

(f) Coincidence information and bent crystal spectroscopy data of the author, presented in Chapters 5 and 6.

The measurements of (d) above are more precise than those made here, and have sufficient accuracy that an excellent low level diagram up to 270 kev could be constructed by means of Ritz combinations, which confirmed the independent studies of (a) and (b) above. Buschhorn's measurements range only up to 350 kev and are superceded by the initial values of (e) above. Gruber's initial data range up to 790 kev and are generally more accurate and more comprehensive than those reported in Chapter 5. Consequently, it has not been felt worthwhile to form many Ritz combinations on the author's data to build up the level diagram. However, the coincidence information of Chapter 6 allows a few obvious features to be noted and added to the scheme of Buschhorn.

The probable 176-176 kev coincidence implies a level at 350 kev in view of the existence of a well established level at 181 kev which decays directly to ground. The level taken is 358.75 kev, since there is a measured 358.75 kev transition and because excellent Ritz combinations can be made with Gruber's data as follows:

(180.86 + 177.88) = 358.74 kev

(97.11 + 261.67) = 358.78 kev

The probable coincidence of 92 and 320 kev suggests a level at 421 kev since there is a well established level at 97 kev above ground. The level is taken as 420.89 kev, since there is a measured 420.89 kev transition and because Ritz combinations can be made with Gruber's data as follows:

(323.88 + 97.11) = 420.99 kev

(197.88 + 222.93) = 420.81 kev

(213.10 + 207.55) = 420.65 kev

(358.75 + 62.14) = 420.89 kev

The possible coincidence of 92 and 441 kev suggests a level at 538 kev since there is a well known level at 97 kev. This level is taken as 537.60 kev because Ritz combinations can be made with Gruber's data as follows:

(97.11 + 440.59) = 537.70 kev
(420.89 + 116.94) = 537.83 kev
(358.75 + 178.84) = 537.59 kev

The definite coincidence of 179 and 634 kev suggests a level at 824 kev because there is a definite level at 181 kev and because there is a strong transition of 643.4 kev. The value of this level then is 824.2 kev, though it is not substantiated by further Ritz combinations. It is to be noted here that the author's measurement of that transition is 645.4 kev, which differs significantly from Gruber. Nevertheless, the Ritz combinations above have been made using Gruber's data consistently, since his better sensitivity allows measurement of transitions used in these combinations that were not detected by the author.

Figure 31 shows the level diagram formed by combining the observations above with the basic scheme of Buschhorn. The absence of agreement with the (d,p) data is surprising, even when one takes into account the possibility that the supposed ground state is the 51 kev level. Completion of the level scheme up to 1 Mev may be expected when Gruber obtains the final measurements.

7.3 IRIDIUM

No attempt has been made to make isotopic assignments to the capture gamma rays measured on the bent crystal spectrometer and listed in Table 2. Those measurements were made in the low flux port of the M.I.T. reactor and, in view of the experience with scandium, the non-observance of gamma rays above 350 kev does not imply the absence of strong transitions above that energy. Consequently, it has not been possible to make Ritz combinations with the values obtained. Fiebiger, however, has made some fourfold measurements on separated isotopes of iridium with the Brookhaven scintillation pair spectrometer, though his results are not yet published. Hopefully, the measurements made here will be of use in formulating level schemes of the two isotopes, Ir^{192} and Ir^{194}. It is worth noting, however, that a precision measurement

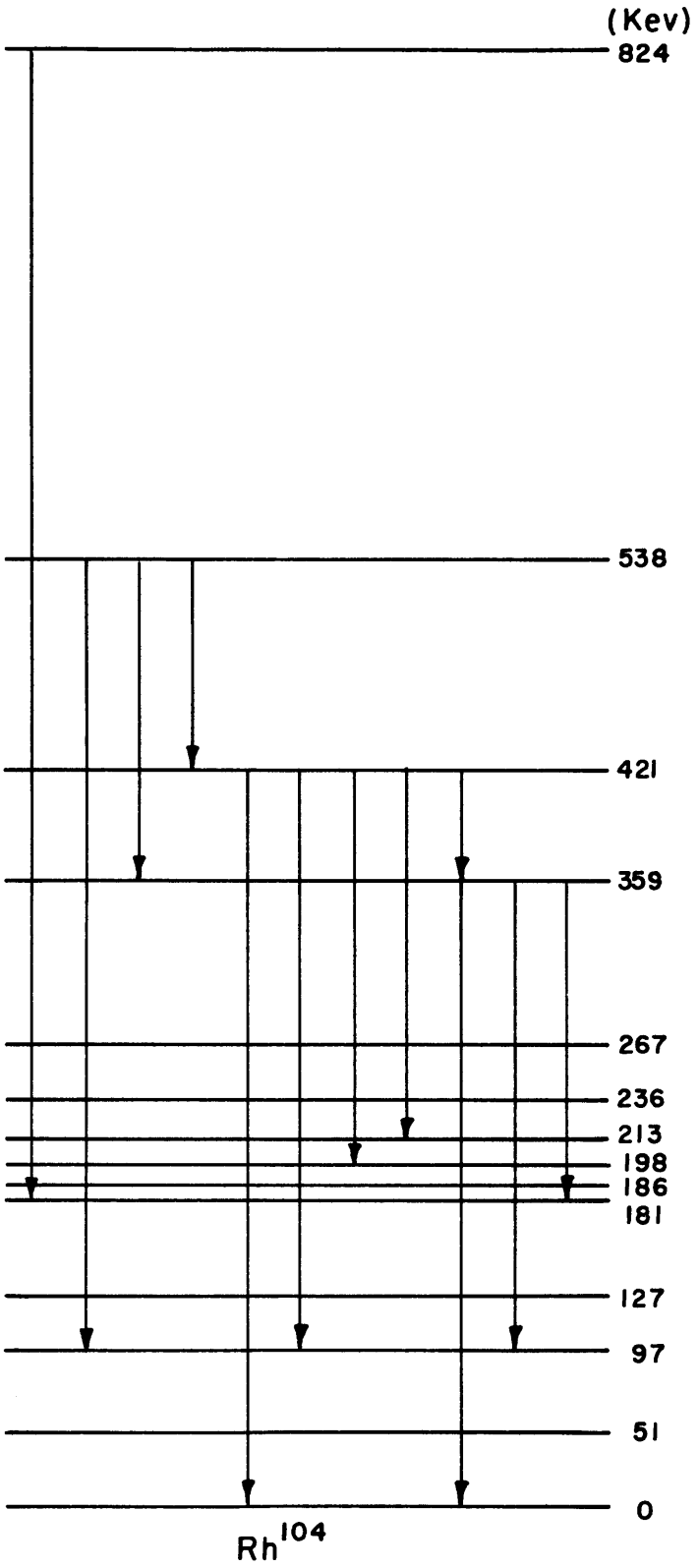

FIG 31. SUGGESTED ADDITIONS TO THE Rh^{104} NUCLEAR ENERGY LEVEL SCHEME OF BUSCHHORN BI

of the gamma ray from Ir^{192m} has been obtained as 58.844 ± 0.012 kev.

7.4 LEVELS IN Dy^{162}

Information on gamma rays from neutron irradiation of Dy^{161} is given by Mihelich (M5) and Jorgensen (J1) and is listed in Table 20 with a tentative identification from the data of Hickson (H1), which was obtained with natural dysprosium. The gamma-ray coincidences of Table 7 confirm the level scheme of Jorgensen. The level ordering may be well interpreted as a series of rotational excitation levels of a deformed nucleus based on the ground state single particle level of 0^+.

The excitation energy E_I of these levels can be related to the total angular momentum I by Eq. (7.4.1).

$$E_I = A(I+1)\, I - BI^2(I+1)^2 , \qquad (7.4.1)$$

where A and B are constants. The transitions between these levels have an energy given by

$$(E_I - E_{I-2}) = 2A(2I-1) - 4B[(I-1)^3 + I^3] . \qquad (7.4.2)$$

A weighted, least squares fit of the first three transitions is made to Eq. (7.4.2), using the more accurate values of Hickson to obtain A = 13.507 kev and B = 11.16 ev. The calculated values for the first five transitions are also listed in Table 20.

Table 20. Measured and Calculated Gamma-Ray Transitions from Irradiated Dy^{161}.

Previous Data	Reference	Hickson (H1) Value	Calculated Value
80.80 kev	M5	80.649 ± 0.019 kev S	80.638 kev
184.8 kev	M5	184.942 ± 0.034 kev VS	185.029 kev
282.8 kev	M5	282.636 ± 0.084 kev S	281.918 kev
--		369.395 ± 0.451 kev VVW	367.016 kev
--		442.436 ± 0.645 kev VVW	436.036 kev
936	J1	--	--
1219	J1	--	--

Although the last two transitions of Table 20 are tentative, they are not impossible. Since the ground state of Dy^{161} is $\frac{5+}{2}$, the capture states will be 3+ and 2+; it is just possible for the 10+ state to be fed through four intermediate transitions and the 8+ state to be fed through three intermediate transitions. These possibilities have been listed because of the tentative agreement from the coincidence data of Table 7, provided one makes allowance for smearing of the peaks. The final low energy level scheme then is given by Fig. 32. The singles spectrum from the scintillation pair spectrometer provides no assistance in this level scheme. The binding energy of the last neutron in Dy^{162} is given by Johnson (J2) as 8.175 ± 0.050 Mev. No identifiable transition from Dy^{162} is seen within 1 Mev of this figure.

7.5 LEVELS IN Dy^{165}

From the singles pair spectrum taken with the scintillation pair spectrometer, a tentative identification of gamma rays from excited Dy^{165} has been made. The gamma rays are partially listed in Table 21 with the energy values of Motz (M1).

Table 21. High Energy Gamma Rays from Irradiated Dy^{164} Measured by Motz (M1).

Energy, Mev
5.620
5.570
5.463?
5.187
5.151
5.114
4.616
4.463
4.334
4.273
4.124
4.082
3.964
3.886

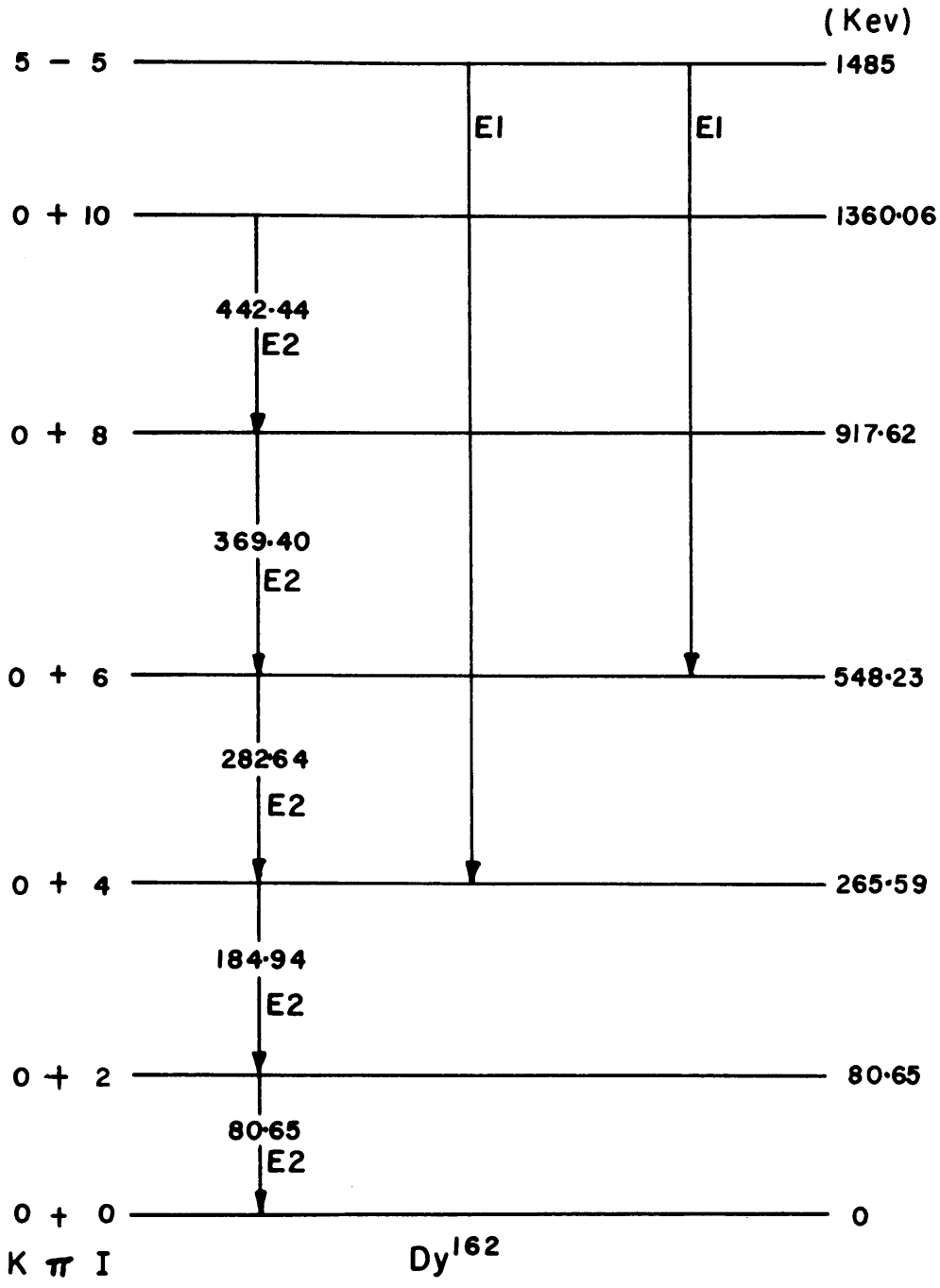

FIG 32. SUGGESTED ADDITIONS TO THE Dy^{162} NUCLEAR ENERGY LEVEL SCHEME OF GALLAGHER G3

Figure 22 indicates clearly that there are essentially no coincidences with either the 5.620 or 5.570 Mev primary gamma rays. Since the capture state is $\frac{1}{2}+$ and the ground state of Dy^{165} is $\frac{7}{2}+$, a direct transition to ground is highly improbable. The isomer Dy^{165m} at 108 kev excitation has a spin $\frac{1}{2}-$, so that it is reasonable to assume that one of the above high energy transitions must feed it directly. Since it is very difficult to postulate a state that is 50 kev below the 108 kev level, and is fed directly from the capture state, but which the isomer may not in turn feed, the 5.620 Mev gamma ray is presumed to go to the isomeric level. The isomeric state is expected to be the ground state of a band of rotational excitation levels, whose spins will be $\frac{1}{2}-$, $\frac{3}{2}-$, $\frac{5}{2}-$, $\frac{7}{2}-$ and so on. It is very likely that if the $\frac{1}{2}-$ level is fed by the $\frac{1}{2}+$ capture state, the $\frac{3}{2}-$ level will also be fed. Since rotational-excitation systematics expect such a $\frac{3}{2}-$ level 50 kev above the $\frac{1}{2}-$ state, the postulate becomes more reasonable. Hickson (H1) finds a very strong 50 kev transition in the gamma spectrum of irradiated dysprosium by means of bent crystal spectroscopy. That the 50 kev transition is not seen in coincidence with the 5.570 Mev gamma ray, requires explanation. It is presumed that the 50 kev transition is a combination of retarded M1 transition and an enhanced E2 transition. The over-all internal conversion coefficient will lie between the extremes of 1.7 for M1 and 27 for E2 which may substantially depress coincidence observation. In addition, the mean lifetime of the level may be expected to lie between the extremes of 2×10^{-5} sec (E2) and 2×10^{-10} sec (M1), the Weisskopf estimates illustrated on page 215 of E1. The resolving time of the pair spectrometer is 5×10^{-8} sec which may be less than the mean lifetime of the level and would further reduce the observable number of gamma-ray coincidences.

These deductions then imply a Q value of 5.728 Mev for the reaction $Dy^{164}(n,\gamma)Dy^{165}$. In addition, the data of Motz in Table 21 implies a series of directly-fed levels and these are illustrated by Fig. 33. In addition to these levels, there is foreknowledge of the rotational band based on the $\frac{1}{2}-$ 108 kev level, [521] Nilsson orbit. Hickson (H1) shows that the levels in this band can be fairly well fitted by his data as follows:

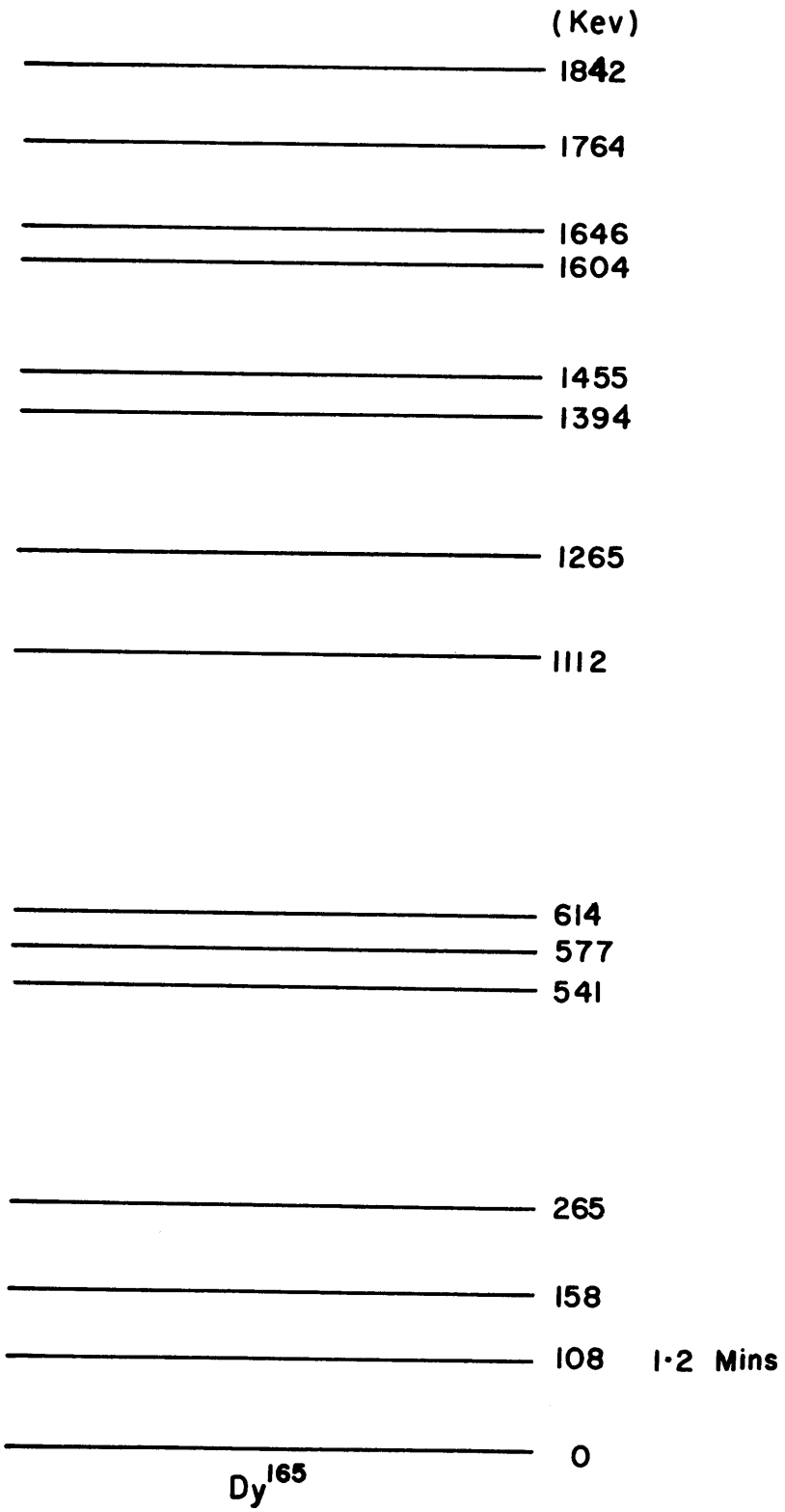

FIG 33. PROBABLE NUCLEAR ENERGY LEVELS IN Dy^{165} FED FROM THE CAPTURE STATE

$\frac{3}{2}-$ 158.570 kev level

$\frac{5}{2}-$ 161.905 kev level

$\frac{7}{2}-$ 281.826 kev level

Hickson also believes he has observed the de-excitation of a rotational band based on the $\frac{7}{2}+$ ground state, [633] Nilsson orbit. In general, though, the spins of the levels in this band are too high to be excited significantly from the low spin capture state, and so any transitions in this band are most unlikely to be observed in the coincidence data.

A transition from the $\frac{7}{2}-$ 281.8 kev level to the $\frac{7}{2}+$ ground state is not observed and this is explained by the K selection rule. This rule states that

$$|K_i - K_f| \leq \lambda \qquad (7.5.1)$$

or the transition will be K forbidden. Here,

K = total angular momentum of the ground state of the rotational band;

i = initial;

f = final;

λ = multipole order of the transition.

Mottelson (M6) states that for each degree of K forbiddeness, the lifetime is ten to a hundred times larger.

The problem now is to fit all this level data with the fourfold coincidence information and the precision measurements of the transitions from Hickson (H1). The latter would be fitted by means of Ritz combinations. It has not been possible to do this satisfactorily because there are too many variants in the level schemes that may be arrived at in this way. This situation arises because there are many unresolved double and triple peaks in the coincidence data and the low energy calibration is not very good. The contrast with the unique picture derived for the Sc^{46} level scheme is very distinct. Consequently, a level scheme is presented in Fig. 34 which represents the combined information mostly from the coincidence work. It is by no

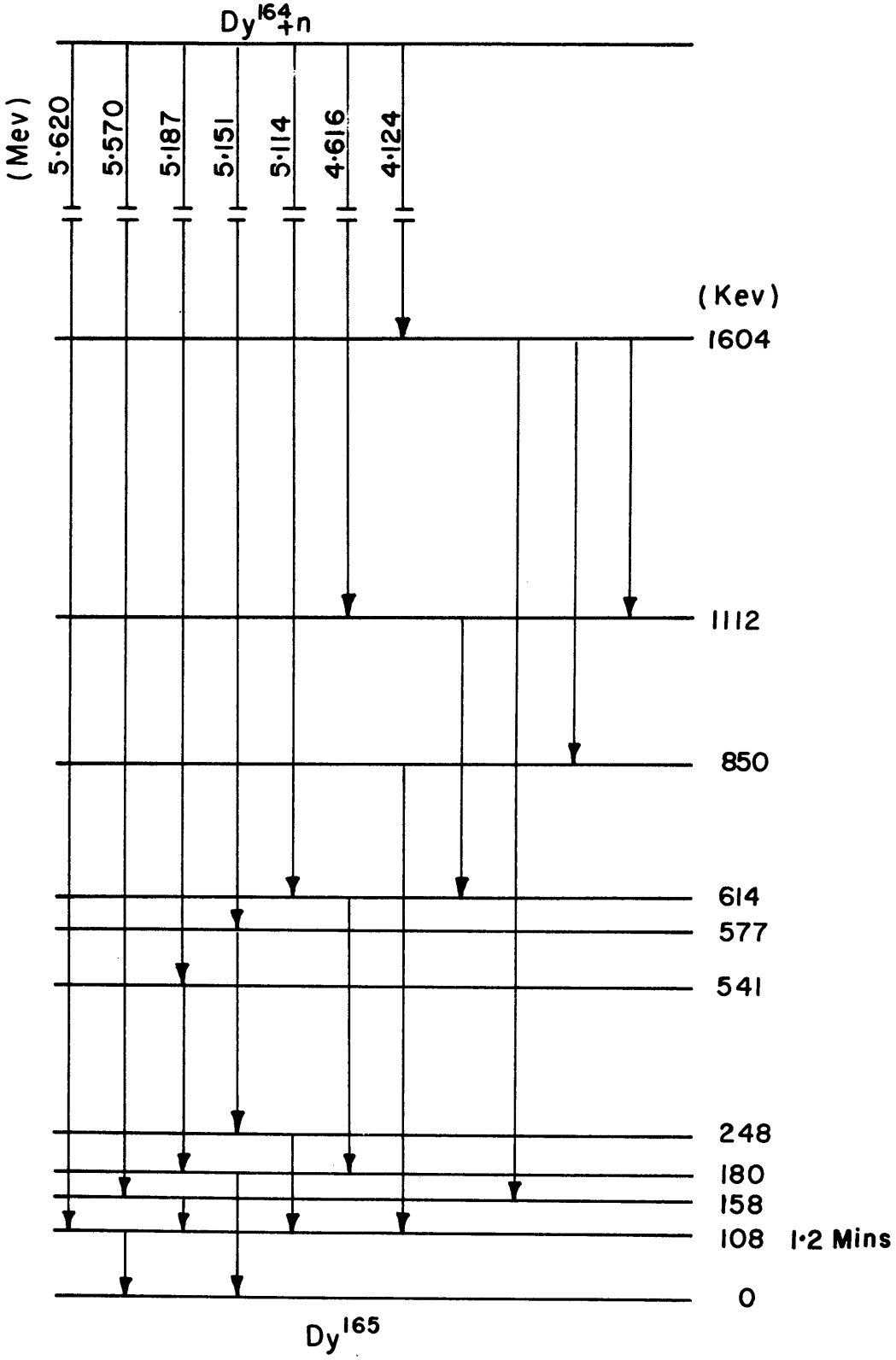

FIG 34. TENTATIVE NUCLEAR ENERGY LEVEL SCHEME OF Dy^{165} SUGGESTED BY THE COINCIDENCE DATA

means unambiguous, but it provides a starting point for fitting the precision measurements of the transitions, and it allows a basis for the discussion of some variants.

The best attempt to combine all the information on Dy^{165} resulted in the level scheme of Fig. 35, which covers the first 650 kev of nuclear excitation. It has not been possible to extend this scheme upwards in a way that allows the precision values of the transitions to be fitted and yet to satisfy the coincidence data. Consequently, no great confidence can be expressed in the level scheme of Fig. 35. The level scheme does fit the measurements fairly well and utilizes some of the strong transitions in Hickson's data. In addition, the agreement with the deduced level data of Fig. 34 is not too bad with the exception of the 595.98 kev level where a 614 kev level had been expected. It is to be noted that a 632.12 kev level can be formed which would decay either to the ground state or, by a strong 448.12 kev transition, to the 184 kev level. It does not fit the coincidence data too well, but the expected 614 kev level could be the combination of the two levels, 596 and 632 kev.

Because of the uncertainty in the proposed level scheme, an extensive interpretation of the levels in terms of single particle levels or rotational excitations is not made. The coincidence data shows a strong gamma ray of about 170 kev which leads either to the isomeric level or, more probably, to the ground state. This gamma ray is taken to be the VVS 184.19 kev transition measured by Hickson. The K selection rule does not allow the 184 kev level to be in the [521] rotational band, and it cannot be in the [633] rotational band because its spin and parity would be $\frac{11}{2}+$, which cannot be excited in a two-step cascade from the $\frac{1}{2}+$ capture state. Consequently, the 184 kev level is presumed to be a single particle level and is probably the $\frac{5}{2}-$ [523] Nilsson orbit. Mottelson (M6) claims to see this [523] orbit 492 kev above the [521] orbit in $_{68}Er^{167}$ and 49 kev below in $_{66}Dy^{161}$.

It is not unreasonable, then, to make this identification, though the $\frac{5}{2}-$ [512] orbit would be a second choice. On this basis, it might be reasonable to identify the 541 kev, the 577 kev and the 614 kev levels as the Nilsson orbits $\frac{5}{2}-$ [512], $\frac{3}{2}-$ [521] and $\frac{5}{2}+$ [642], not necessarily respectively. However, if one allows only M1, E1 and E2 transitions from the capture state, the levels to which the primary transitions

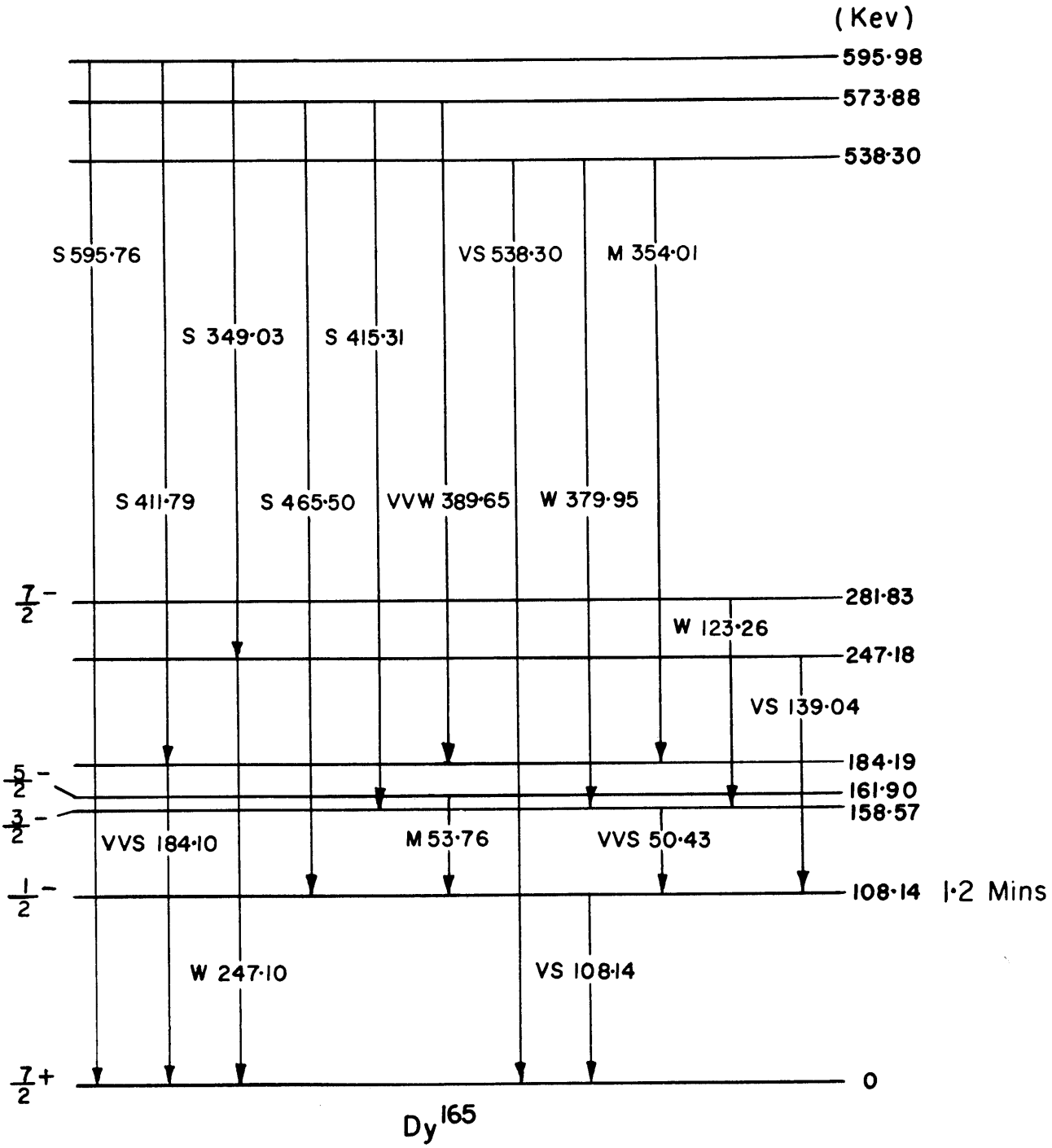

FIG 35. PROPOSED POSSIBLE NUCLEAR ENERGY LEVEL SCHEME OF Dy^{165}

feed may have spins and parities of $\frac{1}{2}+$, $\frac{1}{2}-$, $\frac{3}{2}-$, $\frac{3}{2}+$ and $\frac{5}{2}+$ only. This would eliminate the $\frac{5}{2}-$ [512] orbit from the above identification. This tends to suggest that either one of the three primary gamma rays in the 5.15 Mev group is not from de-excitation of Dy^{165}, or the $\frac{1}{2}-$ [510] and $\frac{3}{2}-$ [512] Nilsson single particle states are the ones at these excited levels.

7.6 LEVELS IN Ho^{166}

Schermer (S2) states that 60% of the thermal cross section of Ho^{165} is to I − 1/2 states. Since the spin of Ho^{165} is $\frac{7}{2}-$, the capture state will be 60% 3− and 40% 4−. The ground state spin of Ho^{166} is 0−, so it is extremely unlikely that there is a direct transition to ground from the capture state. It is desirable then to deduce the binding energy as a starting point to the construction of a nuclear level diagram.

There is evidence available on the low lying levels in Ho^{166} from several sources: beta decay studies by Helmer (H5), neutron capture studies by Estulin (E2), bent crystal spectroscopy data by Hickson (H1), and a discussion paper by Gallagher (G3). There are also some level data from (d,p) excitation by Struble (S3), though these are treated circumspectly due to their incompleteness; nevertheless, they are reproduced in Fig. 36. Excluding the data of Hickson, the existing evidence is summarized by the level diagram of Fig. 38. It is to be noted that 80% of the decay of the 82.5 kev level is to the ground state. Since the E1 transition has a conversion coefficient of about 5, the implication is that the predominant radiation observed in the decay of that level is a holmium K-series X ray. In Section 6.4, it was shown that no coincidences were observed with the 6.07 Mev primary gamma ray. This would imply that this gamma ray excites a level with a significant lifetime or that the decay from this level is highly converted in the L shell. Conversion by the K shell would have led to a coincident K-series X ray.

The best choice would seem to be that the 6.07 Mev gamma ray leads to the 54 kev level, which is possible from spin considerations and satisfies the noncoincidence conditions. This gives a binding energy of 6.127 ± 0.022 Mev. The 5.85 Mev gamma ray is in coincidence with a 246 kev peak and perhaps also a 52 kev peak at the same time. This implies a binding energy of 6.15 Mev which agrees within the error limits.

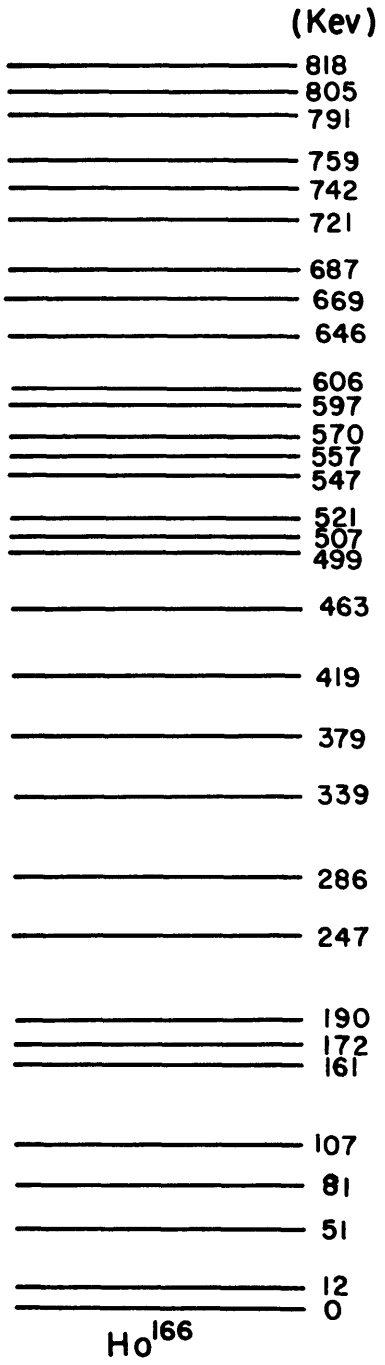

FIG 36. NUCLEAR ENERGY LEVELS IN Ho^{166} MEASURED BY STRUBLE S3

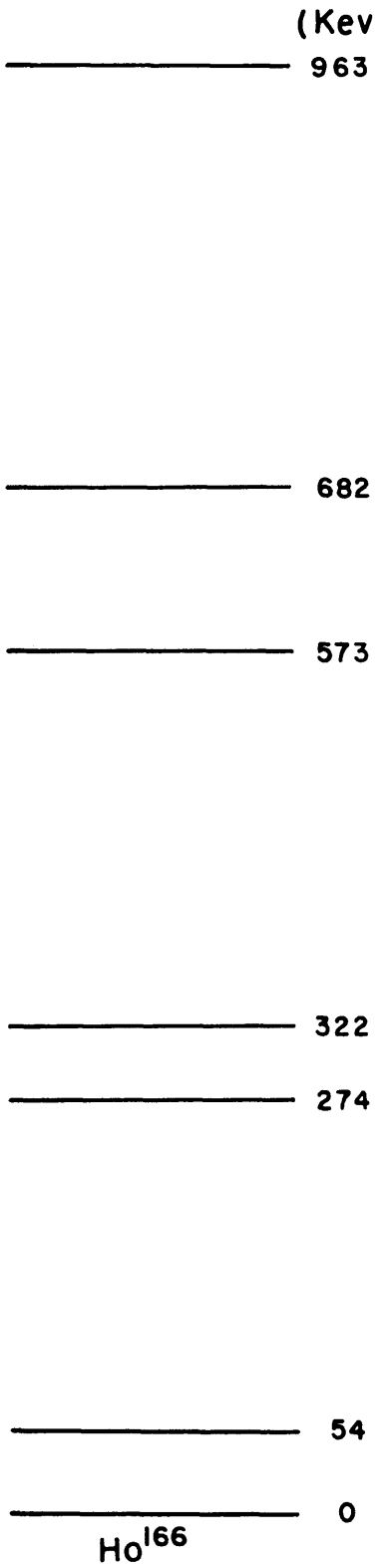

FIG 37. POSSIBLE NUCLEAR ENERGY LEVELS IN Ho^{166} FED FROM THE CAPTURE STATE

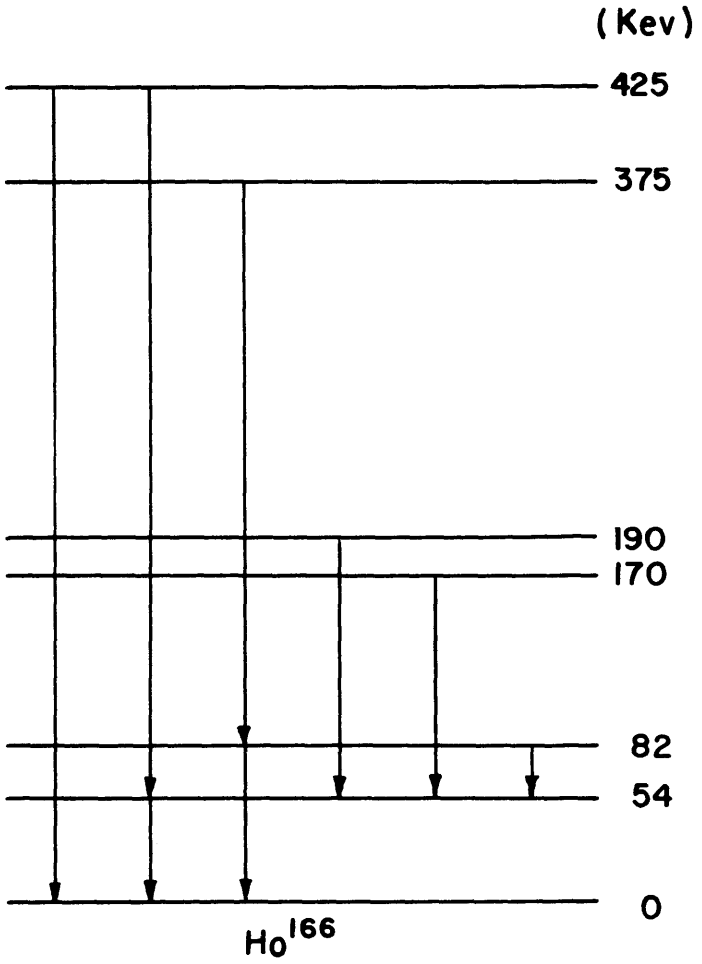

FIG 38. NUCLEAR ENERGY LEVEL SCHEME OF Ho^{166} PROPOSED BY ESTULIN E2

With this deduction made, levels could be determined from the energies of the primary gamma rays, but their energy uncertainty makes this exercise of little use. Despite this, they are shown in Fig. 37 to be compared with the values of Struble (S3).

The next step in the construction of the level diagram is to determine the precise values of the 170 and 190 kev levels, using only the strong transitions that have been measured by Hickson. Several alternatives are possible. Levels are sought at 274 kev and 322 kev, and strong transitions are fitted from these levels to the various alternatives at 170 kev and 190 kev until a precise fit is obtained and the coincident pattern is established. The same procedure is repeated for the 573 and 682 kev levels. The best fit is the level diagram shown in Fig. 39. No great confidence can be expressed in this diagram because it cannot be easily interpreted in terms of rotational levels and because the low energy coincidence data does not fit too well.

As far as possible, the spins and parities are interpreted in terms of rotational bands characterized by the asymptotic quantum number K, which is the projection of the total angular momentum on the axis of symmetry of the deformed nucleus. It seems reasonable to interpret the 426, 576 and 671 kev levels as the 1+, 4+ and 5+ members of the $K = 1[523\uparrow\ 523\downarrow]$ band; since the observed transitions are permissible in this identification and the spins and parities of the upper two members allow excitation from the capture state. One might suppose that the VS 239 kev transition from the 576 kev level would not allow significant population of the lower spin members of that rotational band, but one could look for those 2+ and 3+ states anyway. A tentative fit can be made with 464 and 512 kev levels. The 2+ member can decay to the 82 kev level by a VW 381.35 kev transition. In addition, a measured VVW 409.66 kev gamma ray fits the decay of the 2+ 464 kev level to the 54 kev state.

The 337 kev level appears to be well fitted by the 5− assignment to the $K = 0[523\uparrow\ 633\uparrow]$ rotational band. No spins or parities have been assigned to the other levels because of the tentativeness of this level scheme. Some of them have few choices though, such as the 275 kev level. Since it is fed by the capture state, probably by an E1 transition,

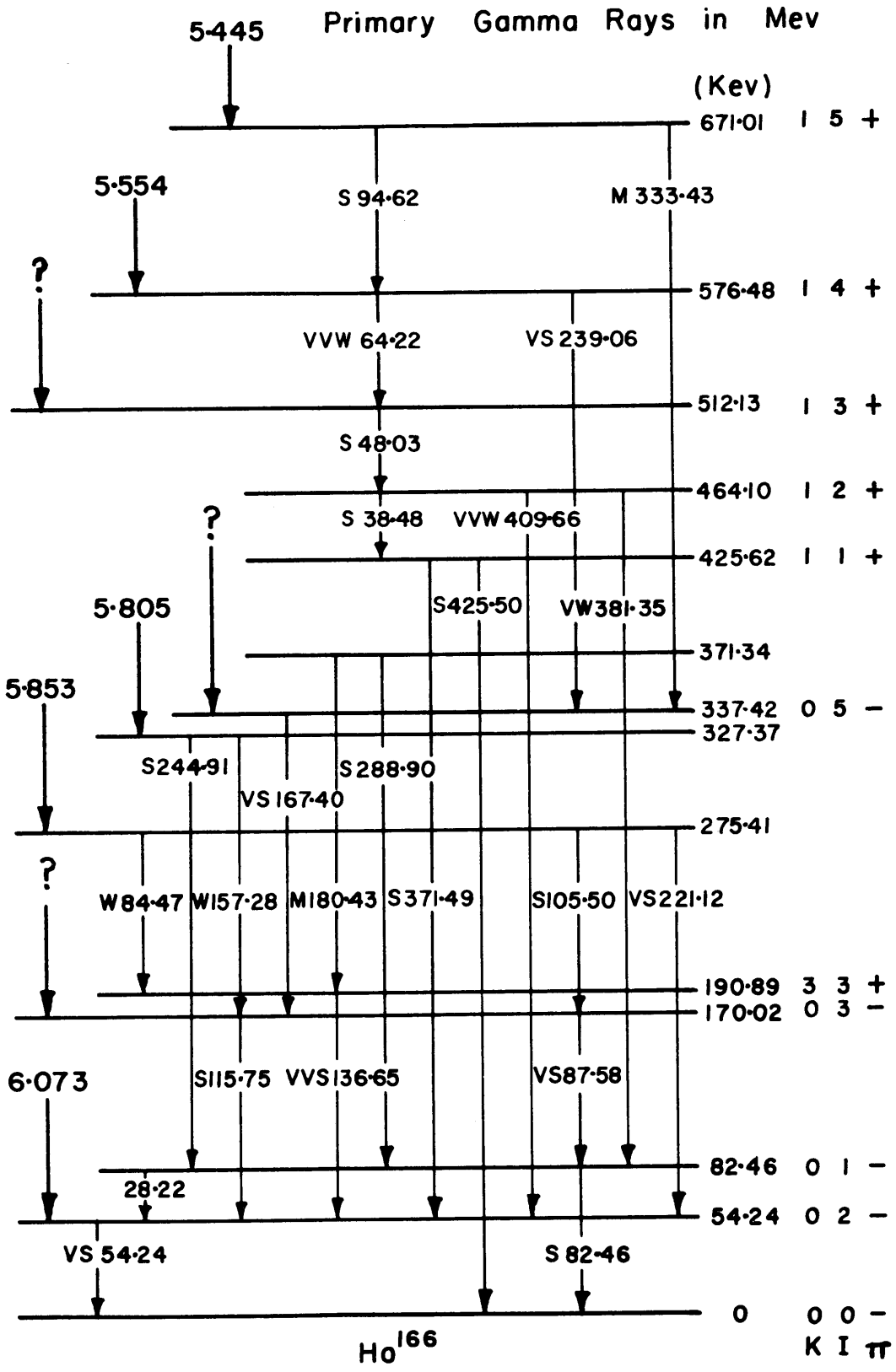

FIG 39. PROPOSED POSSIBLE NUCLEAR ENERGY LEVEL SCHEME OF Ho^{166}

it may be (2−, 2+, 3−, 3+, . . . 5− or 5+). Since it decays to 3+, 3− and 2− levels again, probably by an E1 transition, one may suspect an assignment of 3+ or 3− to the 275 kev level. This level then does not appear to allow assignment of its last two nucleons to the Nilsson orbits mentioned earlier.

CHAPTER 8
CONCLUSIONS AND RECOMMENDATIONS FOR FUTURE WORK

8.1

In the course of this thesis, a comprehensive system has been developed for the determination of neutron-capture gamma-ray spectra by means of bent crystal spectroscopy. This system includes the physical equipment to develop emulsion plates exposed on the bent crystal spectrometer and the perfection of a technique to give good processing. A systematic approach to the reading of these plates has been developed and computer codes have been written to perform the analysis of the readings. In addition, there is now a better understanding of the size of the source needed in relation to its absorption cross section and the available neutron flux. The capability to do this kind of work is considerably improved over the state of the art that existed at the commencement of this work, as exemplified by Kazi (K2).

A comparison can be made with the results that are obtained on the Cauchois type instrument here at M.I.T., and the results obtained from a Dumond type instrument. The latter instrument is a much more costly machine because of the expensive and complicated mechanism required to keep the detector at the correct angle to the crystal as the crystal itself is rotated. It has the advantages that intensity measurements are readily made and that greater precision can be obtained. The greater precision occurs because the Cauchois instrument requires a positive image to be made of the lines. The image is recorded on an emulsion plate, then removed from the spectrometer for processing. This allows various distortions to arise in the image by the time it is read on the comparator. This distortion has been shown to be a random positional fluctuation of about 20 microns. The effect is shown by comparing the author's rhodium data with that of Buschhorn (B1). A new cold developing method for emulsions is being tried at M.I.T. in order to minimize the suspected distortion from processing. Preliminary results have already indicated that the rate at which the emulsion is dried must also be reduced. The conclusion also has been made that

intensity measurements made on the Cauchois instrument by means of photo-density measurements on the emulsion are not at all satisfactory in the type of irradiations carried out in this work. The reasons are detailed in Chapter 5.

8.2

The work on scandium revealed how well the information from the bent crystal spectrometer could be combined with the data from the scintillation pair spectrometer. The latter instrument, located at Brookhaven National Laboratory, was developed by Fiebiger into an extremely capable facility. When coupled to the large two-dimensional analyzer, it permits a considerable amount of data to be recorded during any one run. The use of an IBM 7090 digital computer to reduce these data and to plot them has proved quite helpful and time-saving. The lack of a punched paper tape output from the analyzer reduces the efficiency of the system, since read-out time is longer and the output must be put on cards by hand.

Some conclusions about the operation of the pair spectrometer should be noted. Primarily, this instrument will give good results only if it is able to resolve well the high energy gamma rays. Secondly, the returns in improved statistics by increasing the count rates about normal limits, (0.6×10^6/min for crystal B and 2×10^6/min for crystal A, see Fig. 6), are not really justifiable. There tends to be some pulse pile-up and the stability becomes marginal. Finally, operating the spectrometer with external stabilizing sources proved to be very satisfactory. It is recommended that some low energy gamma-ray sources be available for calibrating the A crystal below 500 kev: the lack of such sources was most noticeable on the first run of Dy^{164}.

8.3

The combination of the data from the bent crystal spectrometer and from the pair scintillation spectrometer plus information from other sources has lead to the construction of a nuclear energy level scheme for Sc^{46}. This scheme looks very satisfactory and is, in fact, the most complete piece of work in this thesis. The level schemes for Ho^{166} and Dy^{165} cannot be regarded so highly and must be taken

as tentative only. The problem with the holmium was that its neutron capture gamma-ray spectrum was notable for its absence of intense high energy peaks, and the statistics for the measured runs were very poor. The problem with the dysprosium was that in both the pair spectrometer and the A crystal, the peaks comprised unresolved doublets or triplets and a unique decay pattern could not be established. With dysprosium, reasonable confidence may be expressed that a good scheme will be deduced when some definite levels have been established between 108 and 540 kev, perhaps by (d,p) excitation.

No definite contributions have been made here to the level schemes of Dy^{162}, Ir^{192} and Ir^{194}. Some additions to the existing level scheme of Rh^{104} have been noted here, which have reasonable substantiation. The superior data of Gruber, with a deeper analysis, should confirm the scheme of Fig. 31 and should provide for considerable extension.

8.4

The response function of the pair spectrometer has been determined in an empirical fashion, and its energy dependence has been calculated approximately. It would be extremely desirable to obtain the response function more accurately. It is suggested that a series of Monte Carlo calculations be made to calculate the response of a scintillation pair spectrometer of variable geometry to several monoenergetic gamma rays. The position and size of the central crystal of the instrument should be varied so that the optimum size and geometry may be determined. In addition, the exact functional dependence of the response may be calculated and a better comparison with measurements from an actual system may be made.

With the response function more accurately determined, more effort may be put into spectrum stripping techniques. The technique used in this thesis was not successful because it used too much computer time, and the uncertainty in the response did not justify further effort at the time. It is expected that more satisfactory results from spectrum stripping will be obtained using the procedure of Trombka (T1). Basically, his procedure is to determine the energy and intensity of line gamma rays whose over-all response fits the measured response

in a least squares manner subject to two restrictions. These restrictions are that no negative intensities may appear and that the number of line components is limited to 40 by computer storage. His results look most promising for the response of an ordinary scintillation spectrometer. The response of the pair spectrometer is much better because the peak is narrower on a percentage basis. In addition, the pair peak contains relatively more area than does the photo-peak of the scintillation spectrometer. Although the pair spectrometer is certainly not the most accurate instrument for measuring high energy gamma rays, it has good resolution coupled to a high efficiency (2×10^{-4}%). It is therefore able to measure the gamma-ray spectrum from the irradiation of separated isotopes in normal reactor fluxes, which can hardly be done with the more precise Compton magnetic spectrometer. Consequently, it seems very desirable to continue the spectrum stripping program in the manner outlined above.

8.5

The difficulty in analyzing the neutron-capture gamma-ray spectrum of a mono-isotopic source is good reason to conclude that the original idea of irradiating a multi-isotopic source such as germanium, in order to determine the level schemes of the individual isotopes, was impractical. However, it is feasible to obtain the line spectrum of a multi-isotope mixture by means of bent-crystal spectroscopy, and couple the results to the coincidence measurements from the scintillation pair spectrometer on each isotope. It is desirable, however, that there should be one principal isotope whose macroscopic cross section is 90% of the total cross section. The experiments performed on the bent-crystal spectrometer at M.I.T. have shown clearly that competitive results will be obtained only if one considers sources of reasonably high cross section and places them in a high flux location (10^{13} n/cms^2-sec). Elements that lend themselves to this sort of studies are titanium, manganese, cobalt*, silver*, indium, cesium, praesodymium*, terbium*, thulium*, lutetium, tantalum*, rhenium, gold* and thorium. Those elements marked with an asterisk may present handling problems, since they will be highly activated. It is not a truism to state that knowledge of the capture

gamma-ray spectrum of the principal isotope in these elements will be useful. It may lead to formulation of the level structure of the capture nuclei, and this will allow extension and refinement of models of the nucleus.

CHAPTER 9
LIST OF REFERENCES

A1. Ad'yasevich, B. P., L. V. Groshev, and A. M. Demidov. Soviet Journal of Atomic Energy 1, 183 (1956). Listed also in G1.

B1. Buschhorn, G. Zeitschrift für Naturforschung, 17a, 241 (1962).

B2. Burrus, W. R. IRE Transactions on Nuclear Science, Vol. INS-7, No. 2-3, February 25-26, 1960.

B3. Burson, S. B., and W. C. Rutledge. Phys. Rev. 86, 633A (1952).

B4. Bartholomew, G. A., and B. B. Kinsey. Phys. Rev. 89, 386 (1953). Listed also in G1.

B5. Bostrom, C. O., and J. E. Draper. Unpublished data, Yale University, 1962.

C1. Chupp, E. L., J. W. M. DuMond, F. J. Gordon, R. C. Jopson, and H. Mark. Phys. Rev. 112, 518 (1958).

C2. Cohan, M. D. Private communication of January 1962.

C3. Cohen, E. R., K. M. Crowe, and J. W. M. DuMond. The Fundamental Constants of Physics, Interscience Publishers, 1957.

C4. Chertok, B. T. S.M. Thesis, Nuclear Engineering Department, Massachusetts Institute of Technology, June 1960.

C5. Cauchois, Y., and H. Hulubei. Longeurs d'Orde des Émissions X et des Discontinuités d'Absorption X, Herman et Cie., Paris, 1947.

D1. DuMond, J. W. M. Spectroscopy of Nuclear Gamma Rays by Direct Crystal Diffraction Methods, p. 232-301, Ergebnisse der Exakten Wissenschaften, Springer Verlag, Berlin, 1955.

E1. Evans, R. D. The Atomic Nucleus, McGraw-Hill, 1955.

E2. Estulin, I. V., A. S. Melioranski, and L. F. Kalinkin. Nuc. Phys. 24, 118 (1961).

F1. Fiebiger, N. F. Private communication to H. Mark, sent on to N. C. Rasmussen, 15 February 1961.

F2. Fiebiger, N. F., N. C. Rasmussen, J. M. Neill, and I. Rahman. Bull. Amer. Phys. Soc., April 1962.

F3. Fiebiger, N. F., W. R. Kane, and R. E. Segel. Phys. Rev. 125, 2031 (1962).

LIST OF REFERENCES (Continued)

G1. Groshev, L. V., A. M. Demidov, V. N. Lutsenko, and V. I. Pelekhov. Atlas of Gamma-Ray Spectra from Thermal-Neutron Capture, Pergamon Press, 1959.

G2. Groshev, L. V., A. M. Demidov, and V. I. Pelekhov. Gamma-Ray Spectra Associated with Thermal-Neutron Capture by Nuclei of Mo, Nd, Ho, Tu and La, AEC-tr-4685.

G3. Gallagher, C. J., Jr., and V. G. Soloviev. Mat. Fys. Skr., Dan Vid Selsk 2, No. 2 (1962). In reference to the Ho^{166} nuclear energy level scheme, this reference cites an unpublished paper by C. J. Gallagher, Jr., O. B. Nielsen, O. K. Skilbreid, and A. W. Sunyar.

G4. Greenwood, R. C. Phys. Rev. 129, 345 (1963).

G5. Gruber, U. Private communication of January 1963.

H1. Hickson, P. J. Ph.D. Thesis, Physics Department, Massachusetts Institute of Technology, June 1963.

H2. House and First. Knolls Atomic Power Laboratory. Data given to the author in a private communication from the Brookhaven National Laboratory cross sections compilation group.

H3. Hildebrand, F. B. Introduction to Numerical Analysis, McGraw-Hill, 1956.

H4. Heath, R. L. Analysis of Complex Gamma-Ray Spectra. Symposium on application of computers to nuclear and radio-chemistry, Gatlinburg, Tennessee, October 18-19, 1962.

H5. Helmer, R. G., and S. B. Burson. Phys. Rev. 119, 788 (1960).

H6. Hammermesh, B. and V. Hummel. Phys. Rev. 88, 916 (1952).

I1. Inglestam, E. Nova Acta Reg. Soc. Sci. Upsalienis 4, No. 5 (1936). Listed also in C5.

J1. Jorgensen, M., O. B. Nielsen, and O. Skilbreid. Nuc. Phys. 24, 443 (1961).

J2. Johnson, W. H., Jr., and V. B. Bharat. Phys. Rev. 107, 1669 (1957).

J3. Johansson, K. E. Arkiv Fysik 10, 247 (1956).

LIST OF REFERENCES (Continued)

K1. Kazi, A. H., N. C. Rasmussen, and H. Mark. Rev. Sci. Instr. 31, 983 (1960).

K2. Kazi, A. H. Ph.D. Thesis, Nuclear Engineering Department, Massachusetts Institute of Technology, February 1961.

K3. Kinsey, B. B. and G. A. Bartholomew. Phys. Rev. 89, 375 (1953). Listed also in G1.

K4. Kinsey, B. B., G. A. Bartholomew, and W. H. Walker. Phys. Rev. 82, 380 (1951). Listed also in G1.

K5. Kalinkin, L. F., A. S. Melioranski, and I. V. Estulin. Soviet JETP 42, 1149 (1962).

L1. Lind, D. A., W. J. West, and J. W. M. DuMond. Phys. Rev. 77, 475 (1950).

L2. Lindquist, T. Arkiv Fysik 6, 123 (1953).

M1. Motz, H. T. and R. E. Carter. P. 299, Proceedings of the international conference on nuclidic masses, McMaster University, 1960. Edited by H. E. Duckworth, University of Toronto Press, 1960.

M2. Mazari, M. Massachusetts Institute of Technology Laboratory for Nuclear Science, Progress Report, p. 44, November 1957.

M3. Muller, D. E., H. C. Hoyt, D. J. Klein, and J. W. M. DuMond. Phys. Rev. 88, 775 (1952).

M4. Mollenauer, J. F. UCRL 9748.

M5. Mihelich, J. W., B. Harmatz, and T. H. Handley. Phys. Rev. 108, 989 (1957).

M6. Mottelson, B. R. and S. G. Nilsson. Mat. Fys. Skr. Dan. Vid. Selsk. 1, No. 8 (1959).

M7. Marklund, I., and B. Lindstrom. Nuc. Phys. 40, 329 (1963).

N1. Neill, J. M. Thesis proposal to N. C. Rasmussen.

O1. Olness, J. W. Private communication of February 1963.

P1. Paik, N. C. S.M. Thesis, Nuclear Engineering Department, Massachusetts Institute of Technology, June 1962.

LIST OF REFERENCES (Concluded)

R1. Rahman, I. U. S.M. Thesis, Nuclear Engineering Department Massachusetts Institute of Technology, January 1962.

R2. Rose, H. J. Nuc. Phys. 19, 113 (1960).

R3. Rapaport, J. Ph.D. Thesis, Physics Department, Massachusetts Institute of Technology, June 1963. To be published in the Physical Review.

S1. Da Silva, A. G. Massachusetts Institute of Technology Laboratory for Nuclear Science, Progress Report, p. 11, November 1961.

S2. Schermer, R. I. Bull. Amer. Phys. Soc., April 1963.

S3. Struble, G. L., N. Shelton, and R. K. Sheline. Phys. Rev. Letters, 10, 58 (1963).

S4. Scofield, N. E. USNRDL-TR 447 (1960).

S5. Segel, R. E. Phys. Rev. 111, 1620 (1958).

T1. Trombka, J. I. Jet Propulsion Laboratory Technical Report, TR 32-373, December 1962.

W1. deWaard, H. Nucleonics 13, No. 7, p. 36 (1955).

APPENDIX I

DATA REDUCTION METHODS FOR THE BENT CRYSTAL SPECTROMETER

I.1

In this appendix, the methods of analysis of the emulsion plates from the bent crystal spectrometer are discussed. The various types of errors that enter the problem are considered in terms of their magnitude and how they enter the analysis. Finally, a description is given of the computer codes that have been written to perform these analyses on the IBM 7090 computer.

As a preliminary, the linearization of the functional dependence of the wavelengths with position is shown. Figure 40 shows an illustration of the bent crystal geometry in which the crystal is bent so that its internal 310 planes, normal to its face, point towards a common focus called the beta point. The figure also shows that the crystal subtends an angle α to the beta point. If two gamma rays of the same energy E are incident upon the crystal edges at the Bragg angle θ, they will be totally reflected to a point P to which the crystal must subtend the same angle α. A well known geometrical theorem states that the locus of a point P, to which two given points subtend a constant angle α, is a circle which passes through these points. Since this must be true for any section of the crystal, then any gamma ray of energy E, incident on the crystal at the Bragg angle θ, will be reflected to point P. This, in effect, is the principle of the bent crystal spectrometer. It can be seen that the diameter R of this focal circle is equal to the bending radius of the crystal. When an emulsion is placed along the focal circle, discrete lines will appear on it, corresponding to discrete gamma-ray energies in the incident beam.

If a photon whose wavelength is λ, is incident on an internal 310 plane of the crystal at angle θ, it will be reflected at angle θ if the Bragg law is satisfied:

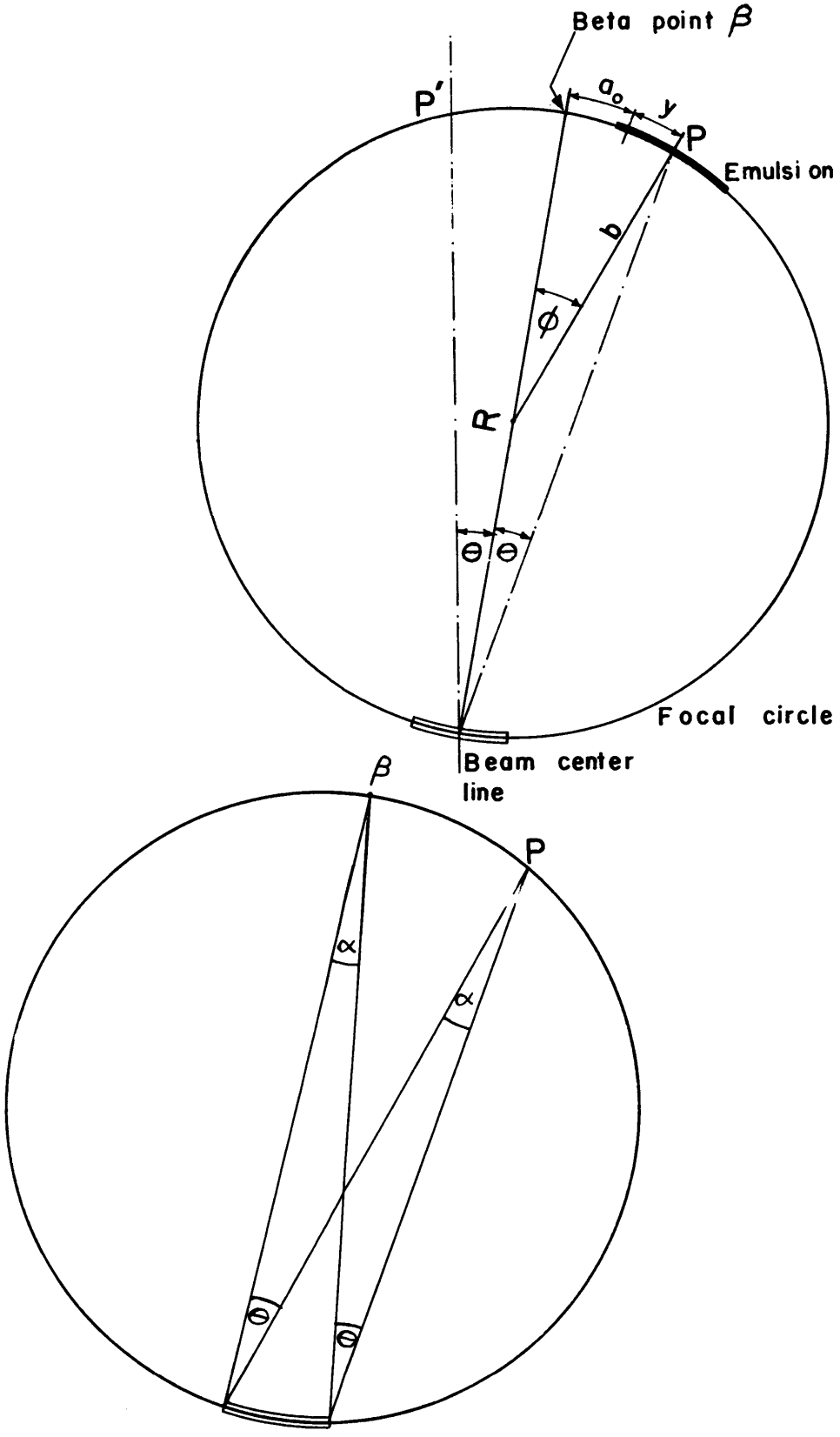

FIG 40. BENT CRYSTAL GEOMETRY

$$\lambda = 2d \sin \theta , \tag{I.1.1.}$$

where d is the spacing between the 310 planes. Note that no corrections to the Bragg angle due to changes of refractive index are necessary in this geometry. This is because the photon wavelength inside the crystal changes exactly to compensate for the variation of the refractive index.

Now, from geometrical considerations as seen in Fig. 40,

$$\phi = 2\theta , \tag{I.1.2}$$

$$R = 2b \tag{I.1.3}$$

and

$$\frac{a_o + y}{b} = \phi , \tag{I.1.4}$$

where a_o is the distance from the beta point to a reference position on the emulsion plate, and y is the distance of a line on the emulsion plate from the reference position.

Equations (I.1.1) to (I.1.4) are combined to give

$$\frac{\lambda}{2d} = \sin\left(\frac{a_o + y}{R}\right) . \tag{I.1.5}$$

This equation can be linearized to give

$$y = a_o + a_1 x \tag{I.1.6}$$

where

$$x = \text{arc sin}\left(\frac{\lambda}{2d}\right) \tag{I.1.7}$$

and

$$a_1 = R . \tag{I.1.8}$$

Although a_1 is a physical quantity, it is more easily calculated than measured. Calibration of the emulsion plate is made by fitting a straight line in the least-squares sense to several values of y for known values of x in order to obtain the coefficients a_o and a_1.

The crystal must be bent to a radius equal to the diameter of the focal circle. The center of the crystal should lie on the focal circle, but this requirement is not compatible with the first one which is more important. That the crystal does not lie true on the focal circle gives rise to a geometrical distortion at large wavelengths. An expression for this geometrical error is derived by Dumond (D1) as a wavelength change,

$$\frac{\delta\lambda}{\lambda} = \frac{\cos\theta\left(1-\cos\frac{\alpha}{2}\right)}{\cos\left(\frac{\alpha}{2}+\theta\right)} \simeq \frac{1}{8}\alpha^2, \quad \text{for small } \alpha \text{ and } \theta, \qquad \text{(I.1.9)}$$

and has a value of about 3×10^{-5} in the worst case. This distortion is manifested by thicker lines on the emulsion plate. Hence, this geometrical error is automatically taken into account in the analysis, since the center of these thick lines is more uncertain due to larger reading errors.

A second geometrical distortion is that as the crystal is bent, the spacing of the planes nearest the convex edge increases while the spacing of the planes nearest the concave edge decreases. Consider a point distance Z from the neutral axis of the crystal towards the convex side. The spacing of the 310 planes d_1 will be given by

$$d_1 = d\left(1+\frac{Z}{R}\right). \qquad \text{(I.1.10)}$$

For a line at the same point on the emulsion, the Bragg angle θ_1 is

$$\theta_1 = \theta\left(\frac{1}{1+\frac{Z}{R}}\right). \qquad \text{(I.1.11)}$$

Hence, the corresponding wavelength λ_1 is

$$\lambda_1 = 2d_1 \sin\theta_1 \qquad \text{(I.1.12)}$$

or

$$\lambda_1 = 2d\left(1+\frac{Z}{R}\right)\sin\left(\theta\left[\frac{1}{1+Z/R}\right]\right). \qquad \text{(I.1.13)}$$

If we expand the sine function in Eqs. (I.1.1) and (I.1.13) in a Taylor series, neglect the third and succeeding terms in the expansion and subtract, we get

$$\lambda - \lambda_1 = 2d\,\frac{\theta^3}{3!}\left[\frac{1}{(1+Z/R)^3} - 1\right] \qquad \text{(I.1.14)}$$

Equation (I.1.14) can be simplified by expansion and normalized by division of the linear expansion of Eq. (I.1.1) to give

$$\frac{\lambda - \lambda_1}{\lambda} = \frac{- Z\theta^2}{2R} . \qquad \text{(I.1.15)}$$

This factor is very small and will not be greater than 10^{-5}, even at the largest Bragg angles capable on the bent crystal spectrometer. In practice, the error is directional and would manifest itself again as a broadening of the lines on the emulsion plate, so that it is automatically taken into account as an increased line position error.

A third geometrical error arises from any incorrect positioning of the focal plate in the original line-up. This type of error will manifest itself by broader lines on the emulsion and a poorer fit of the calibration points to Eq. (I.1.6). The latter is a common feature of errors (a), (b), and (c) below.

Three errors of importance are as follows:

(a) A significant temperature variation between the reactor room where the plate is exposed and the room where the plate is read. A temperature difference of 10°C would result in an over-all expansion of the plate by 30 microns, which is about twice the reading error of one line. It is considered good practice, therefore, to read the plates in a room that is air-conditioned as is the reactor.

(b) The uniform stretching of the emulsion from its position on the circular focal plate to its flat position on the comparator where it is read. This occurs because the emulsion plate bends about its neutral axis which lies in the glass and not in the emulsion.

(c) Improper fastening of the emulsion plate. If the plate is not bound properly on the focal circle, then an error arises since Eq. (I.1.5) does not truly apply.

These three errors have one thing in common, which is that they arise because the functional dependence of wavelengths and position is no longer obeyed rigorously. An error of this type can be seen by the way the residuals in Eq. (I.1.6) are distributed about the mean line. Their distribution should be Gaussian if the functional dependence is correct, but a systematic distribution is suspicious. A chi-squared test can be performed on these residuals as a check. To some extent, this type of error is accounted for in the error analysis by the inclusion of an uncertainty in the crystal plane spacing d. Although this uncertainty is a real physical uncertainty which further justifies

its inclusion, it is not necessary mathematically in the analysis. Of the three errors discussed, (c) is considered the most significant.

A minor error worth mentioning, but not of importance, is the temperature fluctuation in the reactor room of up to 3°C which may distort the spectrometer frame. This distortion will broaden the line thickness, particularly at large Bragg angles, but is automatically taken into account by an increased reading error.

A possible error is distortion of the emulsion during developing and fixing, and for some spectroscopists, this item becomes the residue of all unknown errors. The distortion implied here is a local distortion that is not positionally dependent. Kazi (K2) does not report any significant emulsion movement from an experiment designed specifically to check this point. In addition, Cohan (C2) finds a high degree of correlation between front and back plates of any pair, although they were developed in different batches; and this implies little error due to development distortion. Nevertheless, there is good evidence presented in Sections 5.3 and 5.4 to indicate a positional error on each line that is additional to the reading errors. Whether this is due to emulsion distortion is not at all clear but its magnitude is about 20 microns.

Errors that are taken into account in the formal computer analysis are reading errors, uncertainties in the calibration wavelengths, uncertainty in crystal plane spacing, and a term σ_T to account for unknown errors. σ_T is put in the form of an additional position uncertainty in each line to conform with the treatment by Kazi. It had been intended originally to average several independent values for a given gamma ray and obtain the standard deviation from the set and so avoid concern about unknown errors. This procedure would not have been satisfactory, since a higher weight would be given to calibration lines with small reading errors on each plate and incorrect calibration of each plate would be obtained. Consequently, the positional uncertainty of 20 microns that has been observed is inserted as σ_T in each plate analysis.

One further error must be discussed, which is classified as an unknown error, since it is not taken into account by the error analysis. This error comes from the variation in backlash of the precision screw in the comparator. When a set of lines is read, each side of each line should be read to obtain the central position. In principle, the backlash

can be avoided by making the measurements all in one direction. In practice, it is extremely difficult to measure the second edge of a dark line by moving in the direction across the line. Consequently, the edge of each line is measured by approaching the line. The backlash of the comparator screw enters the measurement and directly affects the measured line widths. However, the analysis makes allowance for a systematic error of this sort, provided it is constant over the whole range. Demanding that the backlash be of constant magnitude over the length of the screw is not a particularly excessive requirement so this error is not considered significant. Good practice, however, demands that the backlash be as small as possible, since useful information is lost by the incorrect measurement of the line width.

I.2

A systematic analysis of the data depends on data being taken in a systematic manner. Most of the plates are read in the following way:

(a) The plate is inspected visually under a strong light and each line is marked and labelled. It is easier to observe lines this way rather than on the comparator because the eye has an integrating effect.

(b) The plate is fastened down temporarily on the comparator, emulsion side up, and the viewing light is switched on.

(c) A low magnification is selected, usually 0.4×6.7, and correct focus is selected by moving the microscope vertically until no parallax is observed.

(d) The emulsion is then put against the horizontal adjusting bar, its lines all within the comparator range, and is lined up. Line-up is achieved by sweeping the carriage, on which the plate is mounted, perpendicular to the screw direction. The emulsion is moved via the adjusting bar until no movement of the edge of a good line, relative to the center of the cross hairs in the microscope, is seen. The plate is then fastened securely to the carriage.

(e) The cross hairs in the microscope are rotated if necessary until the vertical one is parallel to the edge of the good line.

(f) Ten readings of the plate are taken as follows:

1. The plate is read from left to right near its bottom.
2. The plate is read from right to left near its top.

3. The plate is moved horizontally a small amount, its line-up is checked and steps 1 and 2 are repeated.
4. The plate is moved horizontally a small amount, its line-up is checked and step 1 is repeated.
5. The plate is then rotated by 180° , its line-up is checked and steps 1 to 4 are repeated.

(g) The distances of the center of each line, relative to the center of one good line, are then calculated by hand for each set of readings. These data are inspected for gross reading errors and arithmetic errors. Discrepancies looked for are an excessive range in the readings of one line and bad line widths. For reference, the readings of a good line should not range by more than 150 microns. The width of a good gamma-ray line is usually 250 to 450 microns, though an X-ray line may be up to 800 microns in width. This hand calculation is considered desirable at this stage because some judgment is required by the interpreter, which is difficult to program into the computer.

(h) The emulsion is 30 cm long and the comparator range is 25 cm. It is thus possible for some lines to be outside the comparator range. These lines are measured in another set of readings plus one good line in the original set. The distances between these lines and the one good line are calculated for each plate reading. These distances are then added to consecutive readings of the good line in the original set. In this way, the greater uncertainty of the extra lines is reflected in their larger reading errors.

I.3

The computer adjusts each set of readings to a common reference point, which is the centroid of the sum of the good lines. This centroid has the property that the sum of the square of the residuals at the good lines is a minimum. Let there be M good lines on the plate. Any line whose central position is g_i will have been read N times. The i^{th} adjusted reading of the j^{th} line is given by

$$g'_{i,j} = \frac{1}{M}\left[\frac{1}{N}\sum_{i}^{N}\sum_{j}^{M} g_{i,j} - \sum_{j}^{M} g_{i,j}\right] + g_{i,j} \,. \qquad \text{(I.3.1)}$$

In this connection, a good line implies a line that is strong enough to be well read. In practice, a very dark line can prove difficult to read accurately. In addition, a line that is extremely weak and uncertain may have small reading errors because its identifying mark was measured instead. It can scarcely be classed as a good line either. The criterion for a well-read line is that the range of its readings is less than 150 microns. The readings are then averaged, so that the mean reading f of the j^{th} line is given by

$$f_j = \frac{1}{N} \sum_{i}^{N} g'_{i,j} \, . \tag{I.3.2}$$

The variance of the mean of these readings is

$$\sigma^2(f_j) = \frac{1}{N(N-1)} \sum_{i}^{N} (g'_{i,j} - f_j)^2 \, , \tag{I.3.3}$$

and $\sigma(f_j)$ is the standard deviation of f_j.

The uncertainty in the mean position of each line is increased by errors either unknown or unmeasured but whose standard deviation is represented by a positional error σ_T. Hence, the variance of the k^{th} line becomes

$$\sigma^2(y_k) = \sigma^2(f_k) + \sigma_T^2 \tag{I.3.4}$$

with y_k now replacing f_k.

I.4

In this section, the analysis for a plate with two or more calibration lines on it is discussed, type (a) of Section 3.2.

From Section I.1, the linearized relationship for the position of line k was obtained as

$$-a_o + a_1 x_k = y_k \tag{I.4.1}$$

The coefficients, a_o and a_1, are obtained from the solution of the normal equations relevant to the set of Eq. (I.4.1). The normal equations are obtained by multiplying each member of Eq. (I.4.1) by its weight w_k, by multiplying by the coefficient of a_o or a_1 and adding the set. This gives

$$-a_o \sum_k^{NCL} w_k + a_1 \sum_k^{NCL} w_k x_k = \sum_k^{NCL} w_k y_k \qquad \text{(I.4.2)}$$

and

$$-a_o \sum_k^{NCL} w_k x_k + a_1 \sum_k^{NCL} w_k x_k^2 = \sum_k^{NCL} w_k x_k y_k \qquad \text{(I.4.3)}$$

where NCL is the number of calibration lines. The weight w_k associated with each equation is the inverse of the sum of the variances in each equation, normalized by the sum of all the variances, i.e.,

$$w_k = \frac{1}{\sigma_k^2} \Bigg/ \sum_k^{NCL} \frac{1}{\sigma_k^2}, \qquad \text{(I.4.4)}$$

with

$$\sigma_k^2 = \sigma^2(y_k) + a_1^2 \sigma^2(x_k). \qquad \text{(I.4.5)}$$

$\sigma^2(y_k)$ is defined by Eq. (I.3.4) and $\sigma^2(x_k)$ by Eq. (I.4.6) below if we assume no correlation between errors in λ_k and d.

$$\sigma^2(x_k) = \left[\sigma^2(\lambda_k) + \sigma^2(d)\,\frac{\lambda_k^2}{d^2}\right] \Bigg/ \left(4d^2 - \lambda_k^2\right). \qquad \text{(I.4.6)}$$

Since a_1 appears in the weighting function, direct solution of Eqs. (I.4.2) and (I.4.3) is difficult and they are consequently solved by iteration on a_1.

If Eqs. (I.4.2) and (I.4.3) are rewritten in matrix form, we obtain:

$$\begin{bmatrix} B_{11} & B_{12} \\ B_{21} & B_{22} \end{bmatrix} \begin{bmatrix} -a_o \\ a_1 \end{bmatrix} = \begin{bmatrix} E_1 \\ E_2 \end{bmatrix} \qquad \text{(I.4.7)}$$

where

$$B_{11} = \sum_k^{NCL} w_k = 1, \qquad \text{(I.4.8)}$$

$$B_{12} = B_{21} = \sum_k^{NCL} w_k x_k, \qquad \text{(I.4.9)}$$

$$B_{22} = \sum_k^{NCL} w_k x_k^2, \qquad \text{(I.4.10)}$$

$$E_1 = \sum_{k}^{NCL} w_k y_k , \tag{I.4.11}$$

and

$$E_2 = \sum_{k}^{NCL} w_k x_k y_k . \tag{I.4.12}$$

The solution of Eq. (I.4.7) is

$$a_o = \frac{B_{12}E_2 - B_{22}E_1}{D} , \tag{I.4.13}$$

where D is the determinant of the B matrix and is given by

$$D = B_{11}B_{22} - B_{12}B_{21} . \tag{I.4.14}$$

Hence,

$$a_1 = \frac{E_1 + a_o B_{11}}{B_{12}} . \tag{I.4.15}$$

Using a_1 and a_o, the wavelength λ_m of the unknown line is

$$\lambda_m = 2d \sin\left(\frac{a_o+u_m}{a_1}\right) \tag{I.4.16}$$

where u_m = the mean comparator reading of the center of the m^{th} unknown line. The error in λ_m is obtained as follows. On differentiating Eq. (I.4.16), we get

$$\delta\lambda_m = 2 \sin\left(\frac{a_o+u_m}{a_1}\right) \delta d + 2d \cos\left(\frac{a_o+u_m}{a_1}\right)\left\{\frac{\delta a_o + \delta u_m}{a_1} - \frac{(a_o+u_m)\delta a_1}{a_1^2}\right\} . \tag{I.4.17}$$

We may square both sides of this equation and ignore cross product terms of uncorrelated variables. Replacing the squared-error terms by the square of the standard deviation gives

$$\sigma^2(\lambda_m) = 4\sigma^2(d) \sin^2\left(\frac{a_o+u_m}{a_1}\right) + 4d^2 \cos^2\left(\frac{a_o+u_m}{a_1}\right)\left\{\frac{\sigma^2(a_o) + \sigma^2(u_m)}{a_1^2} + \right.$$

$$\left. + \frac{(a_o+u_m)^2 \sigma^2(a_1)}{a_1^4} - \frac{2r\sigma(a_o)\sigma(a_1)\cdot(a_o+u_m)}{a_1^3}\right\} . \tag{I.4.18}$$

In Eq. (I.4.18), $\sigma^2(u_m)$ is the variance in u_m due to both reading and unknown errors analogous to $\sigma^2(y_k)$ of Eq. (I.3.4).

A correlation factor r between a_o and a_1 now appears because those parameters are obtained from the same information. We now calculate $\sigma(a_o)$, $\sigma(a_1)$ and r for substitution into Eq. (I.4.18). It is simpler to quote the results than derive them here from the general expression given by Hildebrand (H3, Page 266).

$$\sigma^2(a_o) = \frac{B_{22}}{D \sum_{k}^{NCL} \frac{1}{\sigma_k^2}} \tag{I.4.19}$$

$$\sigma^2(a_1) = \frac{B_{11}}{D \sum_{k}^{NCL} \frac{1}{\sigma_k^2}} \tag{I.4.20}$$

The correlation factor r can be derived in our case from a more general expression given by Cohan (C3, Page 243). It is

$$r = \frac{B_{12}}{\sqrt{B_{22}B_{11}}}. \tag{I.4.21}$$

If the calibration lines provide a poor fit to Eq. (I.4.1), then the residuals given by

$$R_k = a_o + y_k - a_1 x_k \tag{I.4.22}$$

may be comparable to the error σ_k associated with the parameters in that equation. (See Eq. I.4.5.) Consequently, the weighted mean-square error, $(wE^2)_m$, given by

$$(wE^2)_m = \frac{1}{\sum_{k}^{NCL} \frac{1}{\sigma_k^2}} \tag{I.4.23}$$

is replaced by the estimate below, as indicated by Hildebrand (H3, Page 267), if the latter is larger.

$$(wE^2)_m \simeq \frac{1}{(NCL-2)} \sum_{k}^{NCL} w_k R_k^2 \tag{I.4.24}$$

Clearly an estimate such as this is not possible when only two calibration lines are used.

I.5

The analysis for the case in which only one calibration line is available, type (b) of Section 3.2, is now considered. In this case, the focal length of the bent crystal a_1 and its standard deviation $\sigma(a_1)$ must be fed in as input parameters. In general, these parameters will be available from cases with two or more calibration lines. a_o is immediately determined as

$$a_o = a_1 \arcsin\left(\frac{\lambda_o}{2d}\right) - y_o, \tag{I.5.1}$$

using the nomenclature of the last section and λ_o = calibration line wavelength at position y_o.

Differentiating Eq. (I.5.1), we obtain

$$\delta a_o = \delta a_1 \arcsin\left(\frac{\lambda_o}{2d}\right) - \delta y_o + a_1\left(\frac{\delta\lambda_o}{2d} - \frac{\lambda_o \delta d}{2d^2}\right)\left(1 - \left[\frac{\lambda_o}{2d}\right]^2\right)^{1/2} \tag{I.5.2}$$

or

$$\delta a_o = a_1\left[\frac{\delta\lambda_o - 2\delta d \sin\left(\frac{a_o+y_o}{a_1}\right)}{2d\cos\left(\frac{a_o+y_o}{a_1}\right)} - \frac{\delta y_o}{a_1} + \frac{(a_o+y_o)}{a_1^2}\delta a_1\right]. \tag{I.5.3}$$

The wavelength of an unknown line λ_m is determined from Eq. (I.4.16) as before, and we can substitute for δa_o into Eq. (I.5.4) to find $\delta\lambda_m$ as

$$\delta\lambda_m = 2\delta d\left[\sin\left(\frac{a_o+u_m}{a_1}\right) - \frac{\sin\left(\frac{a_o+y_o}{a_1}\right)\cos\left(\frac{a_o+u_m}{a_1}\right)}{\cos\left(\frac{a_o+y_o}{a_1}\right)}\right]$$

$$+ 2d\cos\left(\frac{a_o+u_m}{a_1}\right)\left[\left(\frac{\delta u_m - \delta y_o}{a_1}\right) + \frac{\delta a_1}{a_1^2}(y_o - u_m)\right]$$

$$+ \delta\lambda_o \cos\left(\frac{a_o+u_m}{a_1}\right) \Big/ \cos\left(\frac{a_o+y_o}{a_1}\right). \tag{I.5.4}$$

We now square both sides of the above equation and treat all variables as independent parameters. Replacing the squared-error terms by the square of the standard deviation gives

$$\sigma^2(\lambda_m) = \frac{4\sigma^2(d)}{\cos^2\left(\frac{a_o+y_o}{a_1}\right)} \sin^2\left(\frac{u_m-y_o}{a_1}\right) + \frac{\sigma^2(\lambda_o)\cos^2\left(\frac{a_o+u_m}{a_1}\right)}{\cos^2\left(\frac{a_o+y_o}{a_1}\right)}$$

$$+ 4d^2 \cos^2\left(\frac{a_o+u_m}{a_1}\right)\left[\frac{\sigma^2(y_o)+\sigma^2(u_m)}{a_1^2} + \frac{\sigma^2(a_1)}{a_1^4}(y_o-u_m)^2\right]. \tag{I.5.5}$$

I.6

In this section, the case is considered in which there is at least one calibration line and there is at least one pair of known or unknown lines straddling the beta point of the bent crystal spectrometer, i.e., case (c) of Section 3.2.

If we have NCLP calibration line pairs denoted by Y_{1i} and Y_{2i} and NULP unknown line pairs denoted by U_{1j} and U_{2j}, we can obtain a_o of Eq. (I.1.6) in the following way:

$$AO_i = \frac{1}{2}(Y_{1i}+Y_{2i}), \tag{I.6.1}$$

$$AO_j = \frac{1}{2}(U_{1j}+U_{2j}). \tag{I.6.2}$$

Hence, we get

$$a_o = \frac{\sum_{i}^{NCLP} w_i AO_i + \sum_{j}^{NULP} w_j AO_j}{\sum_{k}^{NP} w_k} \tag{I.6.3}$$

where

$$NP = NCLP + NULP \tag{I.6.4}$$

and

$$w_k = \frac{1}{\sigma_k^2} \Big/ \sum_{k}^{NP} \frac{1}{\sigma_k^2}. \tag{I.6.5}$$

Here, σ_k is shorthand for $\sigma(y_i)$ and $\sigma(u_j)$, with these defined here as

$$\sigma^2(y_i) = \frac{1}{4}\left[\sigma^2(Y_{1i})+\sigma^2(Y_{2i})\right] \tag{I.6.6}$$

and

$$\sigma^2(u_j) = \frac{1}{4}\left[\sigma^2(U_{1j})+\sigma^2(U_{2j})\right]. \tag{I.6.7}$$

In addition, we obtain

$$\sigma^2(a_o) = \frac{1}{\sum_k^{NP} \frac{1}{\sigma_k^2}} . \tag{I.6.8}$$

Equations (I.6.6) and (I.6.7) are derived from Eqs. (I.6.9) and (I.6.10), respectively:

$$y_i = \frac{1}{2}(Y_{1i}-Y_{2i}), \tag{I.6.9}$$

$$u_j = \frac{1}{2}(U_{1j}-U_{2j}). \tag{I.6.10}$$

If these pairs of lines do not straddle the beta point consistently, we express $\sigma^2(a_o)$ in terms of the residuals R_k as in Eq. (I.6.11) if the latter is larger:

$$\sigma^2(a_o) \simeq \frac{\sum_k^{NP} w_k R_k^2}{(NP-1)\sum_k^{NP} w_k}, \tag{I.6.11}$$

where

$$R_k = AO_k - a_o. \tag{I.6.12}$$

Because the pairs of lines do not straddle the beta point exactly in practice, there is an additional uncertainty in the mean distance from the beta point to the average pair line. This added uncertainty is

accounted for by replacing $\sigma^2(y_i)$ and $\sigma^2(u_j)$ from Eqs. (I.6.6) and (I.6.7) by $\{\sigma^2(y_i)+\sigma^2(a_o)\}$ and $\{\sigma^2(u_j)+\sigma^2(a_o)\}$, respectively.

From Eq. (I.6.9) we have the distance of a paired calibration line from the beta point. Equation (I.6.13) gives the distance of a single calibration line from the beta point as

$$y_j = z_j + a_o , \qquad \text{(I.6.13)}$$

where z_j is the mean reading for the j^{th} single calibration line. The variance of this distance is given by

$$\sigma^2(y_j) = \sigma^2(z_j) + \sigma^2(a_o) . \qquad \text{(I.6.14)}$$

The distance of an unknown single line u_j and its variance are defined similarly to y_j above. We can now calculate a_1 of Eq. (I.1.6) as

$$a_1 = \frac{\sum_{k}^{NCL} \rho_k x_k y_k}{\sum_{k}^{NCL} \rho_k x_k^2} , \qquad \text{(I.6.15)}$$

where x is defined in Eq. (I.1.7) and the weighting function ρ_k is defined by

$$\rho_k = \frac{\frac{1}{\sigma_k^2}}{\sum_{k}^{NCL} \frac{1}{\sigma_k^2}} \qquad \text{(I.6.16)}$$

with σ_k defined by Eq. (I.4.5). In addition, NCL is the effective number of calibration lines and comprises the sum of NCLP calibration line pairs and NCLS calibration line singles.

A solution to Eq. (I.6.16) is found by iterative methods since ρ is a function of a_1. The variance of a_1 is then given by

$$\sigma^2(a_1) = \frac{1}{\sum_{k}^{NCL} \frac{x_k^2}{\sigma_k^2}} . \qquad \text{(I.6.17)}$$

Here again, if a_1 is not well fitted in the procedure, the variance of a_1 is replaced by that in Eq. (I.6.18) if the latter is larger.

$$\sigma^2(a_1) \simeq \frac{\sum_{k}^{NCL} \left(\frac{y_k}{x_k} - a_1\right)^2 \rho_k}{(NCL-1) \sum_{k}^{NCL} \rho_k} . \qquad (I.6.18)$$

We now obtain the wavelength of unknown lines λ_m as

$$\lambda_m = 2d \sin\left(\frac{u_m}{a_1}\right) . \qquad (I.6.19)$$

Differentiating, we obtain

$$\delta\lambda_m = 2\delta d \sin\left(\frac{u_m}{a_1}\right) + 2d \cos\left(\frac{u_m}{a_1}\right)\left[\frac{\delta u_m}{a_1} - \frac{u_m \delta a_1}{a_1}\right] . \qquad (I.6.20)$$

If we now square both sides of the above equation and replace squared-error terms by the appropriate variances, the variance of λ_m is then given by

$$\sigma^2(\lambda_m) = 4\sigma^2(d) \sin^2\left(\frac{u_m}{a_1}\right) + \frac{4d^2}{a_1^2} \cos^2\left(\frac{u_m}{a_1}\right)\left[\sigma^2(u_m) + \frac{u_m^2 \sigma^2(a_1)}{a_1^2}\right] . \qquad (I.6.21)$$

It is to be noted that there is no correlation between u_m and a_1.

I.7

Having calculated the wavelength λ_m of an unknown line and its standard deviation $\sigma(\lambda_m)$, a conversion to energy E_m must be made. This conversion is

$$E_m = \frac{K}{\lambda_m} , \qquad (I.7.1)$$

where K is the conversion coefficient and $\sigma(K)$ is its standard deviation, the values being given in Table 23. The variance of E_m is given by

$$\sigma^2(E_m) = \frac{1}{\lambda_m^2}\left[E_m^2 \sigma^2(\lambda_m) + \sigma^2(K)\right] . \qquad (I.7.2)$$

In addition to calculating the total uncertainty of the unknown lines E_m, a section is built into the computer codes for each case which calculates the standard deviation of E_m in the absence of reading errors and is denoted by SG. It has proved useful in that it shows that generally most of the calculated error arises from the uncertainty in the wavelength of the unknown lines and not from the reading errors.

No formal procedure has yet been devised for interpretation of the final values. If there are several values for one line, some sort of averaging procedure must be used to give a final answer. As mentioned before, the difficulties are that the standard deviation of the mean of several values is generally larger than the standard deviation of any one; and the values obtained on a front and back emulsion plate are by no means independent. In addition, some values may be suspect because the residuals are not placed randomly about the calibration lines for the plates from which those values come. In view of these factors, evaluation of the final values is necessarily subjective and cannot be formalized. Where possible, though, a mean is obtained from the sum of the individual values weighted with the inverse of their calculated variance. That is,

$$\bar{\lambda} = \frac{\sum_{i}^{NV} \frac{\lambda_i}{\sigma^2(\lambda_i)}}{\sum_{i}^{NV} \frac{1}{\sigma^2(\lambda_i)}}, \qquad \text{(I.7.3)}$$

where λ_i is the i^{th} value of wavelength of the same line, $\sigma(\lambda_i)$ is its calculated standard deviation and NV is the number of values of the one line. The variance of $\bar{\lambda}$ is obtained as

$$\sigma^2(\bar{\lambda}) = \frac{\sum_{i}^{NV} \frac{(\lambda_i - \bar{\lambda})^2}{\sigma^2(\lambda_i)}}{(NV-1) \sum_{i}^{NV} \frac{1}{\sigma^2(\lambda_i)}}. \qquad \text{(I.7.4)}$$

If only one value is obtained for a line, its standard deviation will be increased by a suitable factor usually between 2 and 3.

I.8

In this section, the inputs to the three codes for the three types of analysis are discussed. The order of the cards is as follows:

(a) Computation center identification card.
(b) Execution card.
(c) Binary cards representing the code instructions for the particular analysis type involved.
(d) Data indicator card.
(e) Data cards comprising the input information.

Card (a) above is a generalized identity card and has the following format:

*Problem number-programmer number, system type, run type, estimated time, maximum time, maximum number of lines output, maximum number of cards output.

The format above must be written with the following general rules:

1. * in Column 1.
2. Each field must be separated by a comma.
3. Blanks may be used freely.

The following specific rules must also be observed:

1. Problem and programmer numbers must be separated by a hyphen.
2. System type is FMS for monitor runs.
3. Admissable run types are DEBUG, TEST and RESULT. (The latter would generally be used in this case.)
4. Numerical values in the last four fields must all be integers.
5. Any room remaining after the last field may be used for comments.

An example of the above format is:

* M1876-646, RESULT, 1,2,1000,20 Mixed Batch.

Card (b) instructs the monitor to have the job executed and has an asterisk in Column 1 and the word XEQ punched in Columns 7 to 9.

Card (d) informs the monitor that data follow, and has an asterisk in Column 1 and the word DATA punched in Columns 7 to 10. The data cards contain the input information for the particular analysis type involved. They are written in one of the following formats:

1. Hollerith, H.
2. Alphanumeric, A.
3. Fixed point, F.
4. Integer, I.

Hollerith and alphanumeric data comprise English letters, Arabic numerals and other characters that appear on the key punch machine. Fixed point data are numbers that must be written with a decimal point. The location of these numbers in their field is immaterial, though. Integer numbers have no decimal point and must be placed at the right-hand side of their field.

The data cards for the three types of analysis (a), (b), (c) of Section 3.2 can be described in terms of the following blocks:

A. Identity card.
B. Control card.
C. Instrument parameter cards.
D. Calibration line positions.
E. Wavelength cards.
F. Unknown line positions.

Table 22 details this description. Samples of the input data for the three case types are given, followed by a sample of the output information as taken from the punched cards. Fortran listings are included of all the computer codes written to perform analysis of the bent crystal spectrometer data.

I.9

In this section, a detailed list of constants and physical parameters is given, together with the references.

Table 23 details crystal parameters and conversion factors. Table 24 details wavelengths of the gamma rays and X rays used as calibration standards. Sometimes the references quote the gamma rays in terms of energy, and conversion to wavelength in xu is made by the conversion factor K in Table 23.

Table 22. Input for Computer Analysis of Bent Crystal Spectrometer Data

Block	Case	Column Number	Item	Input Form	Code Symbol	Units
A	a,b,c	1-72	Identification. Plate number, isotope, energy range, date, etc.	H	-	-
B	a	1-10	Case type number (a) = 1	I	NOCASE	-
	b	1-10	Case type number (b) = 2	I	NOCASE	-
	c	1-10	Case type number (c) = 3	I	NOCASE	-
	a,b,c	11-20	Number of readings. Can be between 2 and 24.	I	NR	-
	a	21-30	Number of calibration lines.	I	NCL	-
	b	21-30	Number of good unknown lines.	I	NGUL	-
	c	21-30	Number of calibration line singles.	I	NCLS	-
	a	31-40	Number of good unknown lines.	I	NGUL	-
	b	31-40	Number of bad unknown lines.	I	NBUL	-
	c	31-40	Number of calibration line pairs.	I	NCLP	-
	a	41-50	Number of bad unknown lines.	I	NBUL	-
	b	41-50	Print option number. NPRNT1 = 0 or -ve. Punch out final data on cards. NPRNT1 = 0. Print out all useful data. |NPRNT1| = 1. Print out less of the intermediate data. |NPRNT1| > 1. Print out no intermediate data.	I	NPRNT1	-
	c	41-50	Number of good unknown line singles.	I	NGULS	-
	a	51-60	Print option number.	I	NPRNT1	-
	c	51-60	Number of good unknown line pairs.	I	NGULP	-
	c	61-70	Number of bad unknown lines.	I	NBUL	-
	c	71-80	Print option number.	I	NPRNT1	-

Table 22. (continued)

Block	Case	Column Number	Item	Input Form	Code Symbol	Units
C	a,b,c	1-12	Estimate of focal circle diameter.	F	A1	cms
	a,b,c	13-24	Standard deviation of focal circle diameter.	F	SIGA1	cms
	a,b,c	25-36	Spacing of crystal planes used. d.	F	D	xu
	a,b,c	37-48	Standard deviation of spacing d.	F	SIGD	xu
	a,b,c	49-60	Positional uncertainty from unknown errors. σ_T.	F	SIGT	cms
	b	61-72	Wavelength of the single calibration line.	F	WVLNTH	xu
	b	1-12	Standard deviation of wavelength.	F	SIGWL	xu
D	a	1-72	Reading I of calibration line J in a field width of 12 at 6 readings to a card for I = 1 to NR. A fresh card for each new line J on the emulsion is used.	F	Z(I,J)	cms
	b	1-72	As in (a) above. Pair lines come first and must be consecutive with the more positive value of the pair followed by the less positive one.	F	Z(I,J)	cms
	a,b	1-48	Identification card for the set of readings of calibration line J placed behind each set, [Z(I,J), I = 1, NR].	A	DNAM(J,K)	-
E	a,c	1-12	Wavelength #1 corresponding to calibration line #1, (single or pair).	F	WVLNTH(I)	xu
		13-24	Standard deviation of wavelength #1.	F	SIGWL(I)	xu
			Repeat the above two items in order for J = 2 to the total number of calibration wavelengths at 6 readings to a card in a field width of 12.	F F	WVLNTH(J) SIGWL(J)	xu xu

Table 22. (concluded)

Block	Case	Column Number	Item	Input Form	Code Symbol	Units
F	a,b	1-72	Reading I of unknown line J in a field width of 12 at 6 readings to a card for J = 1 to the total number of unknown lines. A fresh card for each new line on the emulsion is used. Good lines come before the bad lines.	F	W(I,J)	cms
	c	1-72	As in (a) and (b) above. Pair lines come first and must be consecutive with the larger value of the pair before the smaller.	F	W(I,J)	cms
	a,b,c	1-48	Identification card for the set of readings of unknown line J placed behind each set [W(I,J), I = 1, NR].	A	DNAME(J,K)	-

Table 23. Crystal Parameters and Conversion Factors.

Item	Value	Reference
Spacing of 310 planes in quartz at 68°C.	1177.67 xu	L2
Standard deviation of item above.	0.02 xu	L2
Conversion coefficient of wavelength to energy, K of Eq. (I.7.1).	12372.44 kev - xu	p. 270 C3
Standard deviation of the item above.	0.16 kev - xu	p. 270 C3
Conversion coefficient of angstrom to Siegbahn x unit	1.002039×10^{-3} xu/Å	p. 267 C3
Standard deviation of the item above.	0.000014×10^{-3} xu/Å	p. 267 C3

Table 24. Wavelength Standards

Source		Value in xu	Reference
Annihilation radiation		24.2132 ± 0.0004	p. 269, C3
Ta^{182}	67.74 kev	182.638 ± 0.018	M3
	100.09 kev	123.599 ± 0.014	"
	113.66 kev	108.849 ± 0.013	"
	116.40 kev	106.283 ± 0.013	"
	152.41 kev	81.171 ± 0.012	"
	156.37 kev	79.116 ± 0.012	"
	179.36 kev	68.974 ± 0.011	"
Ir^{192}	604.53 kev	20.464 ± 0.020	M3
	588.40 kev	21.025 ± 0.010	"
	467.984 kev	26.435 ± 0.004	"
	316.462 kev	39.092 ± 0.004	"
	308.454 kev	40.107 ± 0.004	"
	295.942 kev	41.803 ± 0.004	"
	205.736 kev	60.131 ± 0.011	"
Rh^{104}	333.557 kev	37.0924 ± 0.0034	B1
	266.750 kev	46.3822 ± 0.0037	"
	217.915 kev	56.7764 ± 0.0112	"
	215.489 kev	57.4156 ± 0.0102	"
	186.045 kev	66.5024 ± 0.0100	"
	180.859 kev	68.4093 ± 0.0053	"
	169.402 kev	73.0360 ± 0.0104	"
	134.617 kev	91.9084 ± 0.0052	"
	127.318 kev	97.1775 ± 0.0059	"
	100.796 kev	122.747 ± 0.0060	"
	97.114 kev	127.402 ± 0.0041	"
	85.355 kev	144.952 ± 0.0060	"
	51.422 kev	240.604 ± 0.0078	"

Table 24. (concluded)

Source	Value in xu	Reference
W $K\alpha_2$	213.382 ± 0.010	I1, C5
W $K\alpha_1$	208.571 ± 0.010	"
W $K\beta_3$	184.795 ± 0.010	"
W $K\beta_1$	183.991 ± 0.010	"
W $K\beta_2^I$	179.049 ± 0.010	"
Ta $K\alpha_2$	219.846 ± 0.010	I1, C5
Ta $K\alpha_1$	215.050 ± 0.010	"
Ta $K\beta_1$	189.693 ± 0.010	"
Ir $K\alpha_2$	195.494 ± 0.010	I1, C5
Ir $K\alpha_1$	190.648 ± 0.010	"
Ir $K\beta_3$	169.016 ± 0.010	"
Ir $K\beta_1$	168.193 ± 0.010	"
Ir $K\beta_2^I$	163.613 ± 0.010	"
Ba $K\alpha_2$	388.861 ± 0.010	I1, C5
Ba $K\alpha_1$	384.313 ± 0.010	"
Ba $K\beta_3$	340.797 ± 0.010	"
Ba $K\beta_1$	340.102 ± 0.010	"
Ba $K\beta_2$	332.074 ± 0.010	"
Cs $K\alpha_2$	403.996 ± 0.010	I1, C5
Cs $K\alpha_1$	399.461 ± 0.010	"
Cs $K\beta_3$	354.317 ± 0.010	"
Cs $K\beta_1$	353.633 ± 0.010	"

```
 J.M.NEILL. SCANDIUM-46.  PLATE 52.   RUN 1.  RANGE 180 TO -300 KEV.
       3        10          3          1          8          0          4
    592.0       0.5      1177.67       0.02            0.0020
  20.9956    20.9945    20.9950    20.9919    20.9952    20.9930
  20.9917    20.9911    20.9927    20.9904       .          .
  7 VVS GOOD  295   PLATE 52. SC-46.
   0.         0.         0.         0.         0.         0.
   0.         0.         0.         0.         .          .
 17   M  GOOD  295  PLATE 52. SC-46.
  24.8178    24.8152    24.8191    24.8151    24.8180    24.8243
  24.8141    24.8156    24.8159    24.8122       .          .
  2 VVS GOOD 216    PLATE 52. SC-46.
  27.5338    27.5317    27.5321    27.5336    27.5320    27.5256
  27.5177    27.5238    27.5200    27.5199       .          .
  1  VW GOOD 182    PLATE 52. SC-46.
  16.5637    16.5664    16.5654    16.5655    16.5631    16.5626
  16.5615    16.5583    16.5603    16.5567       .          .
 10   W GOOD  511   PLATE 52. SC-46.
   41.926      0.045      57.194      0.038      68.011      0.025
   24.2132       0.0004
  24.1025    24.0980    24.1014    24.0986    24.1026    24.1009
  24.0964    24.0975    24.0989    24.0961       .          .
  3 VVS GOOD  227   PLATE 52. SC-46.
  24.0449    24.0425    24.0444    24.0405    24.0444    24.0449
  24.0398    24.0397    24.0422    24.0401       .          .
  4  VS GOOD  228   PLATE 52. SC-46.
  21.5395    21.5392    21.5408    21.5386    21.5414    21.5372
  21.5301    21.5341    21.5301    21.5320       .          .
  6   W GOOD         PLATE 52. SC-46.
  16.8753    16.8693    16.8741    16.8706    16.8722    16.8681
  16.8628    16.8665    16.8646    16.8670       .          .
  9   M GOOD         PLATE 52. SC-46.
  16.2414    16.2460    16.2418    16.2431    16.2415    16.2414
  16.2379    16.2339    16.2341    16.2305       .          .
 11   W GOOD         PLATE 52. SC-46.
  16.0908    16.0894    16.0860    16.0867    16.0879    16.0863
  16.0850    16.0827    16.0871    16.0789       .          .
 13   M  GOOD        PLATE 52. SC-46.
  15.7951    15.8001    15.8040    15.7958    15.7978    15.7979
  15.7943    15.7953    15.7929    15.7912       .          .
 14   M  GOOD        PLATE 52. SC-46.
  15.4348    15.4377    15.4378    15.4378    15.4402    15.4367
  15.4370    15.4340    15.4350    15.4293       .          .
 15   M  GOOD        PLATE 52. SC-46.
  23.0019    22.9954    23.0000    22.9935    22.9967    22.9880
  22.9802    22.9820    22.9810    22.9811       .          .
  5 VVW  BAD          PLATE 52. SC-46.
  18.5717    18.5759    18.5787    18.5755    18.5780    18.5671
  18.5689    18.5651    18.5652    18.5635       .          .
  8 VVWQ BAD          PLATE 52. SC-46.
  16.1723    16.1701    16.1714    16.1680    16.1695    16.1655
  16.1637    16.1613    16.1653    16.1514       .          .
 12  VW  BAD         PLATE 52. SC-46.
  14.4990    14.4986    14.5036    14.4949    14.4947    14.4917
  14.4935    14.4820    14.4889    14.4885       .          .
 16 VVWQ  BAD         PLATE 52. SC-46.
```

SAMPLE INPUT

λ_m	$\sigma(\lambda_m)$	Arclength	E_m	$\sigma(E_m)$	Identification
67.9976	0.0210	17.0305	181.9540	0.0562	1 VW GOOD 182 PLATE 52. SC-46.
57.1786	0.0183	14.3202	216.3825	0.0692	2 VVS GOOD 216 PLATE 52. SC-46.
54.3145	0.0174	13.6027	227.7928	0.0732	3 VVS GOOD 227 PLATE 52. SC-46.
54.0871	0.0174	13.5458	228.7503	0.0737	4 VS GOOD 228 PLATE 52. SC-46.
49.8858	0.0181	12.4934	248.0154	0.0900	5 VVW BAD PLATE 52. SC-46.
44.0820	0.0154	11.0397	280.6687	0.0984	6 W GOOD PLATE 52. SC-46.
32.2422	0.0139	8.0744	383.7344	0.1651	8 VVWQ BAD PLATE 52. SC-46.
25.4465	0.0123	6.3725	486.2131	0.2360	9 M GOOD PLATE 52. SC-46.
24.2219	0.0120	6.0658	510.7962	0.2523	10 W GOOD 511 PLATE 52. SC-46.
22.9314	0.0121	5.7426	539.5425	0.2855	11 W GOOD PLATE 52. SC-46.
22.6386	0.0126	5.6693	546.5191	0.3043	12 VW BAD PLATE 52. SC-46.
22.3201	0.0118	5.5895	554.3184	0.2942	13 M GOOD PLATE 52. SC-46.
21.1635	0.0118	5.2999	584.6112	0.3247	14 M GOOD PLATE 52. SC-46.
19.7244	0.0115	4.9395	627.2663	0.3664	15 M GOOD PLATE 52. SC-46.
15.9609	0.0122	3.9970	775.1728	0.5910	16 VVWQ BAD PLATE 52. SC-46.
41.9133	0.0138	10.4966	295.1915	0.0973	17 M GOOD 295 PLATE 52. SC-46.

SAMPLE OUTPUT

```
C       MAIN PROGRAM NO 1
        DIMENSION Z(80,24),WVLNTH(80),SIGWL(80),W(80,24),PART(24),Y(80),
       1 SIGY2(80),SIGY(80),U(80),SIGU2(80),SIGU(80),SIN1(80),SGNG(80),
       2 WVLN2(80),SIGW2(80),X(80),SIGX2(80),SIGX(80),SIG2(80),SIGXY2(80),
       3 GISXY2(80),WT(80),DLM(80),SIN2(80),COS2(80),SG2(80),SGDLM2(80),
       4 SG(80),SGDLM(80),ENERGY(80),RES(80),RES2W(80),DNAM(80,8),DNAME(80
       5,8),ARCLN(80)
C       THIS PROGRAM ANALYSES EMULSION PLATES WHICH DO NOT STRADDLE THE
C       BETA POINT, AND HAVE TWO OR MORE CALIBRATION LINES.
        NIT=4
        NOT=2
        CON=12372.44
         SGCON2=0.0256
  3     WRITE OUTPUT TAPE NOT,4
  4     FORMAT (50H1BENT-CRYSTAL GAMMA-RAY SPECTROMETER DATA ANALYSIS)
        WRITE OUTPUT TAPE NOT,700
        WRITE OUTPUT TAPE NOT,710
        WRITE OUTPUT TAPE NOT,720
        WRITE OUTPUT TAPE NOT,725
        WRITE OUTPUT TAPE NOT,730
        WRITE OUTPUT TAPE NOT,740
        WRITE OUTPUT TAPE NOT,750
        WRITE OUTPUT TAPE NOT,760
        WRITE OUTPUT TAPE NOT,770
C       STATEMENTS 5 TO 102. READ THE INPUT DATA AND WRITE THEM OUT.
  5     READ INPUT TAPE NIT ,6
  6     FORMAT (72H0 PROBLEM
       1 IDENTIFICATION  )
  10    READ INPUT TAPE NIT,20,NOCASE,NR,NCL,NGUL,NBUL,NPRNT1
  20    FORMAT(6I10)
  25    READ INPUT TAPE NIT,40,A1,SIGA1,D,SIGD,SIGT
  28    FORMAT (8A6)
  29    FORMAT (1H1)
        DO 32 J=1,NCL
        READ INPUT TAPE NIT,40,(Z(J,I),I=1,NR)
  32    READ INPUT TAPE NIT,28,(DNAM(J,K),K=1,8)
  40    FORMAT (6E12.6)
        READ INPUT TAPE NIT,40,(WVLNTH(J),SIGWL(J),J=1,NCL)
        NPRNT=XABSF(NPRNT1)
        NL=NGUL+NBUL
  50    FORMAT (6E14.5)
        DO 52 J=1,NL
        READ INPUT TAPE NIT,40,(W(J,I),I=1,NR)
  52    READ INPUT TAPE NIT,28,(DNAME(J,K),K=1,8)
        WRITE OUTPUT TAPE NOT,29
        WRITE OUTPUT TAPE NOT,6
        WRITE OUTPUT TAPE NOT,60
  55    FORMAT (6F14.5)
  60    FORMAT (61H0    NOCASE        NR        NCL        NGUL       NBUL
       1NPRNT1)
        WRITE OUTPUT TAPE NOT,20,NOCASE,NR,NCL,NGUL,NBUL,NPRNT1
        WRITE OUTPUT TAPE NOT,70
  70    FORMAT (70H0       A1           SIGA1            D              SIGD
       1       SIGT     )
        WRITE OUTPUT TAPE NOT,55,A1,SIGA1,D,SIGD,SIGT
        WRITE OUTPUT TAPE NOT,80
  80    FORMAT (84H0    WVLNTH         SIGWL         WVLNTH          SIGWL
       2     WVLNTH          SIGWL     )
        WRITE OUTPUT TAPE NOT,55,((WVLNTH(J),SIGWL(J)),J=1,NCL)
        IGO=1
  88    WRITE OUTPUT TAPE NOT,90
```

```
 90   FORMAT (28H0     (Z(J,I),I=1,NR),J=1,NCL)
      DO 92 J=1,NCL
      WRITE OUTPUT TAPE NOT,55,(Z(J,I),I=1,NR)
 92   WRITE OUTPUT TAPE NOT,28,(DNAM(J,K),K=1,8)
      WRITE OUTPUT TAPE NOT,100
 100  FORMAT (27H0     (W(J,I),I=1,NR),J=1,NL)
      DO 102 J=1,NL
      WRITE OUTPUT TAPE NOT,55,(W(J,I),I=1,NR)
 102  WRITE OUTPUT TAPE NOT,28,(DNAME(J,K),K=1,8)
      GO TO (105,150),IGO
 105  IF (NOCASE-1)550,108,550
C     STATEMENTS 108 TO 130. ADJUST READINGS TO A COMMON REFERENCE POINT
 108  FNCL=FLOATF(NCL)
      FNR=FLOATF(NR)
      DIV=FLOATF(NCL+NGUL)
      SUM=0.
      DO 120 I=1,NR
      PART(I)=0.
      DO 110 J=1,NCL
 110  PART (I)= PART(I)+Z(J,I)
      DO 115 J=1,NGUL
 115  PART(I)=PART(I)+W(J,I)
 120  SUM=SUM+PART(I)
      SUM=SUM/FNR
      DO 130 I=1,NR
      ADD=(SUM-PART(I))/DIV
      DO 125 J=1,NCL
 125  Z(J,I)=Z(J,I)+ADD
      DO 128 J=1,NL
 128   W(J,I)=W(J,I)+ADD
 130  CONTINUE
      IF (NPRNT)140,140,150
 140  WRITE OUTPUT TAPE NOT,145
 145  FORMAT(26H1ADJUSTED POSITIONS BELOW.)
      IGO=2
      GO TO 88
C     STATEMENTS 150 TO 200. OBTAIN AVERAGE VALUES OF Z AND W, AND THEIR
C     STANDARD DEVIATIONS.
 150  CALL AVRGE (Z,NCL,NR,Y,SIGY,SIGY2)
 200  CALL AVRGE (W,NL,NR,U,SIGU,SIGU2)
      IF (NPRNT-1)210,210,230
 210  WRITE OUTPUT TAPE NOT,211
 211  FORMAT (110H1Y(J) = AVERAGE READING OF CALIBRATION LINE J IN CMS
     1       SIGY(J) = STANDARD DEVIATION OF Y(J) IN CMS        )
      WRITE OUTPUT TAPE NOT,212
 212  FORMAT (110H U(J) = AVERAGE READING OF UNKNOWN LINE J IN CMS
     1       SIGU(J) = STANDARD DEVIATION OF U(J) IN CMS        )
 214  WRITE OUTPUT TAPE NOT,215
 215  FORMAT (25H0     Y(J),SIGY(J),J=1,NCL)
      WRITE OUTPUT TAPE NOT,55,(Y(J),SIGY(J),J=1,NCL)
      WRITE OUTPUT TAPE NOT,220
 220  FORMAT (24H0     U(J),SIGU(J),J=1,NL)
      WRITE OUTPUT TAPE NOT,55,(U(J),SIGU(J),J=1,NL)
C     STATEMENTS 230 TO 320. CALCULATE THE WEIGHTS OF EACH CALIBRATION
C     POINT
 230  SIGT2=SIGT*SIGT
      JGO=1
      D2=D*D
      D24=4.*D2
      SIGA12=SIGA1*SIGA1
      TWOD=2.*D
```

```
      SIGD2=SIGD*SIGD
      SIGD24=4.*SIGD2
      DO 260 J=1,NCL
      WVLN2(J)=WVLNTH(J)*WVLNTH(J)
      SIGW2(J)=SIGWL(J)*SIGWL(J)
      X(J)=ARCSN(WVLNTH(J)/TWOD)
      SIGX2(J)=(SIGW2(J)+WVLN2(J)*SIGD2/D2)/(D24-WVLN2(J))
      SIGX(J)=SQRTF(SIGX2(J))
 260  SIG2(J)=SIGY2(J)+SIGT2
      IF (NPRNT)265,265,290
 265  WRITE OUTPUT TAPE NOT,268
 268  FORMAT (24H0   X(J),SIGX(J),J=1,NCL)
      WRITE OUTPUT TAPE NOT,50,(X(J),SIGX(J),J=1,NCL)
 290  AT1=A1
      MANY=0
 300  A12=A1*A1
      TOTAL=0.
      ADD=0.
      DO 310 J=1,NCL
      DATA=A12*SIGX2(J)
      SIGXY2(J)=SIG2(J)+DATA
      GISXY2(J)=1./SIGXY2(J)
      ADD=ADD+1./DATA
 310  TOTAL=TOTAL+GISXY2(J)
      DO 320 J=1,NCL
 320  WT(J)=GISXY2(J)/TOTAL
C     STATEMENTS 326 TO 345. CALCULATE THE LEAST SQUARE VALUE OF THE
C     FOCAL LENGTH A1, AND THE DISTANCE A0 FROM THE BETA POINT TO THE
C     ZERO REFERENCE OF THE MEASUREMENTS.
 326       CALL REDUCE(WT,X,Y,NCL,A0,A1,SIGA02,SIGA12,TOTAL,RCRELT)
      MANY=MANY+1
      IF (ABSF(1.-AT1/A1)-2.E-7)360,360,330
 330  IF (MANY-20)345,332,332
 332  IF (ABSF(1.-AT1/A1)-1.E-5)360,360,335
 335  WRITE OUTPUT TAPE NOT ,338
 338  FORMAT (52H0NO CONVERGENCE ON A1. MORE THAN 20 ITERATIONS.      )
      WRITE OUTPUT TAPE NOT,340
 340  FORMAT(70H0       A0            AT1             A1            SIGA02
     1   SIGA12      )
      WRITE OUTPUT TAPE NOT,50,A0,AT1,A1,SIGA02,SIGA12
      JGO=2
      GO TO 362
 345  AT1=A1
      GO TO 300
 360  WRITE OUTPUT TAPE NOT,361,MANY
 361  FORMAT (6H0MANY=I2)
      WRITE OUTPUT TAPE NOT,570
      WRITE OUTPUT TAPE NOT,580
      WRITE OUTPUT TAPE NOT,590
 362  WRITE OUTPUT TAPE NOT,363
 363  FORMAT (18H0    WT(J),J=1,NCL)
       WRITE OUTPUT TAPE NOT,55,(WT(J),J=1,NCL)
      GO TO (364,5),JGO
 364  IF (NCL-2)379,379,366
C     STATEMENTS 366 TO 380. CALCULATE CALIBRATION RESIDUALS AND ERROR
C     TERMS
 366  WE2MN1=1./TOTAL
      WE2MN2=0.
      DO 370 J=1,NCL
      RES(J)=Y(J)+A0-A1*X(J)
      RES2W(J)=WT(J)*RES(J)*RES(J)
```

```
 370  WE2MN2=WE2MN2+RES2W(J)
      WE2MN2=WE2MN2/FLOATF(NCL-2,
      IF (WE2MN2-WE2MN1)375,375,372
 372  WRITE OUTPUT TAPE NOT,373
 373  FORMAT (42HOTHE RESIDUALS ARE LARGER THAN THE ERRORS.)
      RATIOP=WE2MN2/WE2MN1
      SIGA02=SIGA02*RATIOP
      SIGA12=SIGA12*RATIOP
      TOTAL=1./WE2MN2
 375  WRITE OUTPUT TAPE NOT,376
 376  FORMAT (15HORES(J),J=1,NCL)
      WRITE OUTPUT TAPE NOT,50,(RES(J),J=1,NCL)
      WRITE OUTPUT TAPE NOT,377
 377  FORMAT (28H0   WE2MN1         WE2MN2     )
      WRITE OUTPUT TAPE NOT ,50,WE2MN1,WE2MN2
 379  RATIO=TOTAL/ADD
      SIGA0=SQRTF(SIGA02)
      SIGA1=SQRTF(SIGA12)
      SGA02=SIGA02*RATIO
      SGA12=SIGA12*RATIO
      SGA0=SQRTF(SGA02)
      SGA1=SQRTF(SGA12)
 380   SGA1=SQRTF(SGA12)
C     STATEMENTS 381 TO 480. CALCULATE THE WAVELENGTH AND ENERGY OF THE
C     UNKNOWN LINES, AND THEIR STANDARD DEVIATIONS.
      A12=A1*A1
      N1=NL
 381  DO 480 J=1,N1
      ARCLN(J)=A0+U(J)
      DATA= ARCLN(J)/A1
      SIN1(J)=SINAC(DATA)
      DLM(J)=TWOD*SIN1(J)
      SIN2(J)=SIN1(J)*SIN1(J)
      COS2(J)=1.-SIN2(J)
      SG2(J)=SIGD24*SIN2(J)
      SQUARE=DATA*DATA
      DATAR=D24*COS2(J)/A12
      SGDLM2(J)=SG2(J)+DATAR*(SIGA02+SIGU2(J)+SIGT2+SQUARE*SIGA12-2.*
     1 RCRELT*DATA*SIGA0*SIGA1)
      SG2(J)=SG2(J)+DATAR*(SGA02+SQUARE*SGA12-2.*RCRELT*DATA*SGA0*SGA1)
      SG(J)=SQRTF(SG2(J))
      ENERGY(J)=CON/DLM(J)
      SGDLM(J)=SQRTF(SGDLM2(J))
 480  SGNG(J)=SQRTF(SGDLM2(J)*ENERGY(J)*ENERGY(J)+SGCON2)/DLM(J)
      WRITE OUTPUT TAPE NOT,500
 500  FORMAT (114H1   DLM         SGDLM         SG        ARCLN        ENERG
     1Y        SGNG                        IDENTIFICATION                )
      WRITE OUTPUT TAPE NOT,502,(DLM(K),SGDLM(K),SG(K),ARCLN(K),ENERGY(K
     1),SGNG(K),(DNAME(K,L),L=1,8),K=1,N1)
 502  FORMAT (F11.4,2F11.6,2F11.4,F11.6,8A6)
      IF (NPRNT1)503,503,508
 503  PUNCH 504,(DLM(K),SGDLM(K),ARCLN(K),ENERGY(K),SGNG(K),(DNAME(K,J),
     1 J=1,6),K=1,N1)
 504  FORMAT (F9.4,F8.4,F9.4,F10.4,F8.4,6A6)
 508  IF (NPRNT-1)510,510,5
 510  WRITE OUTPUT TAPE NOT,515
 515  FORMAT (70H0         A0            SIGA0          A1             SIGA1
     1          RCRELT)
      WRITE OUTPUT TAPE NOT,55,A0,SIGA0,A1,SIGA1,RCRELT
      IF (NCL-2)5,5,518
 518  DO 520 J=1,NCL
```

```
      U(J)=Y(J)
      SIGU(J)=SIGY(J)
      DO 520 K=1,8
520    DNAME(J,K)=DNAM(J,K)
      N1=NCL
      JGO=1
      NPRNT=2
      GO TO 381
550   WRITE OUTPUT TAPE NOT,560
560   FORMAT (58H0 YOU HAVE THE WRONG CASE NUMBER. ANALYSIS IS DISCONTIN
     1UED)
      GO TO 5
570   FORMAT (110H0 WT(J) = WEIGHT OF CALIBRATION POINT J IN CMS
     1       RES(J) = RESIDUAL AT CALIBRATION POINT J IN CMS    )
580   FORMAT (110H0 WE2MN1 = MEAN WEIGHTED SQUARE OF ERRORS AT THE CALIB
     1RATION POINTS IN CMS2                                     )
590   FORMAT (110H0 WE2MN2 = MEAN WEIGHTED SQUARE OF RESIDUALS AT THE CA
     1LIBRATION POINTS IN CMS2                                  )
700   FORMAT (110H0NOCASE = PROBLEM TYPE NUMBER
     1       NR = NUMBER OF READINGS OF EACH LINE               )
710   FORMAT (110H NCL = NUMBER OF CALIBRATION LINES
     1       NGUL = NUMBER OF GOOD UNKNOWN LINES                )
720   FORMAT (110H NBUL = NUMBER OF BAD UNKNOWN LINES
     1       NPRNT1 = PRINT OPTION NUMBER                       )
725   FORMAT(111H A0 = DISTANCE FROM THE BETA POINT TO THE ZERO REFERENC
     1E OF THE MEASUREMENTS IN CMS                              )
730   FORMAT (110H A1 = DIAMETER OF FOCAL CIRCLE IN CMS
     1       SIGA1 = STANDARD DEVIATION OF A1 IN CMS            )
740   FORMAT (110H D = ATOMIC PLANE SPACING IN CRYSTAL IN XU
     1       SIGD = STANDARD DEVIATION OF D IN XU               )
750   FORMAT (110H SIGT = UNCERTAINTY IN EACH LINE MEASUREMENT FROM EMUL
     1SION SHRINKAGE,GEOMETRICAL EFFECTS,ETC IN CMS             )
760   FORMAT (110H WVLNTH(J) = WAVELENGTH OF CALIBRATION LINE J IN XU
     1       SIGWL(J) = STANDARD DEVIATION OF WVLNTH(J) IN XU   )
770   FORMAT (110H Z(J,I) = READING I OF CALIBRATION LINE J IN CMS
     1       W(J,I) = READING I OF UNKNOWN LINE J IN CMS        )
      END
```

```
C      MAIN PROGRAM NO 2
       DIMENSION Z(24),W(80,24),PART(24),U(80),SIGU2(80),DLM(80),SIGU(80)
      1,SGDLM2(80),SGDLM(80),ENERGY(80),SGNG(80),SG2(80),SG(80)
      2 ,ZD(80,24),YD(80),SIGYD(80),SIGYD2(80),DNAM(8),DNAME(80,8),ARCLN(
      3 80)
C      THIS PROGRAM ANALYSES EMULSION PLATES WHICH DO NOT STRADDLE THE
C      BETA POINT AND HAVE ONLY ONE CALIBRATION LINE.
       NIT=4
       NOT=2
       CON=12372.44
       SGCON2=0.0256
  3    WRITE OUTPUT TAPE NOT,4
  4    FORMAT (50H1BENT-CRYSTAL GAMMA-RAY SPECTROMETER DATA ANALYSIS)
       WRITE OUTPUT TAPE NOT,700
       WRITE OUTPUT TAPE NOT,710
       WRITE OUTPUT TAPE NOT,720
       WRITE OUTPUT TAPE NOT,725
       WRITE OUTPUT TAPE NOT,730
       WRITE OUTPUT TAPE NOT,740
       WRITE OUTPUT TAPE NOT,750
       WRITE OUTPUT TAPE NOT,760
       WRITE OUTPUT TAPE NOT,770
C      STATEMENTS 5 TO 102. READ THE INPUT DATA AND WRITE THEM OUT.
  5    READ INPUT TAPE NIT ,6
  6    FORMAT (72H0        PROBLEM
      1 IDENTIFICATION  )
 10    READ INPUT TAPE NIT,20,NOCASE,NR,NGUL,NBUL,NPRNT1
 20    FORMAT (5I10)
 25    READ INPUT TAPE NIT,40,A1,SIGA1,D,SIGD,SIGT,WVLNTH,SIGWL
 28    FORMAT (8A6)
 29    FORMAT (1H1)
       READ INPUT TAPE NIT,40,(Z(I),I=1,NR)
 32    READ INPUT TAPE NIT,28,(DNAM(K),K=1,8)
 40     FORMAT (6E12.6)
       NPRNT=XABSF(NPRNT1)
       NL=NGUL+NBUL
 50    FORMAT (6E14.5)
       DO 52 J=1,NL
       READ INPUT TAPE NIT,40,(W(J,I),I=1,NR)
 52    READ INPUT TAPE NIT,28,(DNAME(J,K),K=1,8)
       WRITE OUTPUT TAPE NOT,29
       WRITE OUTPUT TAPE NOT,6
       WRITE OUTPUT TAPE NOT,60
 55    FORMAT (6F14.5)
 60    FORMAT (50H0   NOCASE         NR       NGUL       NBUL     NPRNT1)
       WRITE OUTPUT TAPE NOT,20,NOCASE,NR,NGUL,NBUL,NPRNT
 70    WRITE OUTPUT TAPE NOT,80
 80    FORMAT (98H0      A1             SIGA1             D              SIGD
      1      SIGT           WVLNTH         SIGWL      )
       WRITE OUTPUT TAPE NOT,85,A1,SIGA1,D,SIGD,SIGT,WVLNTH,SIGWL
 85    FORMAT (7F14.5)
       IGO=1
 88    WRITE OUTPUT TAPE NOT,90
 90    FORMAT (16H0    Z(I),I=1,NR)
       WRITE OUTPUT TAPE NOT,55,(Z(I),I=1,NR)
       WRITE OUTPUT TAPE NOT,28,(DNAM(K),K=1,8)
 98    WRITE OUTPUT TAPE NOT,100
 100   FORMAT (27H0     (W(J,I),I=1,NR),J=1,NL)
       DO 102 J=1,NL
        WRITE OUTPUT TAPE NOT,50,(W(J,I),I=1,NR)
 102   WRITE OUTPUT TAPE NOT,28,(DNAME(J,K),K=1,8)
```

```
      GO TO (105,150),IGO
  105 IF (NOCASE-2)550,108,550
C     STATEMENTS 108 TO 130. ADJUST READINGS TO A COMMON REFERENCE POINT
  108 FNR=FLOATF(NR)
      SUM=0.
      DIV=FLOATF(NGUL)+1.
      DO 120 I=1,NR
      PART(I)=Z(I)
      DO 115 J=1,NGUL
  115 PART(I)=PART(I)+W(J,I)
  120 SUM=SUM+PART(I)
      SUM=SUM/FNR
      M=1
      DO 130 I=1,NR
      ADD=(SUM-PART(I))/DIV
      Z(I)=Z(I)+ADD
      ZD(M,I)=Z(I)
      DO 128 J=1,NL
  128  W(J,I)=W(J,I)+ADD
  130 CONTINUE
      IF (NPRNT)140,140,150
  140 WRITE OUTPUT TAPE NOT,145
  145 FORMAT(26H1ADJUSTED POSITIONS BELOW.)
      IGO=2
      GO TO 88
C     STATEMENTS 150 TO 200. OBTAIN AVERAGE VALUES OF Z AND W, AND THEIR
C     STANDARD DEVIATIONS.
  150 CALL AVRGE (ZD,M,NR,YD,SIGYD,SIGYD2)
      Y=YD(M)
      SIGY=SIGYD(M)
      SIGY2=SIGYD2(M)
  200 CALL AVRGE (W,NL,NR,U,SIGU,SIGU2)
      IF (NPRNT-1)210,210,230
  210 WRITE OUTPUT TAPE NOT,211
  211 FORMAT (110H1    Y = AVERAGE READING OF CALIBRATION LINE    IN CMS
     1         SIGY  = STANDARD DEVIATION OF    Y  IN CMS        )
      WRITE OUTPUT TAPE NOT,212
  212 FORMAT (110H U(J) = AVERAGE READING OF UNKNOWN LINE J IN CMS
     1       SIGU(J) = STANDARD DEVIATION OF U(J) IN CMS        )
      WRITE OUTPUT TAPE NOT,214
  214 FORMAT (28H0       Y            SIGY      )
      WRITE OUTPUT TAPE NOT,50,Y,SIGY
      WRITE OUTPUT TAPE NOT,220
  220 FORMAT (24H0    U(J),SIGU(J),J=1,NL)
      WRITE OUTPUT TAPE NOT,50,(U(J),SIGU(J),J=1,NL)
C     STATEMENTS 230 TO 250. CALCULATE THE WAVELENGTH AND ENERGY OF THE
C     UNKNOWN LINES, AND THEIR STANDARD DEVIATIONS.
  230 SIGD2=SIGD*SIGD
      D2=D*D
      SIGT2=SIGT*SIGT
      SIGTWO=2.*SIGT2
      SIGD24=4.*SIGD2
      A12=A1*A1
      A14=A12*A12
      SIGA12=SIGA1*SIGA1
      TWOD=2.*D
      D24=4.*D2
      EX=WVLNTH/TWOD
      EX2=EX*EX
      OMEX2=1.-EX2
      FACT=ARCSN(EX)
```

```
      A0=A1*FACT-Y
      DATA=D24*OMEX2/A12
      SIGWL2=SIGWL*SIGWL
      N1=NL+1
      U(N1)=Y
      DO 240 K=1,8
  240 DNAME(N1,K)=DNAM(K)
      DO 250 J=1,N1
      ARCLN(J)=A0+U(J)
      X=SINAC(ARCLN(J)/A1)
      X=SINAC((A0+U(J))/A1)
      X2=X*X
      YD=Y-U(J)
      YD2=YD*YD
      COSX2=1.-X2
      SINYD=SINAC(YD/A1)
      SINYD2=SINYD*SINYD
      DLM(J)=TWOD*X
      SG2(J)=(SIGD24*SINYD2+SIGWL2*COSX2)/OMEX2+D24*COSX2*YD2*SIGA12/A14
      SGDLM2(J)=SG2(J)+D24*COSX2*(SIGY2+SIGU2(J)+SIGTWO)/A12
      SGDLM(J)=SQRTF(SGDLM2(J))
      ENERGY(J)=CON/DLM(J)
      SGNG(J)=SQRTF(SGDLM2(J)*ENERGY(J)*ENERGY(J)+SGCON2)/DLM(J)
  250 SG(J)=SQRTF(SG2(J))
      WRITE OUTPUT TAPE NOT,500
  500 FORMAT (114H1   DLM         SGDLM         SG        ARCLN        ENERG
     1Y        SGNG                      IDENTIFICATION                  )
      WRITE OUTPUT TAPE NOT,502,(DLM(K),SGDLM(K),SG(K),ARCLN(K),ENERGY(K
     1),SGNG(K),(DNAME(K,L),L=1,8),K=1,N1)
  502 FORMAT (F11.4,2F11.6,2F11.4,F11.6,8A6)
      IF (NPRNT1)503,503,508
  503 PUNCH 504,(DLM(K),SGDLM(K),ARCLN(K),ENERGY(K),SGNG(K),(DNAME(K,J),
     1 J=1,6),K=1,N1)
  504 FORMAT (F9.4,F8.4,F9.4,F10.4,F8.4,6A6)
  508 WRITE OUTPUT TAPE NOT,510,A0
  510 FORMAT (12H0          A=F10.4)
      GO TO 3
  550 WRITE OUTPUT TAPE NOT,560
  560 FORMAT (58H0 YOU HAVE THE WRONG CASE NUMBER. ANALYSIS IS DISCONTIN
     1UED)
      GO TO 3
  700 FORMAT (110H0NOCASE = PROBLEM TYPE NUMBER
     1       NR = NUMBER OF READINGS OF EACH LINE                )
  710 FORMAT (36H NGUL = NUMBER OF GOOD UNKNOWN LINES)
  720 FORMAT (110H NBUL = NUMBER OF BAD UNKNOWN LINES
     1       NPRNT1 = PRINT OPTION NUMBER                        )
  725 FORMAT(111H A0 = DISTANCE FROM THE BETA POINT TO THE ZERO REFERENC
     1E OF THE MEASUREMENTS IN CMS                               )
  730 FORMAT (110H A1 = DIAMETER OF FOCAL CIRCLE IN CMS
     1       SIGA1 = STANDARD DEVIATION OF A1 IN CMS             )
  740 FORMAT (110H D = ATOMIC PLANE SPACING IN CRYSTAL IN XU
     1       SIGD = STANDARD DEVIATION OF D IN XU                )
  750 FORMAT (110H SIGT = UNCERTAINTY IN EACH LINE MEASUREMENT FROM EMUL
     1SION SHRINKAGE,GEOMETRICAL EFFECTS,ETC IN CMS              )
  760 FORMAT (110H     WVLNTH = WAVELENGTH OF CALIBRATION LINE    IN XU
     1          SIGWL = STANDARD DEVIATION OF   WVLNTH  IN XU   )
  770 FORMAT (110H    Z(I) = READING I OF CALIBRATION LINE    IN CMS
     1       W(J,I) = READING I OF UNKNOWN LINE J IN CMS         )
      END
```

```
C       MAIN PROGRAM NO 3
        DIMENSION Z(80,24),WVLNTH(80),SIGWL(80),W(80,24),PART(24),Y(80),
       1 SIGY(80),SIGY2(80),U(80),SIGU(80),SIGU2(80),S(80),AOP(80),
       2SGAOP2(80),SGAOP(80),SIGS2(80),SIGS(80),R(80),SIGR(80),SIGR2(80),
       3 WVLN2(80),X(80),SIGW2(80),SIGX2(80),SIGX(80),SIG2(80),SIGXY2(80),
       4 GISXY(80), WT(80),SIN1(80),DLM(80),SIN2(80),COS2(80),R2(80),
       5SG2(80),SGDLM(80),SGDLM2(80),SG(80),ENERGY(80),SGNG(80),GISXY2(80)
       6 , RES(80),RES2W(80),DNAM(80,8),DNAME(80,8)
C       THIS PROGRAM ANALYSES EMULSION PLATES THAT STRADDLE THE BETA POINT
        NOT=2
        NIT=4
        CON=12372.44
        SGCON2=0.0256
  3     WRITE OUTPUT TAPE NOT,4
  4     FORMAT (50H1BENT-CRYSTAL GAMMA-RAY SPECTROMETER DATA ANALYSIS)
        WRITE OUTPUT TAPE NOT,700
        WRITE OUTPUT TAPE NOT,710
        WRITE OUTPUT TAPE NOT,715
        WRITE OUTPUT TAPE NOT,720
        WRITE OUTPUT TAPE NOT,725
        WRITE OUTPUT TAPE NOT,730
        WRITE OUTPUT TAPE NOT,740
        WRITE OUTPUT TAPE NOT,750
        WRITE OUTPUT TAPE NOT,760
        WRITE OUTPUT TAPE NOT,770
C       STATEMENTS 5 TO 102. READ THE INPUT DATA AND WRITE THEM OUT.
  5     READ INPUT TAPE NIT ,6
  6     FORMAT (72H0 PROBLEM
       1 IDENTIFICATION  )
  10    READ INPUT TAPE NIT,20,NOCASE,NR,NCLS,NCLP,NGULS,NGULP,NBUL,NPRNT1
  20    FORMAT (8I10)
        NCL=NCLS+NCLP
  25    READ INPUT TAPE NIT,40,A1,SIGA1,D,SIGD,SIGT
  28    FORMAT (8A6)
  29    FORMAT (1H1)
  30    FORMAT(5E14.6)
  32    NX1=2*NCLP
        NX2=NX1+NCLS
        DO 35 J=1,NX2
        READ INPUT TAPE NIT,40,(Z(J,I),I=1,NR)
  35    READ INPUT TAPE NIT,28,(DNAM(J,K),K=1,8)
  40     FORMAT (6E12.6)
        READ INPUT TAPE NIT,40,(WVLNTH(J),SIGWL(J),J=1,NCL)
        NPRNT=XABSF(NPRNT1)
        NUL=NGULS+NBUL
        NL=NUL+NGULP
        NX3=2*NGULP
        NX4=NX3+NUL
         NX5=NX3+NGULS
  50    FORMAT (6E14.5)
        DO 52 J=1,NX4
        READ INPUT TAPE NIT,40,(W(J,I),I=1,NR)
  52    READ INPUT TAPE NIT,28,(DNAME(J,K),K=1,8)
  55    FORMAT (6F14.5)
        WRITE OUTPUT TAPE NOT,29
        WRITE OUTPUT TAPE NOT,6
        WRITE OUTPUT TAPE NOT,60
  60    FORMAT (80H0   NOCASE         NR       NCLS       NCLP       NGULS
       1NGULP       NBUL     NPRNT1)
        WRITE OUTPUT TAPE NOT,20,NOCASE,NR,NCLS,NCLP,NGULS,NGULP,NBUL,
       1 NPRNT1
```

```
      WRITE OUTPUT TAPE NOT,70
 70   FORMAT (70H0       A1           SIGA1            D              SIGD
     1       SIGT     )
      WRITE OUTPUT TAPE NOT,55,A1,SIGA1,D,SIGD,SIGT
      WRITE OUTPUT TAPE NOT,80
 80   FORMAT (84H0     WVLNTH         SIGWL         WVLNTH          SIGWL
     1     WVLNTH          SIGWL     )
      WRITE OUTPUT TAPE NOT,55,((WVLNTH(J),SIGWL(J)),J=1,NCL)
      IGO=1
 88   WRITE OUTPUT TAPE NOT,90
 90   FORMAT (30H0      (Z(J,I),I=1,NR),J=1,NX2 )
      DO 92 J=1,NX2
      WRITE OUTPUT TAPE NOT,55,(Z(J,I),I=1,NR)
 92   WRITE OUTPUT TAPE NOT,28,(DNAM(J,K),K=1,8)
      WRITE OUTPUT TAPE NOT,98
 98   FORMAT (28H0     (W(J,I),I=1,NR),J=1,NX4)
      DO 102 J=1,NX4
      WRITE OUTPUT TAPE NOT,55,(W(J,I),I=1,NR)
 102  WRITE OUTPUT TAPE NOT,28,(DNAME(J,K),K=1,8)
      GO TO (105,150),IGO
 105   IF (NOCASE-3)550,108,550
C     STATEMENTS 108 TO 130. ADJUST READINGS TO A COMMON REFERENCE POINT
 108  DIV=FLOATF(NCLS+NGULS+2*(NCLP+NGULP))
      SUM=0.
      FNR=FLOATF(NR)
      SIGD2=SIGD*SIGD
      SIGT2=SIGT*SIGT
      TWOD=2.*D
      SIGA12=SIGA1*SIGA1
      D2=D*D
      D24=4.*D2
      SIGD24=4.*SIGD2
      AT1=A1
      MANY=0
      DO 120 I=1,NR
      PART(I)=0.
      DO 110 J=1,NX2
 110  PART (I)= PART(I)+Z(J,I)
      IF(NX5)120,120,114
 114  DO 115 J=1,NX5
 115  PART(I)=PART(I)+W(J,I)
 120  SUM=SUM+PART(I)
      SUM=SUM/FNR
      DO 130 I=1,NR
      ADD=(SUM-PART(I))/DIV
       DO 122 J=1,NX2
 122  Z(J,I)=Z(J,I)+ADD
      DO 126 J=1,NX4
 126  W(J,I)=W(J,I)+ADD
 130  CONTINUE
      IF (NPRNT)140,140,150
 140  WRITE OUTPUT TAPE NOT,145
 145  FORMAT(26H1ADJUSTED POSITIONS BELOW.)
      IGO=2
      GO TO 88
C     STATEMENTS 150 TO 200. OBTAIN AVERAGE VALUES OF Z AND W, AND THEIR
C     STANDARD DEVIATIONS.
 150   IF (NCLP)162,162,152
 152   DO 155 J=1,NCLP
      JP=2*J
      DO 155 K=1,8
```

```
 155   DNAM(J,K)=DNAM(JP,K)
 158   IF (NCLS)162,162,159
 159   DO 160 J=1,NCLS
      JP1=J+NCLP
      JP2=J+NX1
      DO 160 K=1,8
 160   DNAM(JP1,K)=DNAM(JP2,K)
 162   IF (NGULP)180,180,164
 164   DO 167 J=1,NGULP
      JP=2*J
      DO 167 K=1,8
 167   DNAME(J,K)=DNAME(JP,K)
      NK=NBUL+NGULS
      IF (NK)180,180,170
 170   DO 173 J=1,NK
      JP2=J+NX3
      JP1=J+NGULP
      DO 173 K=1,8
 173   DNAME(JP1,K)=DNAME(JP2,K)
 180   CALL AVRGE (Z,NX2,NR,Y,SIGY,SIGY2)
 200   CALL AVRGE (W,NX4,NR,U,SIGU,SIGU2)
      IF (NPRNT-1)210,210,230
 210   WRITE OUTPUT TAPE NOT,211
 211   FORMAT (110H1Y(J) = AVERAGE READING OF CALIBRATION LINE J IN CMS
     1       SIGY(J) = STANDARD DEVIATION OF Y(J) IN CMS        )
      WRITE OUTPUT TAPE NOT,212
 212   FORMAT (110H U(J) = AVERAGE READING OF UNKNOWN LINE J IN CMS
     1       SIGU(J) = STANDARD DEVIATION OF U(J) IN CMS        )
 214   WRITE OUTPUT TAPE NOT,215
 215   FORMAT (26H0     Y(J),SIGY(J),J=1,NX2 )
      WRITE OUTPUT TAPE NOT,55,(Y(J),SIGY(J),J=1,NX2)
      WRITE OUTPUT TAPE NOT,220
 220   FORMAT (25H0     U(J),SIGU(J),J=1,NX4)
      WRITE OUTPUT TAPE NOT,55,(U(J),SIGU(J),J=1,NX4)
C     STATEMENTS 230TO 242. CALCULATE THE DISTANCE A0 FROM THE BETA
C     POINT TO THE ZERO REFERENCE OF THE MEASUREMENTS AND ITS STANDARD
C     DEVIATION.
 230   SIGA02=0.
      IF(NCLP)233,233,231
 231   DO 232 J=1,NCLP
      J2=2*J
      J2M1=J2-1
      S(J)=0.5*(Y(J2M1)-Y(J2))
      A0P(J)=0.5*(Y(J2M1)+Y(J2))
      SGA0P2(J)=0.25*(SIGY2(J2M1)+SIGY2(J2))
      SIGS2(J)=SGA0P2(J)
      SGA0P2(J)=SGA0P2(J)+0.5*SIGT2
      SGA0P(J)=SQRTF(SGA0P2(J))
 232   SIGA02=SIGA02+1./SGA0P2(J)
 233   IF (NGULP)236,236,234
 234   DO 235 J=1,NGULP
      J2=2*J
      J2M1=J2-1
      JPNCLP=J+NCLP
      A0P(JPNCLP)=0.5*(U(J2M1)+U(J2))
      R(J)=0.5*(U(J2M1)-U(J2))
      SGA0P2(JPNCLP)=0.25*(SIGU2(J2M1)+SIGU2(J2))
      SIGR2(J)=SGA0P2(JPNCLP)
      SGA0P2(JPNCLP)=SGA0P2(JPNCLP)+0.5*SIGT2
      SGA0P(JPNCLP)=SQRTF(SGA0P2(JPNCLP))
 235   SIGA02=SIGA02+1./SGA0P2(JPNCLP)
```

```
 236  A0=0.
      NLAST=NCLP+NGULP
      DO 238 J=1,NLAST
 238           A0=A0+A0P(J)/SGA0P2(J)
      A0=A0/SIGA02
      FNL=FLOATF(NLAST-1)
      SGRA02=0.
      DO 239 J=1,NLAST
 239  SGRA02=SGRA02+(A0P(J)-A0)**2/SGA0P2(J)
      SGRA02=SGRA02/(FNL*SIGA02)
      SIGA02=1./SIGA02
      WRITE OUTPUT TAPE NOT,240
 240   FORMAT (28H0     SIGA02       SGRA02      )
      WRITE OUTPUT TAPE NOT,50,SIGA02,SGRA02
      IF (SIGA02-SGRA02)241,242,242
 241  SIGA02=SGRA02
 242  SIGA0=SQRTF(SIGA02)
      IF (NPRNT1-1)243,243,245
 243  WRITE OUTPUT TAPE NOT,244
 244   FORMAT (43H0     ((A0P(J),SGA0P(J)),J=1,NLAST),A0,SIGA0)
      WRITE OUTPUT TAPE NOT,55,((A0P(J),SGA0P(J)),J=1,NLAST),A0,SIGA0
 245   IF (NCLP)248,248,246
 246   DO 247 J=1,NCLP
      SIGS2(J)=SIGS2(J)+SIGA02
      SIGS(J)=SQRTF(SIGS2(J))
 247   SIGS2(J)=SIGS2(J)+0.5*SIGT2
 248   IF (NGULP)251,251,249
 249   DO 250 J=1,NGULP
      SIGR2(J)=SIGR2(J)+SIGA02
      SIGR(J)=SQRTF(SIGR2(J))
 250   SIGR2(J)=SIGR2(J)+0.5*SIGT2
 251   IF (NCLS)265,265,252
 252   DO 260 J=1,NCLS
      JPNCLP=J+NCLP
      JPNX1=J+NX1
      S(JPNCLP)=Y(JPNX1)-A0
      DATA=SIGY2(JPNX1)+SIGA02
      SIGS(JPNCLP)=SQRTF(DATA)
 260  SIGS2(JPNCLP)=DATA+SIGT2
 265  IF (NUL)272,272,268
C     STATEMENTS 268 TO 320. CALCULATE THE WEIGHTS OF EACH CALIBRATION
C     POINT.
 268  DO 270 J=1,NUL
      JPNX3=J+NX3
      JNGULP=J+NGULP
      R(JNGULP)=U(JPNX3)-A0
      DATA=SIGU2(JPNX3)+SIGA02
      SIGR(JNGULP)=SQRTF(DATA)
 270  SIGR2(JNGULP)=DATA+SIGT2
 272  DO 280 J=1,NCL
      WVLN2(J)=WVLNTH(J)*WVLNTH(J)
      X(J)=ARCSN(WVLNTH(J)/TWOD)
      SIGW2(J)=SIGWL(J)*SIGWL(J)
      SIGX2(J)=(SIGW2(J)+WVLN2(J)*SIGD2/D2)/(D24-WVLN2(J))
 280  SIGX(J)=SQRTF(SIGX2(J))
      IF (NPRNT-1)293,293,300
 293  WRITE OUTPUT TAPE NOT,295
 295  FORMAT (18H0     WT(J),J=1,NCL)
 300  A12=A1*A1
      TOTAL=0.
      NT=0
```

```
      ADD=0.
      DO 310 J=1,NCL
      DATA=A12*SIGX2(J)
      SIGXY2(J)=SIGS2(J)+DATA
      GISXY2(J)=1./SIGXY2(J)
      ADD=ADD+1./DATA
  310 TOTAL=TOTAL+GISXY2(J)
      DO 320 J=1,NCL
  320 WT(J)=GISXY2(J)/TOTAL
      IF (NPRNT-1)321,321,326
  321  WRITE OUTPUT TAPE NOT,55,(WT(J),J=1,NCL)
C     STATEMENTS 326 TO 345. CALCULATE THE FOCAL LENGTH A1.
  326 A1=0.
      DEN=0.
      DO 328 J=1,NCL
      FACT=WT(J)*X(J)
      A1=A1+FACT*S(J)
  328 DEN=DEN+FACT*X(J)
      A1=A1/DEN
      MANY=MANY+1
      SIGA12=1./(TOTAL*DEN)
      IF (ABSF(1.-AT1/A1)-2.E-7)360,360,330
  330 IF (MANY-20)345,332,332
  332 IF (ABSF(1.-AT1/A1)-1.E-5)360,360,335
  335 WRITE OUTPUT TAPE NOT ,338
  338 FORMAT (52HONO CONVERGENCE ON A1. MORE THAN 20 ITERATIONS.      )
      WRITE OUTPUT TAPE NOT,340
  340 FORMAT(70H0       A0            AT1             A1            SIGA02
     1   SIGA12      )
      WRITE OUTPUT TAPE NOT,50,A0,AT1,A1,SIGA02,SIGA12
      GO TO 5
  345 AT1=A1
      GO TO 300
  360 WRITE OUTPUT TAPE NOT,361,MANY
  361 FORMAT (6HOMANY=I2)
      WRITE OUTPUT TAPE NOT,570
      WRITE OUTPUT TAPE NOT,580
      WRITE OUTPUT TAPE NOT,590
  362 WRITE OUTPUT TAPE NOT,363
  363 FORMAT (18H0    WT(J),J=1,NCL)
       WRITE OUTPUT TAPE NOT,55,(WT(J),J=1,NCL)
C     STATEMENTS 366 TO 380. CALCULATE CALIBRATION RESIDUALS AND ERROR
C     TERMS
      WE2MN2=0.
      IF (NCL-1)379,379,366
  366 WE2MN1=1./TOTAL
      DO 370 J=1,NCL
      RES(J)=(S(J)-A1*X(J))
      RES2W(J)=WT(J)*RES(J)*RES(J)
  370 WE2MN2=WE2MN2+RES2W(J)
      WE2MN2=WE2MN2/FLOATF(NCL-1)
      IF (WE2MN2-WE2MN1)375,375,372
  372 WRITE OUTPUT TAPE NOT,373
  373 FORMAT (42HOTHE RESIDUALS ARE LARGER THAN THE ERRORS.)
      SIGA12=SIGA12*WE2MN2/WE2MN1
      TOTAL=1./WE2MN2
      IF (NPRNT-1)375,375,377
  375 WRITE OUTPUT TAPE NOT,376
  376 FORMAT (15HORES(J),J=1,NCL)
      WRITE OUTPUT TAPE NOT,50,(RES(J),J=1,NCL)
  377 WRITE OUTPUT TAPE NOT,378
```

```
 378  FORMAT (28H0   WE2MN1         WE2MN2     )
      WRITE OUTPUT TAPE NOT ,50,WE2MN1,WE2MN2
 379  RATIO=TOTAL/ADD
      A12=A1*A1
      SGA12=SIGA12*RATIO
      DATAR=SGA12*D24/(A12*A12)
      SIGA0=SQRTF(SIGA02)
      SIGA1=SQRTF(SIGA12)
 380   DATA=SIGA12/A12
C     STATEMENTS 390 TO 500. CALCULATE THE ENERGY AND WAVELENGTH OF THE
C     UNKNOWN LINES AND THEIR STANDARD DEVIATION.
 390   DO 400 K=1,NL
      SIN1(K)=SINAC(R(K)/A1)
      DLM(K)=TWOD*SIN1(K)
      SIN2(K)=SIN1(K)*SIN1(K)
      COS2(K)=1.-SIN2(K)
      R2(K)=R(K)*R(K)
      SG2(K)=SIGD24*SIN2(K)
      SGDLM2(K)=SG2(K)+D24*COS2(K)*((SIGR2(K)+R2(K)*DATA)/A12)
      SGDLM(K)=SQRTF(SGDLM2(K))
      SG2(K)=SG2(K)+R2(K)*DATAR*COS2(K)
      SG(K)=SQRTF(SG2(K))
      ENERGY(K)=CON/DLM(K)
 400  SGNG(K)=SQRTF(SGDLM2(K)*ENERGY(K)*ENERGY(K)+SGCON2)/DLM(K)
      WRITE OUTPUT TAPE NOT,500
 500  FORMAT (114H1   DLM         SGDLM         SG        ARCLN        ENERG
     1Y        SGNG                      IDENTIFICATION                 )
      WRITE OUTPUT TAPE NOT,502,(DLM(K),SGDLM(K),SG(K),R(K),ENERGY(K),
     1 SGNG(K),(DNAME(K,L),L=1,8),K=1,NL)
 502  FORMAT (F11.4,2F11.6,2F11.4,F11.6,8A6)
      IF (NPRNT1)503,503,506
 503  PUNCH 504,(DLM(K),SGDLM(K),R(K),ENERGY(K),SGNG(K),(DNAME(K,J),J=1,
     1 6),K=1,NL)
 504  FORMAT (F9.4,F8.4,F9.4,F10.4,F8.4,6A6)
 506  IF (NT)5,508,5
 508  IF (NPRNT-1)510,510,5
 510  WRITE OUTPUT TAPE NOT,515
 515  FORMAT (53H0      A0            SIGA0           A1              SIGA1)
      WRITE OUTPUT TAPE NOT,520,A0,SIGA0,A1,SIGA1
 520   FORMAT (4F14.5)
      WRITE OUTPUT TAPE NOT,535
 535  FORMAT (25H0     S(J),SIGS(J),J=1,NCL)
      WRITE OUTPUT TAPE NOT,55,(S(J),SIGS(J),J=1,NCL)
      WRITE OUTPUT TAPE NOT,540
 540       FORMAT (24H0     R(J),SIGR(J),J=1,NL)
      WRITE OUTPUT TAPE NOT,55,(R(J),SIGR(J),J=1,NL)
      NL=NCL
      DO 544 J=1,NCL
      R(J)=S(J)
      SIGR2(J)=SIGS2(J)
      DO 544 L=1,8
 544   DNAME(J,L)=DNAM(J,L)
      NT=1
      GO TO 390
 550  WRITE OUTPUT TAPE NOT,560
 560  FORMAT (58H0 YOU HAVE THE WRONG CASE NUMBER. ANALYSIS IS DISCONTIN
     1UED)
      GO TO 5
 570  FORMAT (110H0 WT(J) = WEIGHT OF CALIBRATION POINT J IN CMS
     1       RES(J) = RESIDUAL AT CALIBRATION POINT J IN CMS    )
 580  FORMAT (110H0 WE2MN1 = MEAN WEIGHTED SQUARE OF ERRORS AT THE CALIB
```

```
     1RATION POINTS IN CMS2                                              )
 590  FORMAT (110H0 WE2MN2 = MEAN WEIGHTED SQUARE OF RESIDUALS AT THE CA
     1LIBRATION POINTS IN CMS2                                           )
 700  FORMAT (110H0NOCASE = PROBLEM TYPE NUMBER
     1       NR = NUMBER OF READINGS OF EACH LINE                        )
 710  FORMAT (110H NCLS = NUMBER OF CALIBRATION LINES (SINGLES)
     1        NCLP = NUMBER OF CALIBRATION LINES (PAIRS)                 )
 715  FORMAT (110H  NGULS = NUMBER OF GOOD UNKNOWN LINES (SINGLES)
     1       NGULP = NUMBER OF GOOD UNKNOWN LINES (PAIRS)                )
 720  FORMAT (110H NBUL = NUMBER OF BAD UNKNOWN LINES
     1       NPRNT1 = PRINT OPTION NUMBER                                )
 725  FORMAT(111H A0 = DISTANCE FROM THE BETA POINT TO THE ZERO REFERENC
     1E OF THE MEASUREMENTS IN CMS                                       )
 730  FORMAT (110H A1 = DIAMETER OF FOCAL CIRCLE IN CMS
     1       SIGA1 = STANDARD DEVIATION OF A1 IN CMS                     )
 740  FORMAT (110H D = ATOMIC PLANE SPACING IN CRYSTAL IN XU
     1       SIGD = STANDARD DEVIATION OF D IN XU                        )
 750  FORMAT (110H SIGT = UNCERTAINTY IN EACH LINE MEASUREMENT FROM EMUL
     1SION SHRINKAGE,GEOMETRICAL EFFECTS,ETC IN CMS                      )
 760  FORMAT (110H WVLNTH(J) = WAVELENGTH OF CALIBRATION LINE J IN XU
     1       SIGWL(J) = STANDARD DEVIATION OF WVLNTH(J, IN XU            )
 770  FORMAT (110H Z(J,I) = READING I OF CALIBRATION LINE J IN CMS
     1       W(J,I) = READING I OF UNKNOWN LINE J IN CMS                 )
      END
```

```
      FUNCTION SINAC(W)
      W2=W*W
      SINAC=W*(1.0-W2*(1.666666667E-1-W2*(8.333333333E-3-W2*1.984126984E
     1-4)))
      RETURN
      END


      FUNCTION ARCSN(W)
      W2=W*W
      ARCSN=W*(1.+W2*(1.666666667E-1+W2*(0.075+W2*(4.464285714E-2+W2*(
     1 3.291428571E-2+W2*(2.237215909E-2+W2*1.735276442E-2))))))
      RETURN
      END


      SUBROUTINE AVRGE (VAR,M,N,V,SIGV,SIGV2)
      DIMENSION VAR(80,24),V(80),SIGV(80),SIGV2(80)
      FN=FLOATF(N)
      DENOM=FN*(FN-1.)
      DO 30 J=1,M
      V(J)=0.
      SIGV2(J)=0.
      DO 20 I=1,N
20    V(J)=V(J)+VAR(J,I)
      V(J)=V(J)/FN
      DO 25 I=1,N
25    SIGV2(J)=SIGV2(J)+(VAR(J,I)-V(J))**2
      SIGV2(J)=SIGV2(J)/DENOM
30    SIGV(J)=SQRTF(SIGV2(J))
      RETURN
      END


      SUBROUTINE REDUCE (WT,X,Y,NCL,A0,A1,SIGA02,SIGA12,TOTAL,RCRELT)
      DIMENSION WT(80),X(80),Y(80)
      B11=0.
      B12=0.
      B22=0.
      E1=0.
      E2=0.
      DO 10 J=1,NCL
      B11=B11+WT(J)
      PART=X(J)*WT(J)
      B12=B12+PART
      B22=B22+PART*X(J)
      E1=E1+WT(J)*Y(J)
10    E2=E2+PART*Y(J)
      DET=B11*B22-B12*B12
      A0=(E2*B12-E1*B22)/DET
      A1=(B11*A0+E1)/B12
       DIVD=DET*TOTAL
      SIGA02=B22/DIVD
      SIGA12=B11/DIVD
      RCRELT=B12/SQRTF(B22*B11)
      RETURN
      END
```

APPENDIX II
SPECTRUM ANALYSIS
OF THE SCINTILLATION PAIR SPECTROMETER

II.1

In this appendix, methods are discussed of determining the line spectrum of gamma rays incident on the scintillation pair spectrometer. In particular, the operation of a code PAIRSTRIP is described in which one particular method is programmed for the IBM 7090 digital computer.

The problem is discussed by Mollenauer (M4) for the case of an ordinary sodium iodide crystal, but whose equations have more general application. He shows that the measured complex spectrum $\bar{C}$ can be related to the line spectrum $\bar{N}$ of incident gamma rays and the response function of the system $\bar{R}$ by

$$\bar{C} = \bar{R} \times \bar{N} \, . \qquad \text{(II.1.1)}$$

In theory, the matrix $\bar{R}$ can be inverted to allow calculation of $\bar{N}$ as

$$\bar{N} = \overline{R^{-1}} \times \bar{C} \, . \qquad \text{(II.1.2)}$$

In practice, this procedure is not suitable because $\bar{R}$ is not well enough known and because there are statistical fluctuations in $\bar{C}$. The matrix inversion procedure will invariably produce large fluctuations between positive and negative values in the vicinity of the peaks. Examples of this are shown by Chertok (C4). The cause of these errors is discussed by Burrus (B2) who states that it is due to error amplification when the basic equations are solved exactly. What is required then is a solution of Eq. (II.1.1) in which no negative values of $\bar{N}$ are allowed. An iterative method developed by Scofield (S4) and used by Mollenauer (M4) provides such a solution.

Denote successive approximations to the incident line spectrum by $\bar{N}_i$ and to the calculated complex spectrum by $\bar{C}_i$. The procedure then is as follows:

Set $\bar{N}_1$ as the observed spectrum $\bar{C}_o$, and now apply in succession:

$$\bar{C}_i = \bar{R} \times \bar{N}_i , \tag{II.1.3}$$

$$p = \frac{(C_o)_j}{(C_i)_j} , \tag{II.1.4}$$

where $(C_i)_j$ is the j^{th} element in $\bar{C}_i$, and

$$(N_{i+1})_j = (N_i)_j \times p . \tag{II.1.5}$$

In principle, this procedure is to be applied for a sufficient number of times until satisfactory convergence of $\bar{C}_i$ to $\bar{C}_o$ is obtained. In practice, it has been found that a higher convergence rate is achieved if p is replaced by p^2 after the first iteration. A review of this and other methods is given by Heath (H4).

This method can be used for any instrument in which the response is known well enough, and in which no gamma rays are incident on the detector with an energy greater than the range of the measured spectrum. In addition, proper normalization requires that the range of the measured spectrum extends down to zero energy. These conditions can be met by the pair scintillation spectrometer. The problem that remains then is to determine the response matrix $\bar{R}$.

II.2

Let us consider the processes that take place in the scintillation pair spectrometer, before attempting to calculate the response function. The interaction of interest, which is selected by means of the electronic circuitry, is one in which a high energy gamma ray has a pair interaction in the central sodium iodide crystal of the instrument. An electron pair is created, and each electron of the pair slows down to deposit its kinetic energy in the primary crystal. The positron of the pair annihilates and the two annihilation photons are absorbed completely in the two side crystals.

For a given gamma-ray energy, the number of ion pairs formed by the electrons shows statistical fluctuations and the number of optical photons produced will vary about an average value. The number of optical photons impinging on the photo cathode will vary in a statistical manner, due to self-absorption in the crystal, which in turn depends on

the position at which the electron pair was created and on the directions taken by the electrons in that pair. In addition, the number of ion pairs formed by a positron of a given energy may differ from that of an electron of the same energy, due to their different collision cross sections. The original interaction produces an electron pair with the total energy of the incoming gamma ray less pair formation energy (1.02 Mev) and the very small recoil energy of the nucleus, but there is no single energy distribution between the members of that pair. The energy distribution law for the pair is illustrated on page 704 of Reference El. Consequently, the number of photo-electrons produced at the photocathode will fluctuate in a statistical manner for an incoming gamma ray of a particular energy. Before reaching the analyzer, the amplitude of the fluctuations is further increased by instrumental responses, which include photomultiplier tube intrinsic resolution, fluctuations in the high voltage supply, and noise in the preamplifier and amplifier. At best, the analyzer would produce a Gaussian peak as the response of the system to gamma rays of a constant energy.

There are other interactions which complicate the response. Both electrons being of high energy may create bremsstrahlung. Low energy bremsstrahlung may be reabsorbed in the primary crystal but high energy bremsstrahlung may well escape from the system. Re-absorption of low energy quanta further increases the statistical fluctuations due to the non-linearity of the optical output of the sodium iodide crystal at low energies. The escape of the high energy quanta adds a tail to the low energy side of the primary Gaussian peak. The positron may annihilate in flight and remove energy from the central crystal, and yet the more energetic annihilation photons may still be captured by the side crystals and satisfy each of the two single channel analyzers. There is a possibility that one of the electrons may be energetic enough that it is not stopped inside the crystal so that the remaining energy is lost. These mechanisms provide a further contribution to the tail.

The peak may be distorted by an interaction of one or both annihilation photons in the primary crystal, but which leaves the Compton scattered photon enough energy that the channel requirements on both side crystals are still satisfied. Finally, there remains the possibility that under the tight geometrical arrangement of the crystals, the pair

scintillation spectrometer may absorb, perhaps only partially, a low energy photon that is coincident with the primary high energy gamma ray. All of these processes are folded into a Gaussian distribution due to the statistical nature of the response of the system.

Exact calculation of the functional dependence of the response and efficiency of the instrument is very difficult and has not been attempted. It would be desirable instead to have measured the response for a range of monoenergetic gamma rays and calculate a response function empirically from these measurements. In practice, no such source of monoenergetic gamma rays was available. Decay sources usually provide low energy photons (below 3 Mev) and prompt activation produces a whole spectrum of gamma rays. Methods that can be used to produce monoenergetic photons are annihilation of positrons in flight and crystal monochromation, and neither method could be obtained readily.

An approach to obtain the response function that remains is to assume one $R_a(E,V)$, which is dependent on gamma-ray energy E and pulse-height V. This assumed response is multiplied by a series of separable unknown coefficients to obtain

$$\bar{R} = R_a(E,V)(a_o+a_1V+a_2V^2 \ldots)(b_o+b_1E+b_2E^2 \ldots) . \qquad \text{(II.2.1)}$$

In principle, one may insert the above in Eq. (II.1.1), run several different samples of known $\bar{N}$ and measure their spectra $\bar{C}$. A least squares fit to the coefficients a_i and b_i of Eq. (II.2.1) may be obtained and the assumed functional dependence of the response may be modified, and the process can be repeated if necessary. This approach has not been used because the line spectrum of gamma rays from prompt activation is not well known. The other reason is that this approach would have required considerable programming and experimentation to obtain the response function $\bar{R}$ to an indeterminate accuracy, and $\bar{R}$ was then to be used in the procedure of Section II.1 which was unproven in this case. The effort required did not seem justifiable.

The method actually used is more empirical. The efficiency is assumed to be proportional to the pair cross section of the high energy gamma ray. The response of the instrument is taken as a Gaussian peak with a variable resolution, plus triangular and exponential tails on the low energy side of the peak with variable parameters. These

tails are smoothed in to the peak center to avoid discontinuities. From data of Rose (R2) based on gamma rays from excitation by charged particles, it can be shown that the ratio of the areas of the two tails to the area of the peak varies approximately as $E^{1.7}$ where E is energy. If the area of the triangular tail is A_t and the exponential tail is A_e, we may write

$$(A_t+A_e)/A_p \propto E^{1.7}, \tag{II.2.2}$$

where A_p is the area of the Gaussian peak. This fact provides a basis for the arbitrary division of the energy dependence of A_t and A_e. This division is represented by the following equations:

$$A_t = P_1 E A_p \tag{II.2.3}$$

and

$$A_e = P_2 E^2 A_p, \tag{II.2.4}$$

where P_1 and P_2 are constants.

Figure 41 illustrates the components used to describe the response of the instrument. Using the nomenclature of Fig. 41, we obtain

$$A_p = \sqrt{\frac{\pi}{4 \ln 2}}\, w h_p = 1.065\, R E h_p, \tag{II.2.5}$$

where w is the width at half maximum and R is the resolution of the peak. Also,

$$A_t = \frac{1}{2} E h_t. \tag{II.2.6}$$

If the exponential tail is described as

$$h'_e = h_e\, e^{-C_2(E-E')/E}, \tag{II.2.7}$$

where C_2 is an adjustable parameter fed into the computer, then

$$A_e = \frac{h_e E}{C_2}. \tag{II.2.8}$$

Now

$$\frac{A_t}{A_p} = \frac{\frac{1}{2} E\, h_t}{1.065\, R E\, h_p} = P_1 E \tag{II.2.9}$$

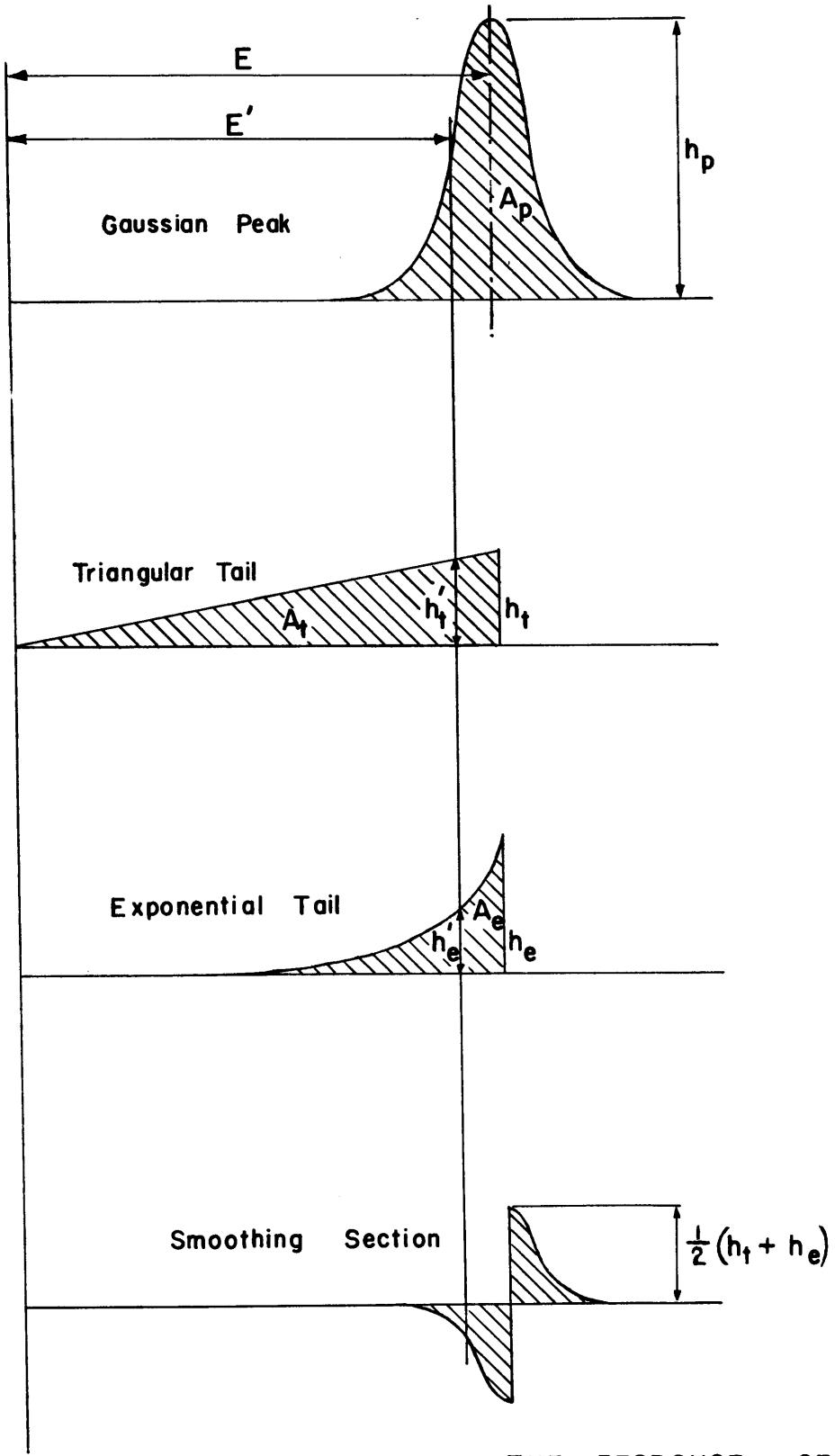

FIG 41. BASIC ELEMENTS DESCRIBING THE RESPONSE OF THE SCINTILLATION PAIR SPECTROMETER

or

$$\frac{h_t}{h_p} = 1.065 \times 2 \times P_1 . \tag{II.2.10}$$

Now put

$$C = 1.065 \times 2 \times P_1 \tag{II.2.11}$$

where C is a constant fed into the computer; and since

$$\frac{h'_t}{h_t} = \frac{E'}{E}, \tag{II.2.12}$$

we obtain

$$\frac{h'_t}{h_p} = CRE' \tag{II.2.13}$$

The above equation is programmed directly into the computer. Now

$$\frac{A_e}{A_p} = \frac{h_e E}{C_2 \times 1.065\ RE h_p} = P_2 E^2 \tag{II.2.14}$$

or

$$\frac{h_e}{h_p} = C_2 \times 1.065\ P_2 RE^2 . \tag{II.2.15}$$

Put

$$C_1 = C_2 \times 1.065 \times P_2 \tag{II.2.16}$$

where C_1 is a constant fed into the computer, so that we obtain

$$\frac{h_e}{h_p} = C_1 RE^2 \tag{II.2.17}$$

which is also programmed directly into the computer.

The resolution R of the peak may be expected to vary inversely with the square root of the number of optical photons created in the crystal. Since the optical output is proportional to the energy deposited in the crystal, the assumed functional dependence of R is taken as

$$R = a + \frac{b}{\sqrt{E}} + \frac{c}{E} . \tag{II.2.18}$$

The third term is added as a convenience. It was found that although the first two terms of Eq. (II.2.18) would fit high-energy data well and also

low-energy decay photons, the resolution predicted for low-energy quanta on the pair scintillation spectrometer was too small. The smearing of the actual peaks may have arisen from capture of coincident gamma rays, but the problem could be treated very easily by the addition of the c/E term above.

Figure 42 illustrates the variation of R with $1/\sqrt{E}$ from the original calibration by the Harshaw Chemical Company, and from the data of Olness (O1).* Both curves can be well fitted by the first two terms of Eq. (II.2.18). The dotted curve is the one that has been used for the reasons described above. The constants describing these curves are given in Table 25.

Table 25. Parameters for the Energy Dependence of the Resolution of the Scintillation Pair Spectrometer.

	$R\% = a + b/E$	$R\% = a + b/\sqrt{E} + c/E$
a	0.82, 1.35	0.70
b	5.44	3.30
c	-	6.00

The values of C, C_1 and C_2 have been adjusted so that a reasonable convergence of the calculated spectrum and measured spectrum of gamma rays from irradiation of iron is obtained. The values finally used are in Table 26, below.

Table 26. Parameters for the Response Function of the Scintillation Pair Spectrometer.

C	C_1	C_2
0.60	0.07	15.5

Figure 15 shows the degree of convergence between the measured and calculated spectrum of gamma rays from irradiation of iron. The agreement provides reasonable confidence in the calculated response function.

---

*The resolution improvement of the second curve has been obtained by the optimization procedure described in Section 4.1.

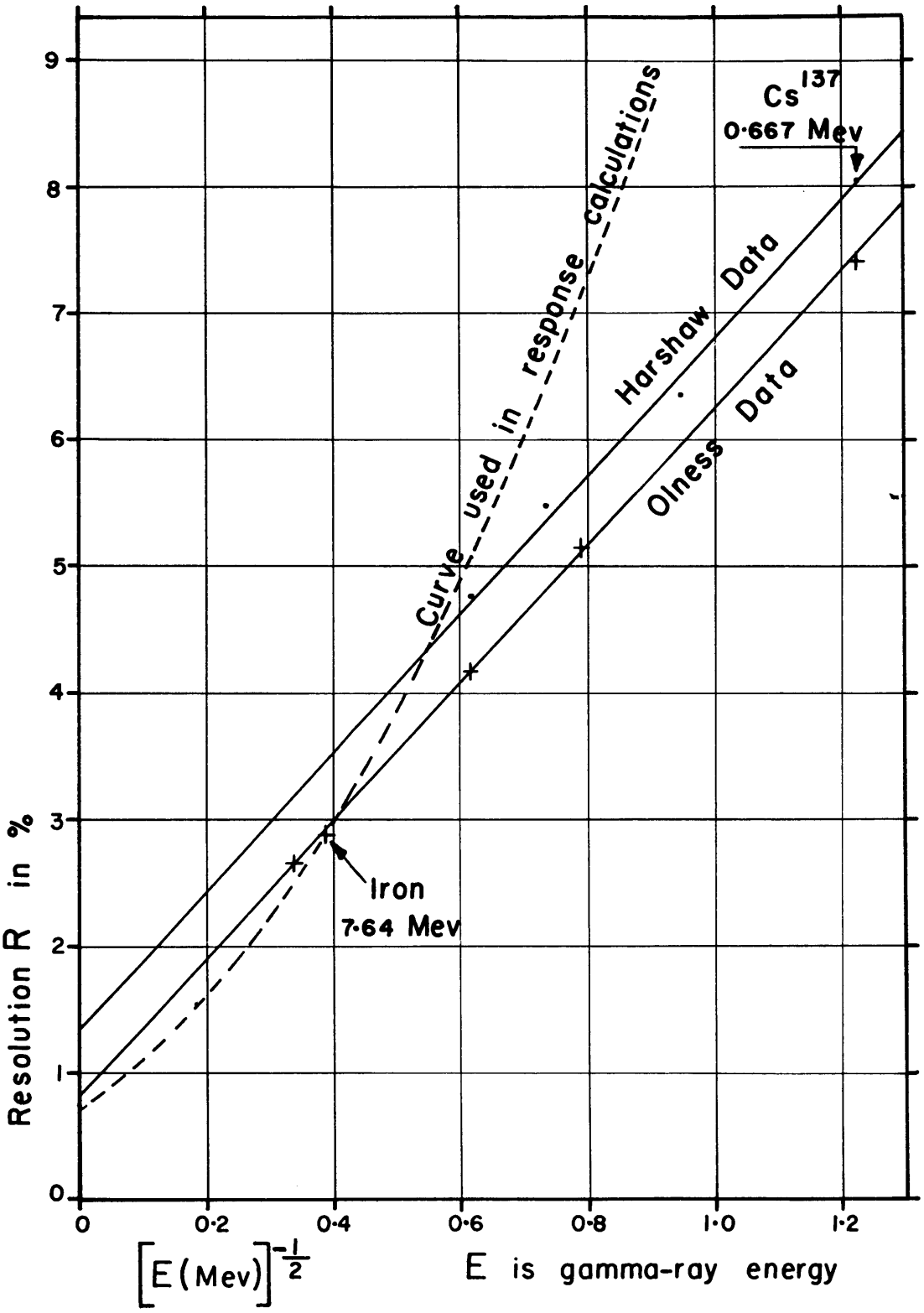

FIG 42. ENERGY DEPENDENCE OF THE RESOLUTION OF THE SCINTILLATION PAIR SPECTROMETER

The calculated response of the instrument to monoenergetic gamma rays is shown in Fig. 16.

The program for the computer is written so that it can either perform the operations indicated by Eqs. (II.1.3) to (II.1.5), or it can calculate an "observed" spectrum from the known line spectrum. In the former case, some smoothing is desirable to eliminate some of the statistical fluctuations without losing information. Smoothing by a third-degree, five-point, least squares formula is used as taken from page 296 of Reference H3. In this process, five consecutive points are used to obtain the smoothed value for the third point of the five. Smoothed values are used for points 1 and 2, and raw data are used for points 3 to 5. The final two and initial two points in the spectrum are smoothed by the specialized formula of Reference H3.

The energy calibration of the spectrum in the 400 channel analyzer is made by means of a third-order polynomial of the form,

$$E = a_o + a_1 I + a_2 I^2 + a_3 I^3 , \qquad \text{(II.2.19)}$$

where I is the channel number. The use of the second- and third-order terms is necessitated because a distinct deviation from a straight line is observed at high energies while below 5 Mev, the calibration is well represented by a straight line.

II.3

The input for the PAIRSTRIP code is described in this section. The card order is the same as that in Section I.8, [(a) to (e)], but the binary cards (c) and the data cards (e) now refer to this code. Data cards comprise the following blocks:

A Identification of runs
B Program type control card
C Parameters for energy calibration and response determination
D Control parameters
E Observed spectrum data
F Energies and intensities of the known line spectrum

Table 27 details the description of these blocks in which the format is that of Section I.8.

Table 27. Input for the PAIRSTRIP Code

Block	Column Number	Item	Input Form	Code Symbol	Units
A	1-60	Identification	A	DENOTE(K)	-
A	1-60	More identification	A		
B	1-10	The number of gamma rays of the known set to be used to calculate an "observed" spectrum NEP will be zero if the line spectrum is to be calculated from a measured spectrum.	I	NEP	
C	1-10	AE = a_o of Eq. (II.2.19)	E	AE	Mev
	11-20	BE = a_1 " " "	E	BE	Mev
	21-30	CE = a_2 " " "	E	CE	Mev
	31-40	DE = a_3 " " "	E	DE	Mev
	41-50	ARTE = a " " (II.2.18)	E	ARTE	%
	51-60	BRTE = b " " "	E	BRTE	$\%(\text{Mev})^{1/2}$
	61-70	CRTE = c " " "	E	CRTE	% Mev
	71-80	C of Eq. (II.2.13)	E	C	Mev^{-1}
C	1-10	C_1 " " (II.2.17)	E	C1	Mev^{-2}
	11-20	C_2 " " (II.2.7)	E	C2	-
D	1-10	Number of iterations to be made, described by Eqs. (II.1.3) to (II.1.5)	I	NUMLT	-
E	1-80	The number of counts in each channel starting with zero and going to the 400th channel. Sections D and E will be read only if NEP = 0.	F	COUNT (I), I = 1,400	-
F	1-10	Energy of monoenergetic gamma ray K	F	ENERGY(K)	Mev
	11-20	Intensity of monoenergetic gamma ray K	F	ENUM(K)	-
	31-80	Repeat items above in order for K = 1 to K = NEP. Section F will be read only if NEP ≠ 0.			

APPENDIX III
DATA REDUCTION METHODS FOR THE BNL APPARATUS

III.1

This appendix describes the handling methods used on the twofold and fourfold coincidence data obtained from the scintillation pair spectrometer at Brookhaven National Laboratory. The data from the 64 X 64 two-parameter analyzer is obtained on a printed paper tape via a Hewlett Packard parallel printer. The information on this tape is transferred by hand onto cards prior to processing by an IBM 7090 digital computer. A code called CAPGAM has been written for this computer which will perform the following operations as requested:

1. Subtract off background.
2. Subtract off accidental counts.
3. Calculate the standard deviation of the corrected count.
4. Subtract off coincident counts arising from the bremsstrahlung tails of high energy gamma rays detected by the pair spectrometer.
5. Print out and plot the corrected data, in subranges if desired.
6. Sum channels in either X or Y directions, and plot and print out these sums.
7. Subtract off a normalized average vector from each row to accentuate differences from the mean. This process is termed singularization. These differences are plotted out and printed.
8. Sum singularized channels, and print out and plot these sums.

Background for the case in question may be post- or prerecorded for a given live time T_B of the analyzer. The corrected counts N_c are related to the actual counts N_a, to the background counts N_B and the live time ratio R_T in the following way:

$$N_c = N_a - N_B R_T \tag{III.1.1}$$

where

$$R_T = \frac{T_a}{T_B}, \tag{III.1.2}$$

and T_a is the live time taken to record N_a. Since further corrections to the data are small, the standard deviation of the corrected counts $\sigma(N_c)$ is represented quite accurately by

$$\sigma(N_c) = \sqrt{N_a + N_B R_T} \, . \qquad \text{(III.1.3)}$$

In practice though, background corrections have not been made in this way.

Fourfold runs generally have extremely low background count rates relative to the true count rate. This is because the scintillation pair spectrometer does not easily detect the gamma rays originating from the reactor that are Compton scattered into the instrument. These scattered gamma rays have, in general, too low an energy to interact by pair formation. The principal background in the fourfold cases arises from neutrons scattered by the source and captured by the surroundings, including the central sodium iodide crystal of the instrument. If the background were to be measured, the source should be replaced by a non-absorbing scattering material. In the past, carbon has been used, but the count rates are low compared with the singles count rate of the pair spectrometer and probably negligible in the fourfold coincidence case.

In the case of twofold coincidence runs, background subtraction is easier if made directly in the analyzer itself. A twofold run takes about 7 hours and it is easy to put the analyzer in the subtract mode, put in a carbon scatterer and run the system for the same live time.

Accidental counts may be subtracted directly in the analyzer as in the case of twofold runs, a procedure which is described in Chapter 4. Alternately, accidental counts may be subtracted by computational means as in the case of fourfold runs. The gross accidental count rate is measured and its ratio R_a to the true fourfold coincidence count rate is obtained. The accidental count rate is a function of the position in the count energy matrix, but it is proportional to the singles count in either the X or the Y directions. Hence, the accidental count in X channel, i, and Y channel, j, is $n_{i,j}$ and is given by

$$n_{i,j} = \frac{R_a S_{x,i} S_{y,j}}{\sum_{j}^{64} \sum_{i}^{64} S_{x,i} S_{y,j}} \sum_{i}^{64} \sum_{j}^{64} N_{i,j} \, , \qquad \text{(III.1.4)}$$

where S_x and S_y represent the singles counts in the X and Y directions. N_{ij} is the true fourfold count in X channel, i, and Y channel, j. This expression will be true only if the analyzer counts all of the true fourfold counts. The analyzer has the feature that channel zero in either direction holds all counts that do not fall below the analyzer range. If the analyzer range is set so that no true counts lie outside its upper end, then Eq. (III.1.4) will be an accurate representation of the accidental counts.

Summing channels is a simple operation, easily performed by the computer, and it is done to improve the statistics for inspection in the direction opposite to that of the summing direction.

In the case of twofold data, there are very many true coincidences which arise from Compton interactions in both crystals. The consequence is that the true coincident peaks of interest sit on a large quantity of coincident counts spread uniformly over the range. The peaks of interest can be accentuated by subtracting off an average count obtained from each side of it, but this necessitates a pre-inspection of the output data and some preliminary interpretation. A more systematic approach is to subtract from each column an average vector normalized to the sum of that column. In practice, it is desirable to leave a quantity that is mostly positive so the normalized average vector is multiplied by a diminution factor DF of about 0.95. This process is called singularization and can be represented by the following equation in which the singularized count N' is related to the actual count N by

$$N'_{ij} = N_{ij} - DF\left\{\frac{\left(\sum_{i=1}^{i=64} N_{ij}\right)\left(\sum_{j=1}^{j=64} N_{ij}\right)}{\sum_{i=1}^{i=64}\sum_{j=1}^{j=64} N_{ij}}\right\} . \qquad \text{(III.1.5)}$$

If desired, these singularized counts may be summed in small groups to improve statistics and may be plotted as such, operations which are also performed by the computer.

Interpretation of the fourfold data is complicated by the tails of the peaks from the scintillation pair spectrometer. These tails permit the coincident spectrum of the peak to be observed at a different energy point, where it may be greater than the true coincident spectrum at the point.

A systematic way of removing the coincidences from these bremsstrahlung tails is desired which does not require a pre-inspection of the data. The method used depends on obtaining a good knowledge of the response function of the pair spectrometer. Define G_{ij} to be the number of counts in channel i which arise from gamma rays whose energy corresponds to channel j and which have one count in that channel. Then the coincidences from bremsstrahlung tails can be subtracted off by pretending that the count in each Y channel arises directly from a true peak. Hence, the corrected counts are given by

$$N_{ik} = N_{ik} - N_{ij} \cdot G_{kj}, \tag{III.1.6}$$

where k goes from 1 to m and where

$$m = j - S \cdot R_j \tag{III.1.7}$$

and R_j = resolution of a peak whose center lies in channel j, in units of numbers of channels and S is an empirical factor, usually about 0.8.

The operation indicated by Eq. (III.1.6) is carried out with j made to vary from 64 to 1, so that essentially a stripping process is performed. The function G is obtained by the methods discussed in Appendix II. It has been shown that a reasonable approximation to the response function of the system is obtained if it is considered to comprise a Gaussian peak and triangular and exponential tails.

To subtract the tails off, the peak is replaced by the area of one channel, which means that the peak area A_p is given by

$$A_p = h_p B, \tag{III.1.8}$$

where h_p is the number of counts in the channel and B is the energy width of one channel or the slope of the energy calibration line. In general, the nomenclature of Section II.2 is used here. Substitute the expression for A_p into Eq. (II.2.3), together with Eq. (II.2.6), and obtain

$$\frac{A_t}{A_p} = \frac{\frac{1}{2} E h_t}{h_p B} = P_1 E. \tag{III.1.9}$$

But P_1 is known from Eq. (II.2.11) so that we get

$$\frac{h_t}{h_p} = \frac{2B \cdot C}{2 \times 1.065} = \frac{B \cdot C}{1.065}. \tag{III.1.10}$$

Now put

$$D = \frac{B \cdot C}{1.065} \tag{III.1.11}$$

and get

$$\frac{h'_t}{h_p} = D \cdot \frac{E'}{E} \tag{III.1.12}$$

for the triangular tail, and this is programmed directly into the computer.

Substitute the expression for A_p into Eq. (II.2.4) together with Eq. (II.2.8) and obtain

$$\frac{A_e}{A_p} = \frac{h_e E}{C_2 h_p B} = P_2 E^2 . \tag{III.1.13}$$

But P_2 is known from Eq. (II.2.16), so that we get

$$\frac{h_e}{h_p} = \frac{BEC_2C_1}{1.065\,C_2} = \frac{BEC_1}{1.065} . \tag{III.1.14}$$

Now put

$$D_1 = \frac{BC_1}{1.065} \tag{III.1.15}$$

and get

$$\frac{h'_e}{h_p} = D_1 E \exp\left\{-C_2 \frac{(E - E')}{E}\right\} \tag{III.1.16}$$

for the exponential tail, and this is programmed directly into the computer.

III.2

In this section, some examples of the operations performed by the computer are given.

Figure 43 shows the counts in one channel from irradiation of scandium as obtained and as singularized data. Both sets of data are taken as plotted by the computer which, in this example, has selected the largest scale possible over a 20-channel range in the X direction. The singularized data indicates that the peak in Y channel No. 6 is a photo peak coincidence while the peak in Y channel No. 21 is not. The example illustrates the positive identification of a coincidence between a 150 kev gamma ray in the X range and a 300 kev gamma ray in the Y range.

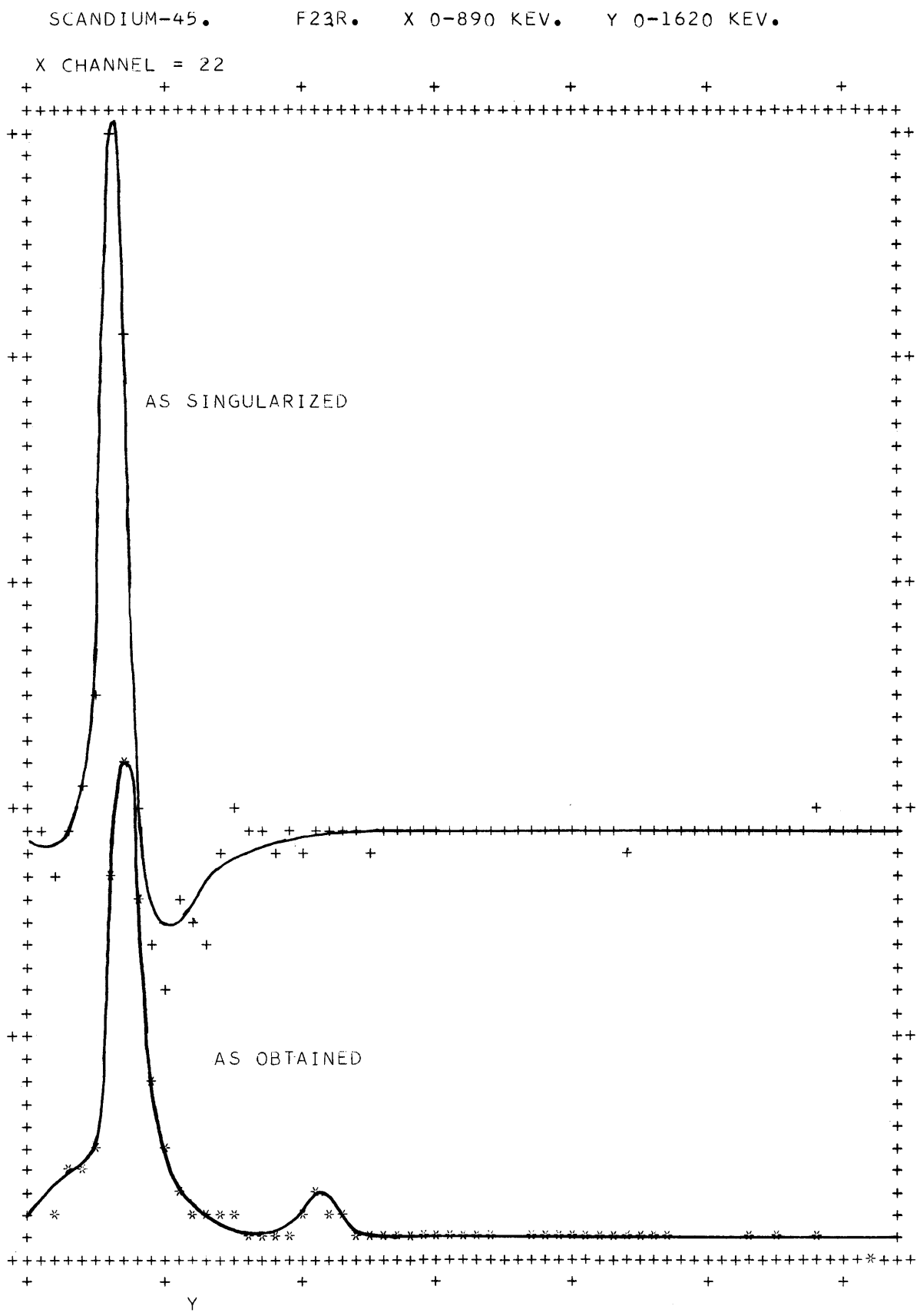

Fig. 43. Twofold coincidence gamma-ray spectra, as obtained and as singularized.

Figure 44 shows the sum of all counts in X channels plotted against the Y channel in a fourfold run on the irradiation of Dy^{164}. One case shows the ordinary corrected data and the other case shows the same data with bremsstrahlung tails removed. The peaks are somewhat more distinct in the latter case.

III.3

The input for the CAPGAM code is described in this section. The card order is the same as that described in Section I.8, (a) to (e), but the binary cards (c) and the data cards (e) now refer to this code.

Data cards comprise the following blocks:

A. Identification of runs.
B. Output from two-parameter analyzer.
C. Operational parameters and numbers.
D. Stored background counts, if any.
E. Singles counts in each direction.

Table 28 details the description of these blocks in which the format is that of Section I.8.

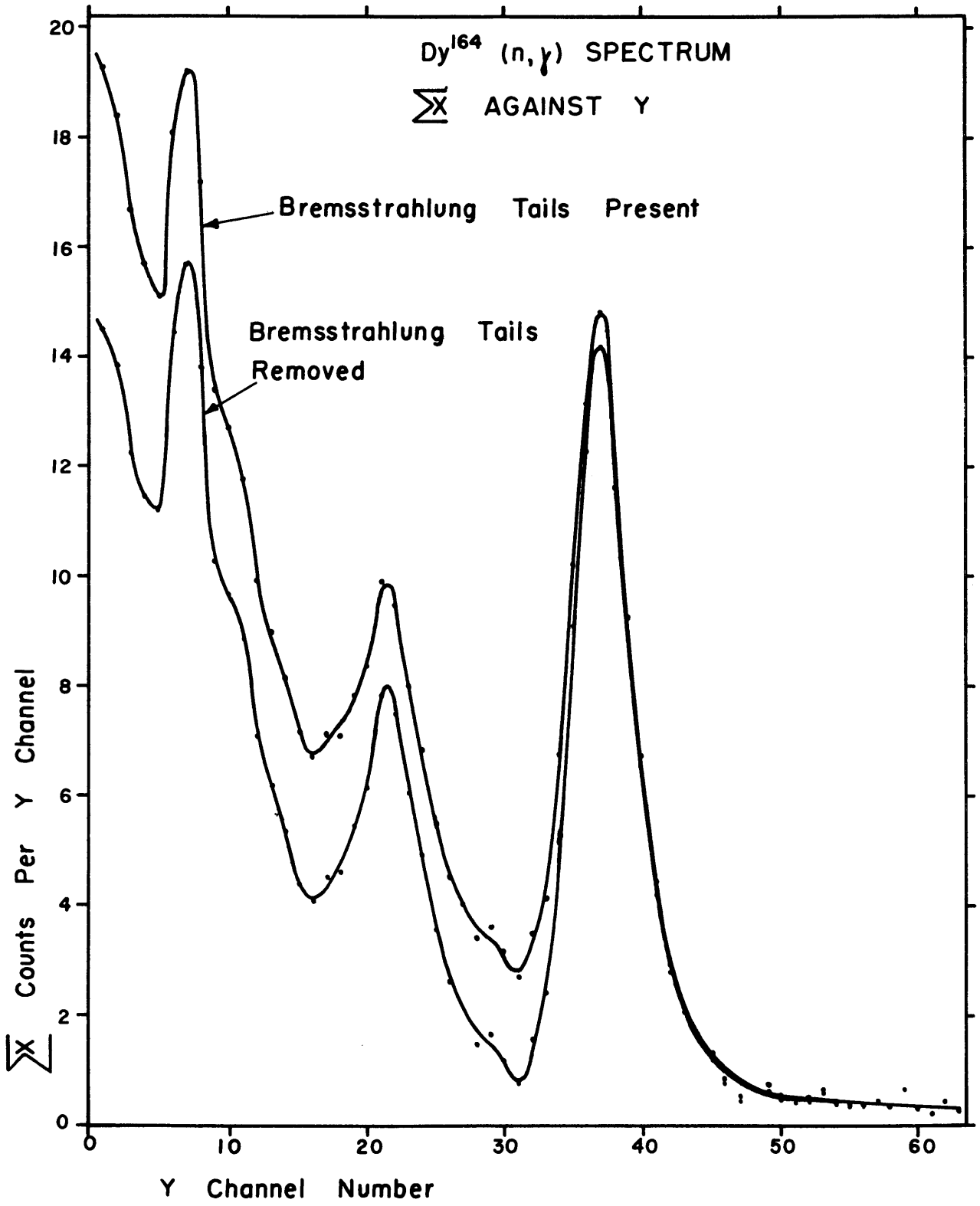

FIG 44. FOUR-FOLD COINCIDENCE GAMMA-RAY SPECTRUM, AS OBTAINED, AND WITH BREMSSTRAHLUNG TAILS REMOVED

Table 28. Input for the CAPGAM Code

Block	Column Number	Item	Input Form	Code Symbol	Units
A	1-60	Identification	A	DENOTE(K)	-
A	1-60	More identification	A		
B	1-77 in sets of 6 cards	Counts in X channel I of each Y channel J. 64 numbers at 11 to a card so that the sixth card has only 9 numbers on it.	F	COUNT(I,J)	-
C	1-10	Operation request #1. If positive, subtract off the background to be read in later. The value of OP(1) is the ratio of the live time taken to record total counts to that for the background counts.	F	OP(1)	-
C	11-20	Operation request #2. If positive, subtract off the accidental counts. The value of OP(2) is the ratio of the accidental count rate to the total count rate.	F	OP(2)	-
C	21-30	Operation request #3. If positive, the output is plotted on a logarithmic scale instead of a linear scale.	F	OP(3)	-
C	31-40	Operation request #4. If positive, print out the standard deviation of each corrected count.	F	OP(4)	-
C	41-50	Operation request #5. If zero, plot out and print the corrected counts in both the X and the Y directions.	F	OP(5)	-
C	51-60	Operation request #6. If positive, sum channels as specified later, then print out and plot these sums.	F	OP(6)	-
C	61-70	Operation request #7. If nonzero, singularize the corrected counts. If negative, sum the singularized channels as specified later. In both cases, the results are printed out and plotted.	F	OP(7)	-
C	71-80	Operation request #8. If positive, subtract off coincidences arising from bremsstrahlung tails.	F	OP(8)	-

Table 28 (continued)

Block	Column Number	Item	Input Form	Code Symbol	Units
C	1-8	AE	E	AE	Mev
C	9-16	BE	E	BE	Mev/channel
C	17-24	Diminution factor DF	E	DF	-
C	25-32	S of Equation (III.1.7)	E	S	-
C	33-40	ARTE	E	ARTE	%
C	41-48	BRTE See Tables 25 and 26	E	BRTE	$\% \cdot (\text{Mev})^{1/2}$
C	49-56	C for suggested values	E	C	-
C	57-64	C1 of these items.	E	C1	-
C	65-72	C2	E	C2	-
C	1-10	The number of values of ND that must be read in where ND are summing instructions described below.	I	NND	-
C	11-20	The number of values of NSR that must be read in where NSR are plotting instructions described below.	I	NNSR	-
C	1-3	Sum starting in this channel.	I	ND(1)	-
C	4-6	Sum for this total number of channels.	I	ND(2)	-
C	7-9	Advance the start channel of the sum at one-channel intervals until this channel is reached. ND(1) numbers come in sets of 3 at 24 to a card in a field width of 3, and a total of 72 numbers is allowed. ND refers to a summation of Y channels until 3 consecutive values of ND are set as zero. After that, ND refers to a summation of X channels until the process is terminated by 3 more consecutive zero values of ND.	I	ND(3)	-

Table 28 (concluded)

Block	Column Number	Item	Input Form	Code Symbol	Units
C	1-3	Initial channel number for sub-range plotting.	I	NSR(1)	-
C	4-6	Final channel number for sub-range plotting. NSR(I) numbers come in sets of 2 at 24 to a card in a field width of 3, and a total of 72 numbers is allowed.	I	NSR(2)	-
D	1-77 In sets of 6 cards	Background counts in the same format as B. There are no D cards unless OP(1) is positive.	F	BKGRND(I,J)	-
E	1-77 In one set of 6 cards	Singles count in the X direction with the format of B.	F	SCNTX(I)	-
E	1-77 In one set of 6 cards	Singles count in the Y direction with the format of B. There are no E cards unless OP(2) is positive.	F	SCNTY(J)	-

APPENDIX IV
BROOKHAVEN SCINTILLATION PAIR SPECTROMETER OPERATING PROCEDURE

IV.1

The procedure for operating the Brookhaven scintillation pair spectrometer on a typical fourfold run is described in this appendix. Extensive reference is made here to the description of the apparatus in Chapter 4, and to Figs. 6 to 8.

The electrical equipment is turned on but no stabilizers are hooked in, and the neutron beam from the reactor is blanked off. A minimum warm-up time of 6 hours is allowed. The high voltages on each crystal have, in general, been set to a value designed to produce the best resolution and these levels are not changed throughout the run. It will have already been determined which energy ranges in the A and B crystals (see Fig. 6) are to be investigated. Stabilization of the B crystal is probably the most important feature of the setting-up procedure. It is considered desirable not to introduce more extraneous sources than necessary, once it is stabilized. Consequently, the procedure described here provides for the A crystal to be set up first. The A system is set to produce the desired energy range on the X channel of the two-parameter analyzer. This is done by changing the gain of the A amplifier, making sure that the range does not exceed the amplifier cut-off limit. Rough calibration of this range is obtained by insertion of sources in the A calibration sample hole. A stabilizing source for the A crystal is then selected, making sure its pulse height is less than 75% of the cut-off limit of the amplifier; and this source is placed near to the A crystal by attaching it to the end of the heavy lead plug in the shielding surrounding A. The A stabilizer is then hooked in.

The procedure for hooking in the A or the B stabilizer is as follows. The channel width of the single-channel analyzer, built into the stabilizer, is set approximately equal to the line width of the stabilization peak. The delayed signal which normally goes to the

two-dimensional analyzer is fed to an oscilloscope, and a signal from the channel position of the stabilizer analyzer is fed to the external trigger position of the oscilloscope. Under these conditions, the channel position of the stabilizer can be readily seen. Changing now to internal triggering, the position of the stabilizing pulse can also be seen. The procedure then is to adjust the base line of the stabilizer-analyzer until the two pulse heights match. The mode switch of the stabilizer is switched from count rate to the integrate mode. The sweep of the stabilizer is then set to vary the base line by an amount equal to the line width of the stabilization peak, and final adjustments to the base line are made. The count range is turned to the maximum and the mode switch of the stabilizer is turned to the stabilize mode. Inspection of the oscilloscope indicates whether stabilization has been achieved. The stabilization source must clearly have been selected so that its peak height does not fall outside the range of the stabilizer-analyzer.

IV.2

A final collimator of the correct bore is now selected. This is done simply by inserting the unknown source at its correct position, opening the neutron beam, and checking the count rate in the A crystal. The collimator is selected usually to provide the A crystal with a total maximum count rate of 2 to 2-1/2 $\times 10^6$ counts/min. During this process, care must be taken to ensure that the A crystal remains stabilized. To achieve this, the external stabilizing peak must be at least twice as large as the counts around it from the (n,γ) reaction on the isotope in question. It is sometimes possible or necessary to use a slightly larger final collimator and to adjust the position of the source in the cross wires to achieve the desired maximum count rate.

With this done, a quick check of the total count rate in the B crystal is made to ensure it is not excessive. The neutron beam is then blanked off and the unknown source is removed from the apparatus. Attention is now paid to the pair spectrometer. In general, stabilization by an external source is used. Its advantage over the prompt source is that it keeps the system stable in the event of a shutdown by the reactor. It is possible that if the system were stabilized on the unknown source, the re-startup of the reactor could lead to stabilization on a different peak with the

consequent loss of the information gathered prior to the shutdown. In addition, stabilization by an external source permits energy calibration measurements to be made when the neutron beam is blanked off and when the crystals are already stabilized. The disadvantage of external source stabilization is that it reduces the useful count rate.

Stabilization of the two side crystals, C and D, is now obtained by insertion of Na^{22} into their respective calibration sample holes, and appropriately adjusting their respective amplifiers and stabilizer-analyzers. The base lines and channel widths for the two slow coincidence requirements are now set, these being independent of the C and D stabilizers. A channel width of 25% of the base-line setting is about normal.

The gain of the B amplifier is now changed to obtain the correct gain for the B system. It is desired that the spectrum, seen on the Y channel of the two-dimensional analyzer, represents the gamma energy range required. One suitable way is to insert some natural iron into the source position, put in the 7 mm-bore final collimator and unblock the neutron beam. The B system is run as a pair spectrometer and attention is paid to the distinct peaks at 6.00 Mev and 7.64 Mev in the iron. The gain of the B amplifier is changed to obtain the desired separation of these peaks. During this process, the base level of the Y channel must be adjusted to keep these two peaks in the range of the analyzer. When this is complete, the position of the Y-channel base level is computed for the energy range of the unknown source and is appropriately moved. If possible, the position of one of these iron peaks, if it comes in this range, is checked to ensure the correct setup. Then the B system is stabilized, using a suitable source placed in the calibration sample hole. When this is done, the gain of the B amplifier and the Y-channel base level control are rechecked. The neutron beam is then blocked off and the correct final collimator is reinserted. Final calibration of the A system is now made, using samples placed in the A calibration sample hole in the absence of neutron capture gamma rays. These single runs are made by putting the operation switch on the analyzer to the singles position, by disconnecting the signal lead to the analyzer from the B system and by appropriately switching in only the correct coincidence requirements

on the coincidence circuitry. A calibration is also taken with the unknown source in position with the neutron beam unblocked, both as an A singles run and also as a run in which a fast coincidence with B is required.

IV.3

When the calibration of the A system is complete, the slow-coincidence requirements are optimized. Essentially, this means varying the base line of the single-channel analyzer on each side crystal until the maximum count is obtained. It is most easily done in the absence of the neutron beam, since the 0.51 Mev peak from Na^{22} is much sharper than the peak seen in the presence of the spectrum coming from neutron capture by the unknown source.

When this is done, the unknown source is reinserted into position, the neutron beam is unblocked and the two Na^{22} sources are removed from the side-crystal calibration sample holes. A check is made to see that all of the detection systems are properly stabilized. A singles run is then made of the pair spectrum from the unknown source. This is done by switching in the correct coincidence requirements, by disconnecting the signal lead from the A system to the two-dimensional analyzer, by putting the operation switch on the analyzer to the singles position, and by putting the display switch to reverse so that the Y channel is displayed horizontally. After the pair spectrum has been taken, it is checked to see that it covers the desired energy range. Hopefully, it will provide the self-calibration of the B crystal.

The signal leads to the analyzer are reconnected, the operation switch is turned to the coincidence position, and the display switch is put to the normal position. The stabilizers are all rechecked. Count rate checks are then made of the pair count rate; A, B, C, and D singles count rates; A + B coincidence count rate; C and D channel count rates; the fourfold count rate and the accidental fourfold count rate. The latter is obtained by switching in a fixed delay in B and turning the variable delays in A and B in the opposite directions.

The coincidence requirements for the fourfold run are then switched in, the stabilizers rechecked again, the switch positions on the two-dimensional analyzer are rechecked and the fourfold run is then allowed to begin. During the run, a continuous monitor of the fourfold count rate is kept by a subsidiary scaler. Print-outs of the accumulated data are

taken each day to observe any drifts, and the stabilizers are checked frequently. When the fourfold run is completed, a final, quick pair run is taken and the A system is recalibrated in the manner described earlier.

AF Cambridge Research Laboratories, Bedford, Mass. MEASUREMENT OF GAMMA-RAY SPECTRA FROM THERMAL-NEUTRON CAPTURE, by J.M. Neill, N.C. Rasmussen, T.J. Thompson, August 1963. 171pp. AFCRL-63-341 Unclassified report

The report describes an investigation of the capture γ rays from Sc-45, Ir-191, Ir-193, Dy-161, Dy-164, Ho-165 using both a six meter bent crystal spectrograph and a NaI detection system capable of identifying γγ coincidences. Using the information obtained in conjunction with that already available, the low energy portion of the decay scheme is proposed for Sc-45, Dy-165, and Ho-166 are presented.

UNCLASSIFIED

1. Nuclear Physics
2. Nuclear Energy Levels

I. Neill, J. M.
II. Rasmussen, N. C.
III. Thompson, T. J.

AF Cambridge Research Laboratories, Bedford, Mass. MEASUREMENT OF GAMMA-RAY SPECTRA FROM THERMAL-NEUTRON CAPTURE, by J.M. Neill, N.C. Rasmussen, T.J. Thompson, August 1963. 171pp. AFCRL-63-341 Unclassified report

The report describes an investigation of the capture γ rays from Sc-45, Ir-191, Ir-193, Dy-161, Dy-164, Ho-165 using both a six meter bent crystal spectrograph and a NaI detection system capable of identifying γγ coincidences. Using the information obtained in conjunction with that already available, the low energy portion of the decay scheme is proposed for Sc-45, Dy-165, and Ho-166 are presented.

UNCLASSIFIED

1. Nuclear Physics
2. Nuclear Energy Levels

I. Neill, J. M.
II. Rasmussen, N. C.
III. Thompson, T. J.

AF Cambridge Research Laboratories, Bedford, Mass. MEASUREMENT OF GAMMA-RAY SPECTRA FROM THERMAL-NEUTRON CAPTURE, by J.M. Neill, N.C. Rasmussen, T.J. Thompson, August 1963. 171pp. AFCRL-63-341 Unclassified report

The report describes an investigation of the capture γ rays from Sc-45, Ir-191, Ir-193, Dy-161, Dy-164, Ho-165 using both a six meter bent crystal spectrograph and a NaI detection system capable of identifying γγ coincidences. Using the information obtained in conjunction with that already available, the low energy portion of the decay scheme is proposed for Sc-45, Dy-165, and Ho-166 are presented.

UNCLASSIFIED

1. Nuclear Physics
2. Nuclear Energy Levels

I. Neill, J. M.
II. Rasmussen, N. C.
III. Thompson, T. J.

AF Cambridge Research Laboratories, Bedford, Mass. MEASUREMENT OF GAMMA-RAY SPECTRA FROM THERMAL-NEUTRON CAPTURE, by J.M. Neill, N.C. Rasmussen, T.J. Thompson, August 1963. 171pp. AFCRL-63-341 Unclassified report

The report describes an investigation of the capture γ rays from Sc-45, Ir-191, Ir-193, Dy-161, Dy-164, Ho-165 using both a six meter bent crystal spectrograph and a NaI detection system capable of identifying γγ coincidences. Using the information obtained in conjunction with that already available, the low energy portion of the decay scheme is proposed for Sc-45, Dy-165, and Ho-166 are presented.

UNCLASSIFIED

1. Nuclear Physics
2. Nuclear Energy Levels

I. Neill, J. M.
II. Rasmussen, N. C.
III. Thompson, T. J.